SATELLITE COMMUNICATIONS IN THE V AND W BAND: NATURAL AND ARTIFICIAL SCINTILLATION EFFECTS

THESIS

David A. Smith, Capt, USAF

AFIT-ENG-MS-17-M-070

DEPARTMENT OF THE AIR FORCE
AIR UNIVERSITY

AIR FORCE INSTITUTE OF TECHNOLOGY

Wright-Patterson Air Force Base, Ohio

AFIT-ENG-MS-17-M-070

SATELLITE COMMUNICATIONS IN THE V AND W BAND: NATURAL AND ARTIFICIAL SCINTILLATION EFFECTS

THESIS

Presented to the Faculty

Department of Electrical and Computer Engineering

Graduate School of Engineering and Management

Air Force Institute of Technology

Air University

Air Education and Training Command

in Partial Fulfillment of the Requirements for the

Degree of Master of Science in Electrical Engineering

David A. Smith, B.S.E.E.

Capt, USAF

March 2017

AFIT-ENG-MS-17-M-070

SATELLITE COMMUNICATIONS IN THE V AND W BAND:

NATURAL AND ARTIFICIAL SCINTILLATION EFFECTS

THESIS

David A. Smith, B.S.E.E.
Capt, USAF

Committee Membership:

Dr. A. J. Terzuoli
Chair

Dr. P. Collins
Member

Lt Col J. Fee
Member

Dr. J. Petrosky
Member

Dr. C. Yardim
Member

AFIT-ENG-MS-17-M-070

Abstract

Secure communications are imperative for government applications. Crowded frequency bands are forcing users to look into higher frequencies in the 40 - 110 GHz band (V and W bands). In a natural atmospheric environment the troposphere will be the primary source of loss with the ionosphere loss being negligible. If the ionosphere was disturbed from a high altitude nuclear explosion (HANE) more than three times the amount of electrons would be present in the ionosphere and could represent a source of significant loss. In order to determine the amount of electrons distributed from a HANE, GSCENARIO, developed by Defense Threat Reduction Agency was used. The two sources of loss that were examined was signal absorption and amplitude scintillation. Signal loss was determined using GSCENARIO and amplitude scintillation loss was determined by using the multiple phase screen method. Nuclear detonation yields of 100 kt, 500 kt, 1 Mt, 2 Mt, and 5 Mt at explosion heights of 150 km and 200 km were investigated. The results show that signal absorption drops off quickly (within 30 sec), while amplitude scintillation loss can linger for up to 6 min after a HANE. Thus, the signal loss in the V and W bands from a HANE will only disrupt transmissions for the first 6 min after a HANE.

Acknowledgements

I would like to thank the sponsor of the research for this thesis AFRL/RIT for their support and feedback during the thesis process. I would also like to thank Dr Terzuoli for his support and direction. I give thanks for the thesis committee members, Dr. Collins, Lt Col Fee, Dr. Petrosky, and Dr. Yazdim, for taking the time to listen and provide feedback on my research. I also thank Elliot Erstein for is insight into MATLAB. Next, I thank the research assistants, Derek Hesser, Lee Burchett, James Ethridge, and Courtney Landis for their work and support that allowed smooth operation of the simulations performed in this research. Also, would like to thank the Joseph Sugrue and Raymond Wasky for steering my in the correct direction. Finally, I especially thank my wife for supporting the energy and countless hours I dedicated to this research.

David A. Smith

Contents

Page

List of Figures

Figure Page

Figure Page

List of Tables

Table Page

SATELLITE COMMUNICATIONS IN THE V AND W BAND:
NATURAL AND ARTIFICIAL SCINTILLATION EFFECTS

I. Introduction

1.1 Introduction

Secure communications is of the utmost importance for the Department of Defense (DoD). The increased use of unmanned aerial vehicles and the desire for real-time intelligence and reconnaissance has driven the need for access to satellite communication (SATCOM). Currently, the radio frequency bands (RFB) for SATCOM are cluttered with many users other than the DoD. Therefore, the DoD, with its increasing demand for SATCOM usage, needs to explore alternate solutions that use the current RFBs. One solution is to take advantage of the unused V and W radio bands, 40 - 75 GHz and 75 - 110 GHz respectively. Currently, no commercial entities are using the V and W bands, leaving two entire bands for exclusive DoD use. Not only are the V and W bands not currently used for SATCOM, but these RFBs provide greater bandwidth capabilities than other RFBs. The greater bandwidth capabilities are particularly attractive to the DoD because greater bandwidth allows more data to be transmitted. [5, 6, 7]

The ionosphere is an atmospheric layer that contains free ions and electrons. This atmospheric layer extends from 50 km to approximately 2000 km above the surface of the Earth. The ionosphere is also divided up into three different regions that are designated by layers D, E, and F. The electron content structure of the ionosphere during day time hours can be described as steadily increasing from 100 km to 300 km

(E and F layers), where it begins to decline and decrease at altitudes greater than 300 km. During night hours, the electron content in the E layer (200 km) drops off, giving the electron content profile seen in Figure 1. Modifications or disturbances in the ionosphere can arise from both natural and artificial causes. Both artificial and natural disturbances can change the electron content of the ionosphere and thus affect SATCOM. A natural disturbance can include severe weather (hurricanes, thunderstorms, etc.), earthquakes, and solar activity (solar flares, solar storms, solar eclipses, etc.), where artificial disturbances include nuclear explosions [5, 6, 7].

Since the V and W bands are not currently used for SATCOM, the particular effects that the troposphere or the ionosphere have on SATCOM communications in these RFBs has not been researched. The main effects on SATCOM from the troposphere and ionosphere are termed scintillation. Scintillation is changes in amplitude and phase of a communication signal caused by small-scale electron structures in the ionosphere. As a plane EM wave transverses through the electron structures of the ionosphere, the irregularities cause phase fluctuations that produces phase variations along the phase front of a plane wave. As the wave continues to propagate through the ionized medium, scintillation develops from the additive and subtractive interference cause from the small scale scattering of the EM wave, see figure 5. Signals at frequencies higher than 10 GHz are more affected by the troposphere, while signals at frequencies below 10 GHz are more affected by the ionosphere. Currently, the International Telecommunication Union Radio-telecommunication (ITU-R) provides recommendations for modeling scintillation on SATCOM primarily for frequencies below 30 GHz. Other models that exist include only tropospheric scintillation effects for frequencies above 10 GHz and ionospheric scintillations effects for frequencies below 10 GHz [3, 8].

The rationale behind the limits imposed on current scintillation models is under-

standable since most SATCOM above 10 GHz are generally not affected by scintillation resulting from natural ionospheric effects. Even with the most intense natural geomagnetic storm, the electron density of the ionosphere would not have a significant effect on SATCOM above 10 GHz. What is perhaps a greater concern to the DoD is effects on SATCOM that ionospheric scintillation would have from artificial disturbances, such as a nuclear explosion. In the event of a nuclear explosion or other cataclysmic event, DoD SATCOM must still be available. Thus, a significant gap in current research is apparent in regards to ionospheric scintillation effects for SATCOM in the V and W bands for both natural and artificial disturbances.

1.2 Problem Statement

Link budget analysis is the accounting of all the gains and losses of a propagating wave. Currently, models do exist to support link budget analysis for V and W band research, but these models only include tropospheric scintillation effects, and have not been expanded to include ionospheric scintillation effects. Models for ionospheric scintillation focus primarily on frequencies below 10 GHz and these models do not include artificial disturbances. Link budget analysis provides a SATCOM user with propagation loss of communication links due to factors including antenna loss, free space propagation loss, and scintillation loss. In theory the effects of ionospheric scintillations should be minimal, nonetheless, it is important to understand the ionosphere's effects. This research explores ionospheric scintillation effects on SATCOM signals in the 40 - 110 GHz range.

1.3 Justification

A critical gap exists in research on the effects of the ionosphere scintillation on SATCOM. Middlestead, LeLevier, and M. Smith have shown that a nuclear detona-

tion can disperse ions and electrons that interfere with satellite crosslinks up to 30 GHz in space where the ionosphere is not a factor. Thus, more electrons injected into an already dense field will only increase ionospheric scintillation effects on SATCOM. This research aims to fill a critical gap in understanding what effects the ionosphere will have on SATCOM during a strong artificial disturbance [3].

1.4 Assumptions and Scope

This research will only consider terrestrial to satellite communications. Also, only the effects of artificial disturbances in the ionosphere will be considered. Only the frequency range of 40 - 110 GHz will be considered. The propagation path considered will be earth normal and one-way.

1.5 Standards

The validity of the model will be verified by comparing the solution of the model to the solution of simple examples. The simple examples will include a basic Gaussian power spectral density (PSD). Additionally, a Gaussian input wave which can be easily solved using the Fresnel-Kirchoff Diffraction Integral will be utilized. Solving the Fresnel-Kirchoff Integral for the simple example will give an exact solution to which the ionosphere scintillation model can be compared.

1.6 Approach and Methodology

In order to model the propagation of SATCOM through the ionosphere the solution to Maxwell's electromagnetic equations was utilized. The solution to Maxwell's electromagnetic equations were determined by using the multiple phase screens (MPS) method. MPS uses the Helmholtz wave equation form of Maxwell's electromagnetic equations. The Helmholtz wave equation was then put into the parabolic form. MPS

takes the phase changes from each phase screen in the model to determine the solution of Maxwells electromagnetic equations. The phase screen was realized by finding the power spectral density (PSD) of the electron content of the ionosphere. The propagation model was used to run simulations on different SATCOM modulation waveforms to determine the effects ionospheric scintillation will have [9, 10, 11, 12, 13, 14, 15].

1.7 Research Question

What effects will the ionosphere have on SATCOM in the V and W band? How will particular SATCOM modulation waveforms will be affected by ionosphere scintillation during natural and artificial (HANE) disturbances?

1.8 Materials

The materials required for this research are the computer software MATLAB, GSCENARIO and computer systems available in LOREnet. The sponsor to this research effort is the Air Force Research Laboratory (AFRL/RIT).

1.9 Other

Research assistants will help conduct the simulations and help in implementing the model. Funding for this research effort was provided by AFRL.

1.10 Chapter Preview

Chapter two provides a brief explanation of ionospheric effects and methods to propagate electromagnetic waves. Chapter three explains the methodology used to model and simulate SATCOM propagation through the ionosphere. Chapter four explains the results of the propagation simulation. Chapter five provides the analysis

of the results. Chapter six is the conclusion and gives recommendations for further research.

II. Literature Review

2.1 Introduction

The purpose of this chapter is to explain the background of the problem of transionic propagation and explain the different approaches that have been used to model the ionospheric propagation. First will be a description of the ionosphere, which will include the ionosphere's composition, disturbances, and specific effects that it has on radio waves. Next, the electromagnetic theory will be introduced and shown how it will be used to model radio wave propagation. Finally, various ionosphere modeling properties will be shown and described.

2.2 Ionosphere

Ionosphere Properties.

Since the launch of Sputnik by the Soviet Union on October 4, 1957, the ionosphere has been brought to the attention of scientists and engineers as a possible source of interference of radio transmissions into space. In general terms, the ionosphere is an atmospheric layer that contains free ions and electrons. The ionosphere is generally defined as a weak cold plasma with the Earth's magnetic field overlaid. In a plasma there are equal amount of negative and positive charged particles, thus a plasma is electrically neutral. The electrons will oscillate around the heavy ions and spiral around an external magnetic field. For particle movement in a plasma, collisions are the most important factor. The collision type that appears in the ionosphere is elastic collisions, which are collisions where kinetic energy and momentum are conserved. These collisions produce ionization, and transfer heat from hot to cold regions of the ionosphere [16, 6, 7].

The ionosphere has been divided up into layers that are characterized by their maximum electron density and electron decay. The layers are also characterized by the critical frequencies, peak heights, and half thickness. There are primarily three distinct layers labeled D, E, and F. The F layer is also partitioned up into three distinct layers of its own, labeled: F1, F2 and F3. The first layer to be detected was the E layer, followed by the F layer, and finally the D layer. The F layer is the most dominant of the three main layers and extends from 150 to 500 km above the Earth. The E layer extends from 90 to 150 km and the D layer is below 90 km. Interestingly, the main ionospheric layers are only distinct during the daytime. At night the F1 layer will decay and a valley manifests to separate the E and F2 layers [16, 6, 7].

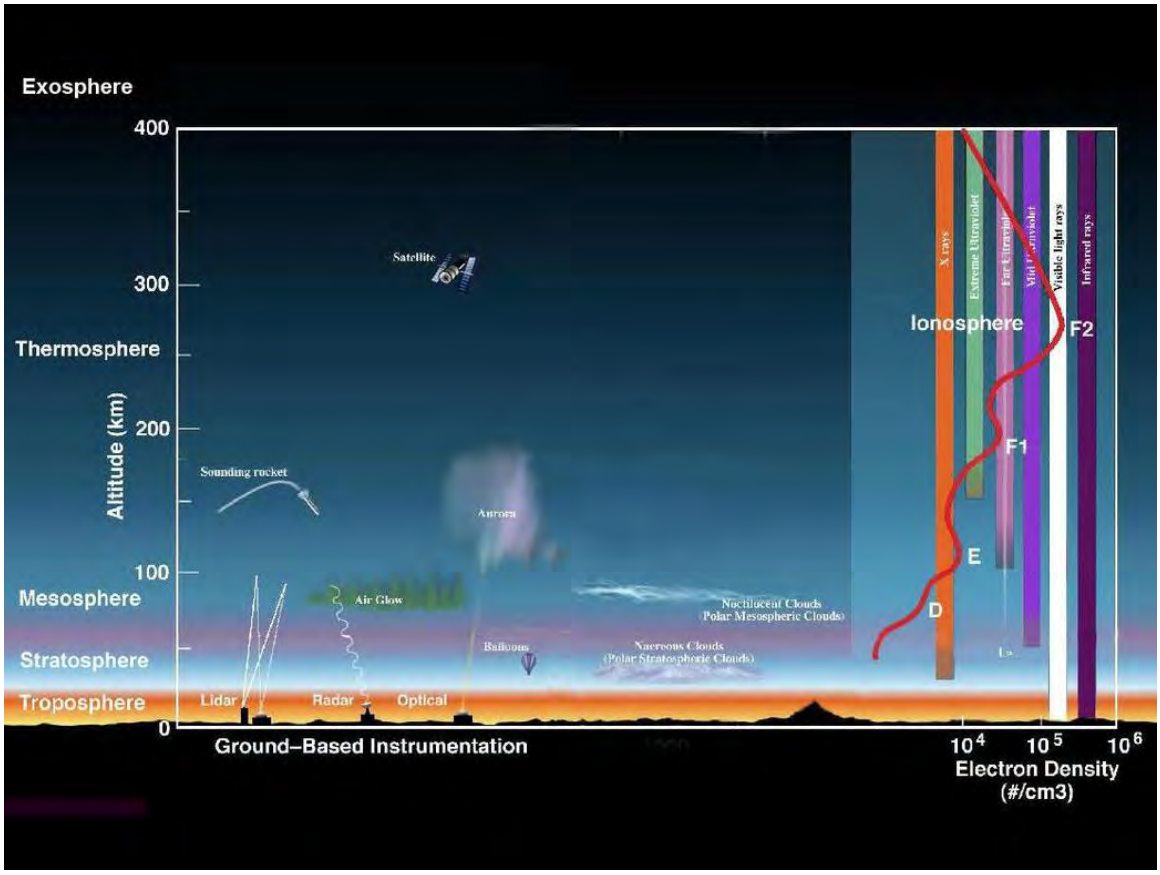

Figure 1. Ionosphere layer map. [1]

As stated previously, the F Layer is comprised of three different sub-layers, F1, F2,

and F3. The F1 layer is only present during the day. It is also more distinct during the summer months when sun spots are low and during ionospheric storms. In the F1 layer the ion atomic interchange process (or ion collisions) becomes important, but it is in the F2 layer where the ion collisions reach a maximum [16, 6, 7].

The F2 layer is the most important of all the layers for radio wave propagation. The peak density of the F2 layer is approximately 10 times greater than the E layer. The F2 layer is where ion collisions become important and must be taken into account [3].

The F3 layer was known to exist more than 50 years ago, but it was not until the 1990's that meaningful characteristics were identified through the use of ionosodes. As the F2 forms near the equator during the day and drifts upward, the F3 layer is formed at altitudes above 500 km. The F3 layer can be present in both the summer and winter sides of the magnetic equator although it becomes weaker with increased activity from the sun. The F3 layer has also been observed to form with magnetic storms. The F3 layer becomes important since occasionally it can have higher peak ion densities than the F2 layer [6].

The main irregularities that exist in the F layer are "spread F" (or bubbles). These bubbles are plasma irregularities and inhomogeneities in the F layer. The dominant feature in spread-F occurrence is the existence of two areas: equatorial regions ($\pm 20^\circ$ latitude), and high-latitude regions ($> 40^\circ$ latitude). There is a region of permanent spread F close to the magnetic dip pole. In this region, during the summer months, spread F occurs 90-100 percent of the time. In these high latitudes, spread F presents itself as filaments that are several kilometers in size [6, 7].

Equatorial spread F (ESF) appears near the geomagnetic equator and occurs during the evening and nighttime. ESF is most prevalent during equinoxes, or during local summer months. The density of ESF bubbles can be anywhere from a few

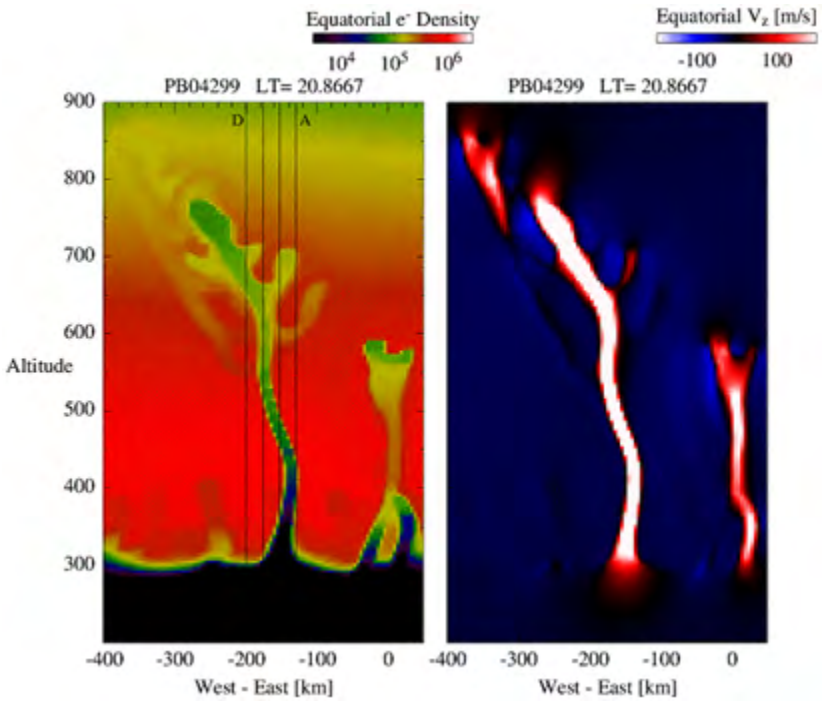

Figure 2. An example of Spread F [2].

centimeters to 100s of kilometers. These bubbles are vertically elongated pockets of depleted plasma that form beneath the bottom-side of the F layer and drift upwards. The resultant bubbles can be up to two orders of magnitude less dense than the surrounding medium [16, 6, 7].

Plasma instabilities in the E layer (or sporadic E) have a critical frequency that is extremely variable in time and space. The critical frequency can vary anywhere from 3 - 30 MHz at a given location. The sporadic E forms between 90 - 120 km and occurs sporadically at all latitudes, hence its name. Close to the equator, the sporadic E has little seasonal variation and is present during both day and night. At higher latitudes (the aurora zone) sporadic E occurs mostly at night. The densities of sporadic E can manifest on the order of a magnitude greater than the surrounding densities. Sporadic E is very narrow (0.6 - 10km) and can occur in multiple layers separated by 6 to 10 km. At mid-latitudes, sporadic E is primarily caused by wind

shears, but the irregularities also are brought on by gravity waves and by diurnal and semi-diurnal tides [16, 6, 7].

Ionosphere Disturbances.

The ionosphere is occasionally disturbed from outside influences that include both natural and artificial sources. Some natural disturbances that affect the ionosphere include severe weather, earthquakes, and solar activity. Severe weather (hurricanes, thunder storms, etc.) affect the ionosphere through tropospheric and ionospheric coupling and acoustic gravity waves. Earthquakes affect the ionosphere by the production of gravity waves that propagate to the ionosphere. During a solar eclipse, as the Moon traverses the sun, the Moon's shadow will cut off the heat radiation from the sun. The sudden loss of solar heating will produce oscillating waves that will disturb the ionosphere [7, 17].

Apart from the aforementioned natural disturbances, the ionosphere can be disturbed artificially as well. The F layer can be altered through chemically increasing the electron density, reducing the electron density, or convecting the ionospheric plasma from one region to another. During a National Aeronautics and Space Administration (NASA) experiment, a spacecraft's engines were used to deposit 280 kg of varying chemicals in the F layer. The results of the deposit of chemicals decreased the electron content by at least two orders of magnitude. [7, 18, 19].

Artificial Disturbances.

Nuclear Explosion.

Another way the ionosphere can be artificially disturbed is through nuclear detonations. Unlike conventional explosions, in which explosive energy is produced by a chemical reaction, a nuclear explosion's energy is produced by the energy output

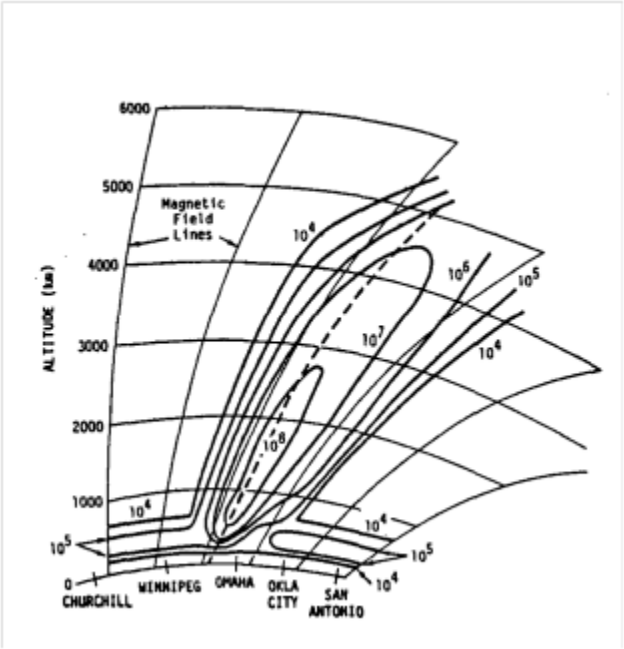

Figure 3. Nuclear explosion plume [3].

due to the nuclear instability resulting from fissile material absorbing a neutron (or fission). The resulting energy output are one million times greater than those from a chemical explosion. This dramatic effect allows nuclear explosions to require significantly less material than conventional explosions to produce the same amount of burst. When a nuclear explosion occurs, radioactive debris, consisting of electrons and ions, is dispersed. Often the yield, or measurement of explosive energy, of a nuclear explosion is quantified in terms of the amount of TNT needed to produce the same explosive energy. For example, a nuclear explosion of 100 kt (kiloton) yield produces the same explosive energy as 100 kt of TNT, regardless of the size of the nuclear weapon [4].

High Altitude Nuclear Explosion.

Nuclear explosions above the Earth's atmosphere can inject a significantly greater density of electrons and ions that occur naturally in the ionosphere. In particular,

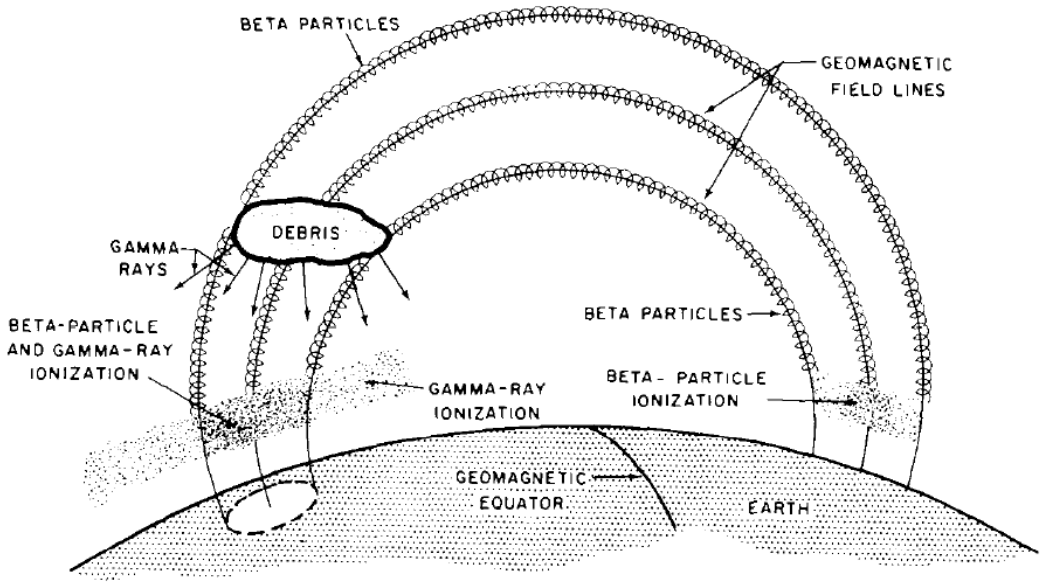

Figure 4. Ionization regions and travel paths along geomagnetic field lines. [4].

a high altitude nuclear explosion (HANE) (high altitude, defined as 100 km above the Earth's surface or higher) could produce upwards of 10^3 times the amount of the electron density currently in the ionosphere. After a nuclear burst above 100 km, the initial ion debris (which contains electron-neutral ions and electron ions) generated from the explosion travels in outwards in all directions, with the Earth's geomagnetic field lines dominating the path the nuclear debris travels. The ion debris that travels down towards the Earth is stopped by the Earth's atmosphere at approximately 80 km. The ionized debris will then expand and rise (spiraling) along the Earths geomagnetic lines (See figures 3 and 4). This spiraling along the Earth's geomagnetic field lines is a result of the Earth acting as a magnetic dipole, with conjugate points north and south of the geomagnetic equator for each geomagnetic field line. The upwards traveling ion debris will then produce similar effects at the conjugate location of the initial explosion. As a result of this process the electron content of the ionosphere can see a rise of electron content upwards of $10^9 \frac{el}{cm^3}$ above the explosion point [7, 20, 3, 4].

Effects on Satellite Communications.

The ionosphere plays a role in producing a variety of effects on SATCOM. In general, even during the most severe natural disturbances the ionosphere will have little effect on SATCOM signals in the 40 - 110 GHz range, in which this thesis investigates, unless a nuclear detonation is taken into account. The increase of electrons may have adverse effects on SATCOM in the 40 to 110 GHz range. The effects observed in the range of frequencies discussed herein are amplitude scintillation and absorption. Other effects from ionized plasmas, such as Faraday rotation, time delay, phase delay, and dispersion, are neglected because of the scope of this research [3].

Amplitude scintillation is defined by rapid fluctuations in amplitude of a signal about a mean level. Irregularities in the plasma structure of an ionized medium cause refraction at small, or narrow, angles. This small angle refraction over a large distance (≈ 100 km +) will cause focusing and defocussing effects on a signal, resulting in fluctuations at a given receiver (see figure 5). As irregularities occur more often in an ion structure, so do the fluctuations. The amount of amplitude scintillation can be determined using the split-step Fourier method discussed below [9].

Absorption of a signal after a HANE comes from the concentrated ion debris. After the initial explosion, the electron density will be very compact. The electron densities will drop off as the electrons begin to disperse along the geomagnetic lines. In order to calculate the absorption from a HANE the following equations can be used:

$$Ab_i = \frac{0.79 N_i \upsilon_{im}}{(\upsilon_{im})^2 + (2 f_c \pi)^2} \tag{1}$$

$$Ab_{en} = \frac{4.6 \times 10^4 v_{em} G}{(v_{em} G)^2 + (2\pi f_c H)^2} \tag{2}$$

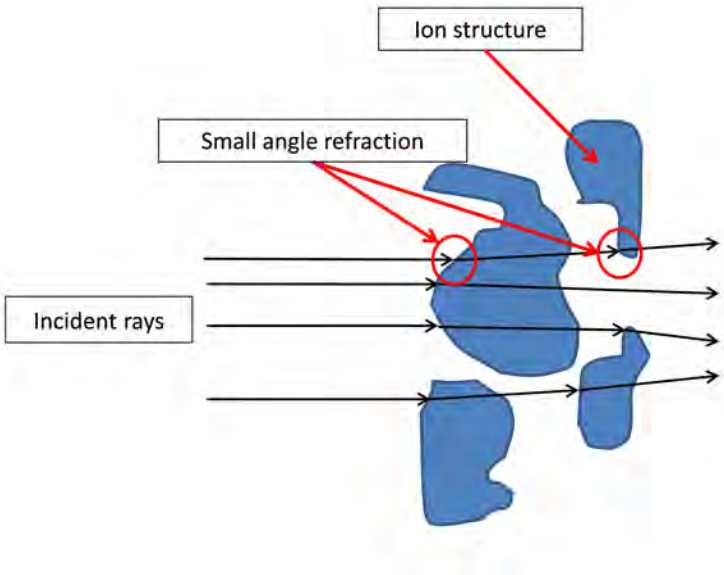

Figure 5. A simple example of refraction in an ionized plasma that causes amplitude scintillation.

$$Ab_e = \frac{4.6 \times 10^4 N_e \upsilon_{ei}}{\upsilon_{ei}^2 + (2\pi f_c)^2} \tag{3}$$

where,

$$G = \begin{cases} 3/5, & \upsilon_{im} > \upsilon_{ei} \\ 1, & \upsilon_{im} \leq \upsilon_{ei} \end{cases} \tag{4}$$

$$H = \begin{cases} 3, & \upsilon_{im} > \upsilon_{ei} \\ 1, & \upsilon_{im} \leq \upsilon_{ei} \end{cases} \tag{5}$$

$$\upsilon_{em} = 8.14 \times 10^{12} \rho_n T_e^{0.64} \tag{6}$$

$$\upsilon_{im} = \frac{\upsilon_{em}}{40} \tag{7}$$

and

$$\upsilon_{ei} = 1.8 N_e T_e^{-3/2} \ln(1.54 \times 10^8 \frac{T_e^3}{N_e} \frac{f_p^2}{f_c^2}). \tag{8}$$

Equation (1) calculates the absorption from neutrals (Ab_i). Here, N_i is the neutral ion density (cm^{-3}), υ_{im} is the collision frequency of neutral ions, ρ_n is the neutral mass density, and f_c is the frequency of the electromagnetic wave. Equation (2) calculates the absorption from electron neutrals Ab_{en}. Variables G and H are weights that depend on the relationship between equations (7) and (8). υ_{em} is the electron neutral collision frequency. Equation (3) calculates the electron neutral absorption (Ab_e), with N_e as the electron density (cm^{-3}), and υ_{ei} as the electron neutral collision frequency. In (8) T_e is defined as the electron temperature, f_p is the electron collision frequency ($f_p = 8.1 \times 10^7 N_e$), and f is the frequency (Hz) of the electromagnetic wave [21].

Middlestead, LeLevier, and Smith have shown that the rise in electron density from a HANE can effect satellite cross-links. However, their research, though, was limited by the effects of a HANEs at 800 km two minutes after the initial explosion, when most of the absorption effects would have already dissipated. This thesis aims to consider the scintillation effects and absorption effects for HANE at 150 km and 200 km both immediately following a nuclear explosion until 10 min following[3].

2.3 Electromagnetic Theory

Maxwell's Equations.

In 1873, James Maxwell developed four partial differential equations to describe electromagnetic propagation. These equations are defined as:

$$\begin{aligned} \nabla \times \vec{E} &= -\tfrac{\delta \vec{H}}{\delta t} \\ \nabla \times \vec{H} &= -\tfrac{\delta \vec{E}}{\delta t} \\ \nabla \bullet \vec{E} &= 0 \\ \nabla \bullet \vec{H} &= 0 \end{aligned} \tag{9}$$

The equations list in (9) are the basis upon which all electromagnetic wave propagation is based. To determine the propagation effects on a signal, one has to simply solve (9). Unfortunately, the solution to ME is not trivial and requires different forms of the original equations.

Ionosphere Propagation Models.

Finite Difference Time Domain.

An exact solution to (9) is always ideal as it gives a precise representation of a propagating wave. The finite difference time domain (FDTD) method that calculates an exact solution to the time dependent equations in equation (9) . In regards to the ionosphere, Nickisch developed a two dimensional FDTD algorithm based on Yee's FDTD algorithm. They both treated the ionosphere as a dispersive medium and were able to get accurate results from their calculations. Yu extended this idea and created a three dimensional FDTD model of the ionosphere that is able to incorporate data from other ionosphere physics models to allow for an exact propagation solution. Unfortunately, the computational requirements for an FDTD algorithm for the ionosphere in the 40 110 GHz range is currently unrealizable, due to the propagation distances and sampling requirements needed for an accurate result. Thus, a different method is needed [22, 23].

Spectral Properties.

There have been many experiments that have measured and recorded different scintillation events. Spectral Fourier analysis was then performed on the events to determine the spectral properties of the scintillation events. The strength of scintil-

lation events are defined by the S_4 scintillation index. S_4 is defined as:

$$S_4 = \sqrt{\frac{\langle (A - A)^2 \rangle}{\langle A^2 \rangle}} \tag{10}$$

where, A is the amplitude of a received signal and $\langle\ \rangle$ denotes the mean. The S_4 index has a value of 0 to 1. An S_4 of above 0.3 is considered signal fading, while an S_4 of 0.6 is considered a strong scatterer, and an S_4 of 1 is Rayleigh saturated.

Recorded scintillation events have revealed that the ion plasma could be modeled as a turbulent medium with both inner and outer scales. The turbulence scale of the ionosphere is shown in Figure 6. Many of the measurements showed that a power law holds for ion plamsa irregularities in both a naturally and artificially disturbed ionosphere. These irregularities show transference of energy from an outer scale of tens of kilometers to a few meters. As a result, power law spectral densities (PSD) were developed. A general and useful PSD was developed by Shkarofsky. This PSD allowed for control over the inner and outer scales of ion plasma turbulence. Thus, with control over the inner and outer scales an ion plasma can be modeled for a given electron density [24, 9, 25, 26, 27].

Parabolic From.

The dependence $e^{-j\omega t}$ is assumed in the following. It is also important to define the electric field, $\vec{E}_y$, in the parabolic form as:

$$\vec{E}(x, z) = U(x, z)e^{-jkz}. \tag{11}$$

The parabolic form of ME is taken from the two dimensional scalar wave equation and defined as:

$$\frac{\partial^2 U}{\partial x^2} - 2jk\frac{\partial^2 U}{\partial z^2} + 2k^2 \Delta n U \tag{12}$$

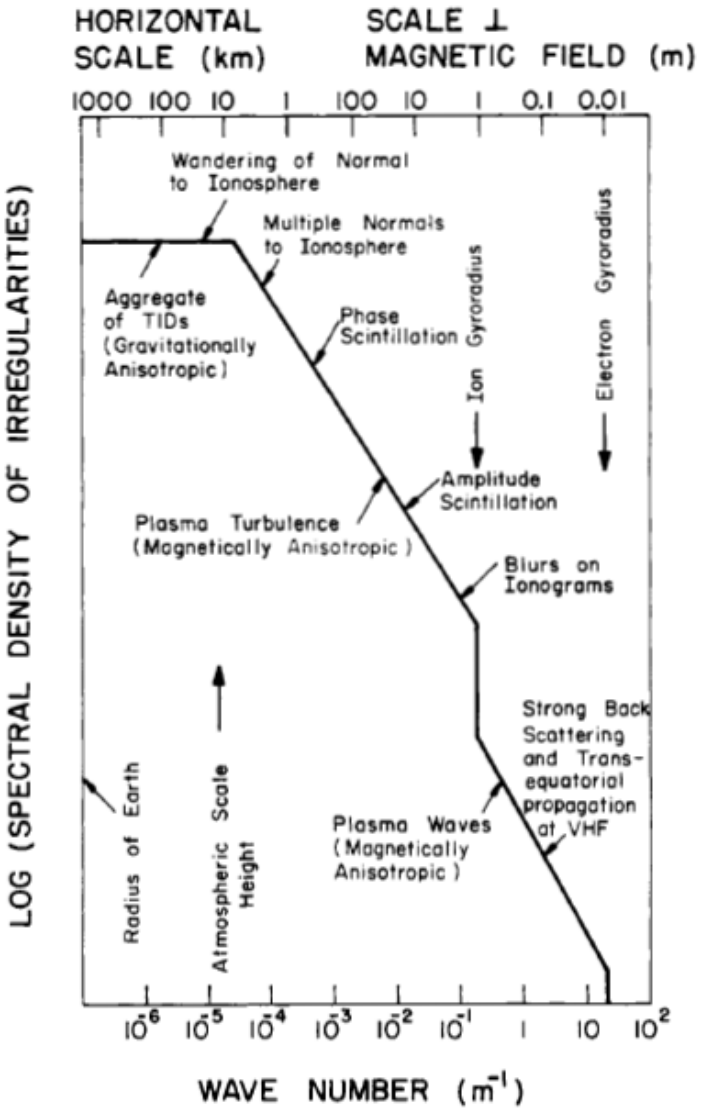

Figure 6. Turbulence scale of the ionosphere.

where k is the wavenumber and Δn is the index of refraction that varies with height x and range z. In the case for ionization irregularities, Δn for a ionospheric plasma is defined as:

$$2\Delta n = -\frac{\Delta N_e}{n_c} = -\frac{r_e \lambda^2}{\pi} \Delta N_e \tag{13}$$

where ΔN_e is the variation of electron density, r_e is the classical electron radius, and n_c is the critical electron density. Once the electron density is obtained, the parabolic equation can be solved using the split-step Fourier method (SSFM) and a series of phase screens [28, 9, 25, 29].

In order to solve the parabolic equation, SSFM will be used. The SSFM is comprised of two steps: a propagation step (14) and a phase change step (15) that are described as:

$$U\left(x, z_2, \omega\right) = \int_{-\infty}^{\infty} \tilde{U}\left(K, z_1, \omega\right) e^{jK^2 \frac{(z_2 - z_1)}{2k} + jKx} dK \tag{14}$$

$$U\left(x, \frac{\Delta z}{2}, \omega\right) = U\left(x, -\frac{\Delta z}{2}, \omega\right) e^{-jk \int_{-\Delta z/2}^{\Delta z/2} \Delta n(x, z', \omega) dz'}. \tag{15}$$

(14) is used to propagate the EM wave by taking the Fourier transform of spatial domain of the E-field and multiplying it with a spatial step in the spatial domain. K is the spatial component of the E-field much like ω is the frequency component of the E-field. k is the wavenumber of the E-field. The E-field is transformed between the spatial domain and frequency domain by using the transform pairs of

$$\tilde{U}\left(K, z, \omega\right) = \frac{1}{2\pi} \int_{-\infty}^{\infty} U\left(x, z, \omega\right) e^{-jKx} dx \tag{16}$$

$$U(x,z,\omega) = \int_{-\infty}^{\infty} \tilde{U}(K,z,\omega)\, e^{jKx} dK. \tag{17}$$

Once the E-field has been propagated to the location of the phase screen, (15) is used to determine the change in phase of the propagated EM wave. The integral in equation (15) is representative of a random process and can found by Monte Carlo sampling defined as

$$\tilde{\phi}(m\Delta K) = r_m [S(m\Delta K)\, L/2\pi]^{1/2}. \tag{18}$$

The PSD of an ionopsheric plasma is given by

$$\sigma_\phi^2 = 2r_e^2 \lambda^2 \Delta z \sigma_{N_e}^2 \tag{19}$$

$$S_{N_e}(K_x) = \frac{\sigma_\phi^2 \frac{1}{\sqrt{2\pi}} {l_i}^2 (l_i/L_0)^{\frac{m-1}{2}}}{H_{\frac{m-1}{2}}\left(\frac{l_i}{L_0}\right)} \frac{H_{\frac{m}{2}}\left(l_i\sqrt{K_x^2 + \frac{1}{L_0^2}}\right)}{\left(l_i\sqrt{K_x^2 + \frac{1}{L_0^2}}\right)^{\frac{m}{2}}}. \tag{20}$$

In (19), r_e is the classical electron radius and $\sigma_{N_e}^2$ is the electron variance of a given ionized plasma. For (20) l_i is the inner scale of the plasma turbulence, L_0 is the outer scale of the plasma turbulence, $H_{\frac{m}{2}}$ and $H_{\frac{m-1}{2}}$ are spherical bessel functions of the third kind, K_x is the spatial spectral component obtained from (16) and m corresponds to a K^{-3} power-law phase spectrum for electron density fluctuations taken from many measurements [26, 9].

In (18), $S(m\Delta K)$ are the discrete values of the PSD obtained from (19) and (20), L is the length of the phase screen in the x-direction, $\Delta K = 2\pi/L$, and $r_m = \sqrt{1/2}(g_{1m} + jg_{2m})$ with g_{1m} and g_{2m} as randomly generated numbers under a Gaussian distribution. These randomly generated numbers are the Fourier coefficients. Numerous generations must be made for each realization and averaged for each phase screen in order achieve a accurate statistical representation the medium

in which the wave is propagating.

This solution process allows for a fast and efficient way to solve ME. Normally, to solve MEs, a finite difference method (similar FDTD to that discussed above) is used, but because of the long propagation distance, such a method would be excessively time consuming and computationally expensive.

SSFM.

The SSFM allows for the solution of the propagating distance needed to solve EM in a timely fashion. Figure 7a depicts marching through the modeled domain for the SSFM process. A comparison of figures 7a and 7b shows the efficiency of the SSFM compared to a finite difference method. When comparing the figures it can be seen that in 7a, the Fourier transform allows solving in the direction of the electric-field (x-direction) and jumping ahead to the next propagation location, while 7b requires a the domain to be solved at all points in the domain.

2.4 Conclusion

In conclusion, this chapter has given a description of the ionosphere and explained what types of natural and artificial disturbances are possible to occur. Next, the effect a disturbed ionosphere can have on signal propagation was described. This chapter has also described current modeling techniques that have been used to model ionospheric propagation. A description of Maxwell's electromagnetic equations were given and the parabolic form used to approximate Maxwell's equations was described. Finally, the SSFM process and the theory of how it can be used to model transmission through an ion plasma was explained. This chapter also showed that the SSFM is the best way to model propagation through the ionosphere. The next chapter will present the methodology.

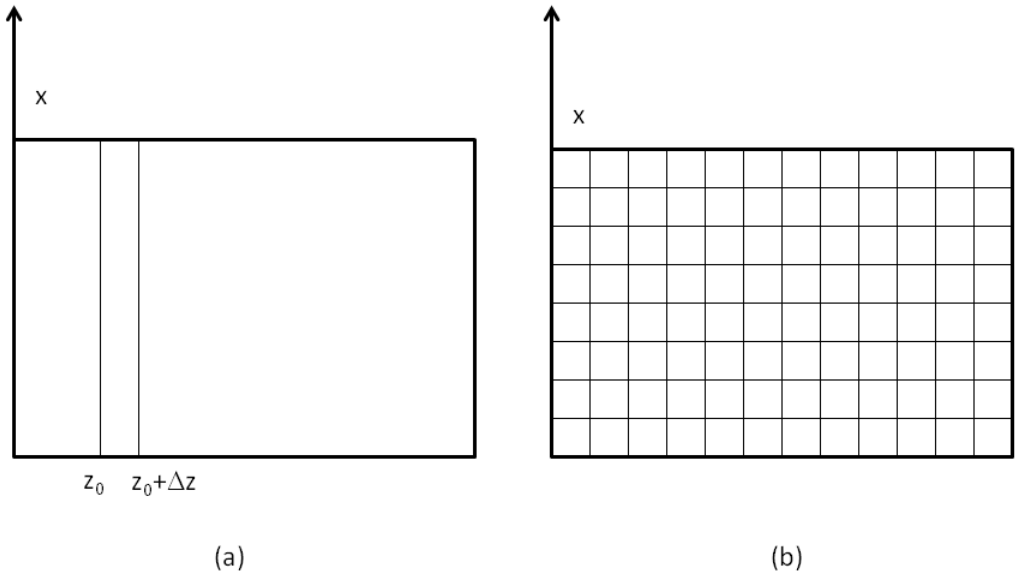

Figure 7. Diagram of the SSFM domain (a) and a diagram of a finite difference domain (b).

III. Chapter 3 Methodology

3.1 Introduction

The purpose of this chapter is to describe the methodology of modeling and simulating ionospheric scintillation on SATCOM. To investigate ionospheric scintillation effects, the split-step Fourier method, described in chapter two, was used to solve the parabolic form of Maxwell's equation. The results from solving the Maxwell's equations were then used to answer the following questions:

- What are the amplitude scintillation effects on SATCOM from a naturally disturbed ionosphere?
- What are the amplitude scintillation effects on SATCOM from an artificially disturbed ionosphere?
- What is the SATCOM outage percentage?

3.2 Theory

Scintillation Index.

The SSFM described in chapter 2 was utilized to determine the effects of the ionosphere in both a naturally and artificially disturbed state. Given a description of the electron content, the amount of amplitude scintillation can be determined by using the SSFM algorithm discussed in the previous chapter. The SSFM solves the parabolic form of Maxwell's equations. Once the input wave has been marched through the solution, the loss from amplitude scintillation can then be determined as well as the S_4 scintillation index. Certain conditions were required to ensure that the results of the simulation were numerically accurate.

SSFM Conditions.

The first condition to guarantee that the SSFM algorithm provides numerically correct results is to ensure that Nyquist sampling of the propagated wave is sufficient. This condition is met by ensuring that

$$\frac{\pi^2 N^2 \Delta z}{kL^2} < \pi \tag{21}$$

where, N is the number of grid points in the x-direction and L is the length of the grid in the x-direction [28]. In this research the maximum Δz value was 3.0×10^7 km, based off of a minimum frequency of 40 GHz, 2^{16} grid points (N), and a grid length of 50 km (L). Since the transmitter and receiver are separated by 4,800 km in distance, the Nyquist sampling conditions are be met.

Another important criterion is to ensure that the phase representation is correct. For a phase representation the length of the grid in the x-direction, L, is at a minimum five to ten times as large as the outer scale (L_0) of the medium [28] or

$$L > 5L_0. \tag{22}$$

Since L_0 was set to 10 km, L was set to 50 km. Next, the space between the grid points (Δx) in the x-direction is at least three times smaller than the inner scale (l_i) of the medium [28] or

$$\Delta x \leq \frac{l_i}{3}. \tag{23}$$

In this research Δx was set to 3.3 m, based off of an inner scale of 10 m. In order to satisfy Nyquist sampling of the phase, the change in phase from grid point to grid

point in the x-direction is less than π. This is verified by

$$\phi(x_{n+1}) - \phi(x_n) < \pi. \tag{24}$$

In this research equation (24) had values between 4.77×10^4 and -5.25×10^4, thus meeting the condition for Nyquist sampling of the phase.

Finally, in order to control edge effects (aliasing) that are inherent for taking Fourier transforms, the distance in the x-direction (L) is greater than the scattering angle distance. This can be controlled by ensuring that

$$L > \frac{\sigma_\phi \lambda z}{\sqrt{2}\pi L_0} \tag{25}$$

where, σ_ϕ is found from (19) and λ is the propagating signal wavelength [28]. Assuming $z = 4800$ km (the total propagation distance) and $\sigma_\phi = 10$ (which would be strong scatterer), equation (25) gives a value of 8.03 km, which is less than $L = 50$ km.

SSFM Verification.

The model was verified by comparing the solution of the model to the solution a of simple example. To verify the calculations of the PSD portion of the SSFM algorithm, a basic Gaussian (PSD) was used. The Gaussian PSD used was

$$S_\phi(K) = \frac{1}{2}\pi^{-\frac{1}{2}} L_0 \sigma_\phi^2 e^{-K^2 L_0^2/4} \tag{26}$$

where, K is the spectral wavenumber, L_0 is the outer-scale, and $\sigma_p hi^2$ is the phase variance [28].

Another check used to determine the accuracy of the propagation step of the

SSFM algorithm was propagation through a Gaussian lens. The Gaussian phase lens was defined as

$$\phi(x) = -\phi_0 e^{\frac{-x^2}{r_0^2}} \tag{27}$$

where, ϕ_0 is the phase, and $r_0 = \lambda$. The negative phase allows the lens to act as a focusing or convergent lens. If the phase was positive the lens would then be considered divergent. The focal length is defined as

$$F = \frac{kr_0^2}{2\phi_0} \tag{28}$$

where, k is the wavenumber. Verification was completed by computing the output of a single Gaussian phase lens and comparing it to analytical solution of the Fresnel-Kirchoff Integral. The Fresnel-Kirchoff Integral is defined as

$$E(x, z_2) = \Big[-\frac{j2\pi(z_2 - z_1)}{k} \Big]^{-\frac{1}{2}} \int_{-\infty}^{\infty} e^{jk(z_2 - z_1)} e^{-\frac{jk(x-\zeta)^2}{2}(z_2 - z_1)} E(\zeta, z_1) d\zeta. \tag{29}$$

Solving the Fresnel-Kirchoff Integral for the Gaussian lens was accomplished numerically by

$$E(x, z) = \frac{e^{(jkz + \frac{jkx^2}{2z})}}{\sqrt{jkz}} \sum_{n=0}^{\infty} \frac{(j\phi_0)^n}{n!} \left(\frac{2n}{k^2 r_0^2} - \frac{j}{kz} \right)^{-\frac{1}{2}} e^{\left(\frac{\frac{-x^2}{2z^2}}{\frac{2n}{k^2 r_0^2} - \frac{j}{kz}} \right)} \tag{30}$$

where, ϕ_0 is the phase, $r_0 = \lambda$, k is the wavenumber of the propagating wave, and $E(x, z)$ is the electric field of the propagating wave [28].

Central Limit Theorem.

In order to ensure that the numerical results of the SSFM model accurately portray a given scenario, the simulations were executed 100 times and averaged to adhere to

the Central Limit Theorem (CLT). The CLT states "the distribution of the sum (or average) of a large number of independent, identically distributed variables will be approximately normal, regardless of the underlying distribution" [30]. The results can be verified by the following:

$$Y = \frac{\sum_{i=1}^{n}(y_i) - \sum_{i=1}^{n}(\mu_i)}{\sqrt{\sum_{i=1}^{n}(\sigma_i^2)}} \tag{31}$$

where, Y is the norm of independent random variables $Y_1, Y_2, ..., Y_n$ and each Y_i has a probability distribution $P(y_1, y_2, ..., y_n)$, μ_i is the mean of Y_i and σ_i^2 is the variance of Y_i. The results of 100 executions of the SSFM simulations had a normal distribution. Therefore, a limitation of 100 simulations is sufficient in order to derive statistically accurate and correct conclusions from the scenario.

3.3 Materials and Equipment

Several types of software and computational sources have been used in the completion of this thesis. The primary software that was used in order to execute the code SSFM algorithm was MATLAB developed by MathWorks. MATLAB stands for Matrix Laboratory and is a high-level computer language used for numerical computation and visualization of results [31].

Another application that was used is NeQuick2. NeQuick2 was developed by the T/ICT4D Laboratory of the Abdus Salam International Centre for Theoretical Physics (ICTP). NeQuick2 is available as a web based tool or a FORTRAN code. NeQuick2 is a model that provides electron densities for propagation through the ionosphere. NeQuick2 uses five semi-Epstein layers to create the profile for the F2 layer, and depends upon the number of sunspots. It provides the electron densities based on geocentric coordinates (latitude and longitude) and altitude. This applica-

tion can also provide an electron density for a given ray-path for a ground to satellite system. This software was used to retrieve electron densities for the natural ionosphere [32].

GSCENARIO, developed by Defense Threat Reduction Agency (DTRA), models a high altitude nuclear explosions' (HANE) effects on the ionosphere. The software simulates different burst yields (1 kiloton - 10 megaton) at various altitudes (120 km - 1000 km) and at any location around the Earth. GSCENARIO adheres to DTRA's "first principle codes." This means that GSCENARIO can be used to validate other simulation codes. The software produces the post-HANE environment with chemically reactive magnetohydrodynamics (MHD) of interacting neutral ions and electron fluids. For data from the atmosphere, GSCENARIO uses AFRL SAG (Sharc/Samm Atmospheric Generator). For input data from the ionosphere, GSCENARIO uses IRI95 (International Reference Ionosphere, 1995 version). GSCENARIO was used to provide electron data for the ionosphere in a nuclear disturbed environment [33, 34].

The computing resources was were HP Z820 Workstations from LORElab laboratory. The HP Z820 Workstations from LORElab are powered by two Intel Xeon 64-bit CPUs clocked at 3.10 GHz each. The Intel Xeon CPUs have eight cores each with sixteen threads per core. The Z820 Workstations also have 128 gigabytes of RAM.

3.4 Processes and Procedures

Signal Absorption.

The electron content of the natural ionosphere is not sufficient (typical values range from $\approx 40 - 250$ TECU (total electron content unit 1 TECU= $10^{16} \frac{el^-}{m^2}$)) to absorb an electromagnetic waves considered in this thesis. Therefore, absorption from the natural ionosphere was not considered in this research.

The electron content in the ionosphere resulting from a HANE is significant enough to consider signal absorption loss. The GSCENARIO software suite was used to calculate the absorption due to the increase of electrons and ions in the ionosphere.

Amplitude Scintillation Calculations.

This thesis answers the question from section 3.1 by utilizing the SSFM to solve the parabolic equation. Figure 8 shows the general process that was followed.

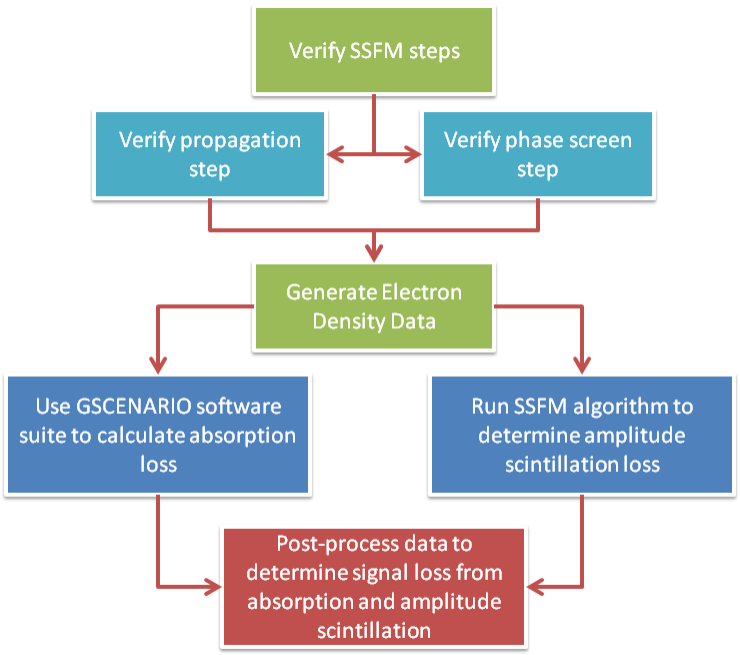

Figure 8. General description of the methodological process of this thesis.

To begin the process of calculating amplitude scintillation effects on a transmitted signal, electron density data was generated for a given scenario. To determine the ionospheric scintillation effects of the natural ionosphere, NeQuick2 was used to generate electron concentrations. Since the ionosphere electron content is dependent on the number of sun spots, the time of day, and season of the year, NeQuick2 was used to determine the electron content when the number of sunspots was particularly

high.

In order to shown scintillation effects from the natural ionosphere on a 40 - 110 GHz EM wave, a scenario was selected from record history that exhibited a strong geomagnetic inference. The scenario selected was March 13, 1989. During March 13, 1989 a geomagnetic storm left most of North American in blackout conditions, because a massive plume of solar plasma reached the Earth. This potential black swan scenario shows amplitude scintillation effect the 40 - 110 GHz frequency band during a severe geomagnetic storm [35].

To determine the amplitude scintillation effects of the ionosphere disturbed artificially by a HANE, GSCENARIO was use to generate the electron densities of the ionosphere. The HANE yields that were selected were 100 kt, 500 kt, 1 Mt, 2 Mt, and 5 Mt. The detonation location was over Dayton, OH, USA, and the altitudes were at 150 km and 200 km. The date of the HANEs was September 23, 2016 for all detonations. The default detonation time of day of 0000 hrs was used. The over all time for the simulation was ten hours.

After the electron content data was generated the from either GSCENARIO or NeQuick2, the SSFM algorithm was used to determine amplitude scintillation effects on the input signal.

The simulation was executed for various frequencies (40 - 110 GHz), and was executed 100 times to adhere to the CLT. Also, the amount of loss (dB) for each channel was determined.

3.5 Conclusion

In conclusion, the questions listed in 3.1 were answered through the methodology outlined in this chapter. Electron densities were generated from one of two verified and validated sources (NeQuick2 or GSCENARIO). The SSFM was used to solve the

parabolic form of Maxwells equations in order to determine amplitude scintillation effects on a SATCOM channel. The SSFM code adhered to the conditions needed for accurate results as stated in this chapter. The SSFM code also was verified using the simple examples outlined in this chapter. This methodology ensured that the data presented in the next chapter was numerically accurate.

IV. Data Analysis

4.1 Introduction

This chapter presents the data from a given scenario and the results of the SSFM algorithm First, the results from NeQuick2 simulations and GSCENARIO will be explained. Furthermore, analysis of the output verifying the accuracy of the SSFM algorithm will be shown. In addition, validation of the phase screen from a PSD, and then the results showing how the CLT was followed will be explained. Finally, the results from propagation loss from a natural ionosphere and a HANE scenario using the SSFM algorithm will be depicted and analyzed

4.2 Natural Ionosphere Data

This section presents the electron density data generated from NeQuick2. Figures 9 and 10 show the electron density of the ionosphere for March 13, 1989. Figure 9 shows that the electron density of the ionsphere peaks at an altitude between $\approx$ 300 km - 450 km from 1100 - 1600 hrs Zulu time. Figure 10 shows that the peak density in the F-layer of the ionosphere occurs at 1300 hrs Zulu and is $\approx 18 \times 10^6 \frac{el^-}{cm^3}$.

4.3 Nuclear Simulation Data

This section will present the electron density data generated from the GSCENARIO software suite. Figures 11 - 30 show various HANE's from 100 kt to 5 Mt and compare HANE's located at altitudes of 150 km to 200 km. The time frame for all figures is directly after the HANE to 6 min after the HANE. These figures show that soon after the HANE, the electrons rise along the magnetic fields lines and move down towards the earth's surface.

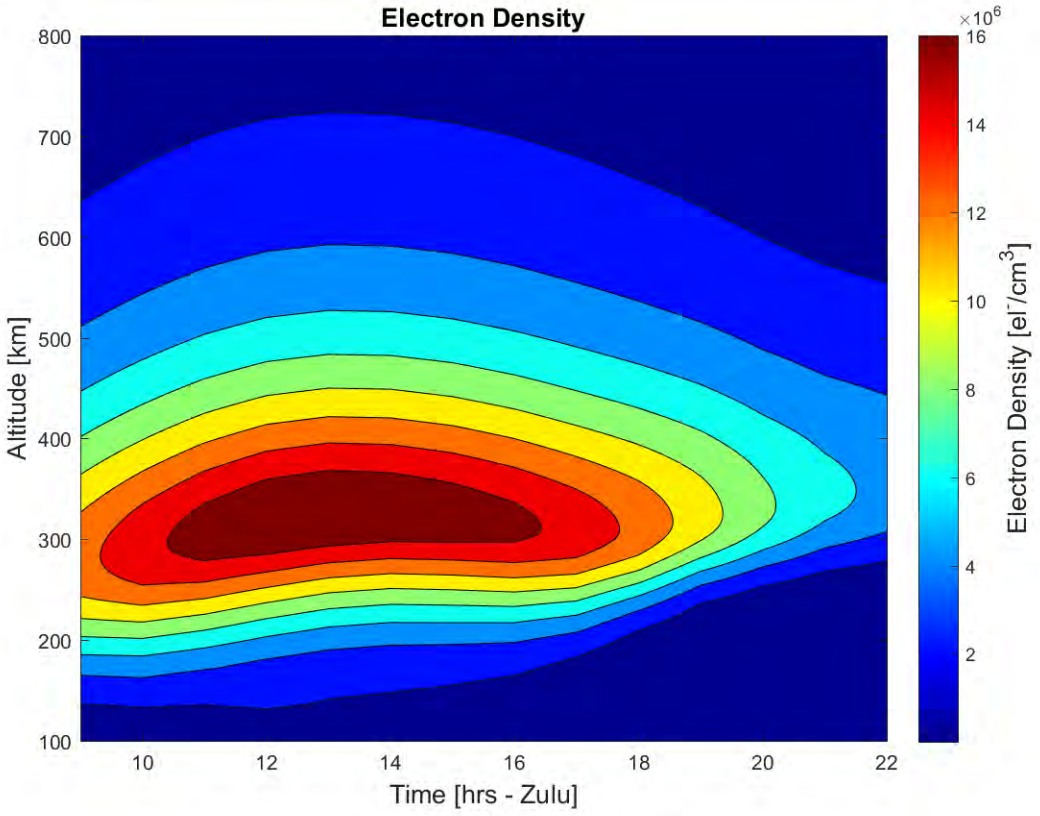

Figure 9. Electron density of ionosphere over 14 hours on March 13, 1989.

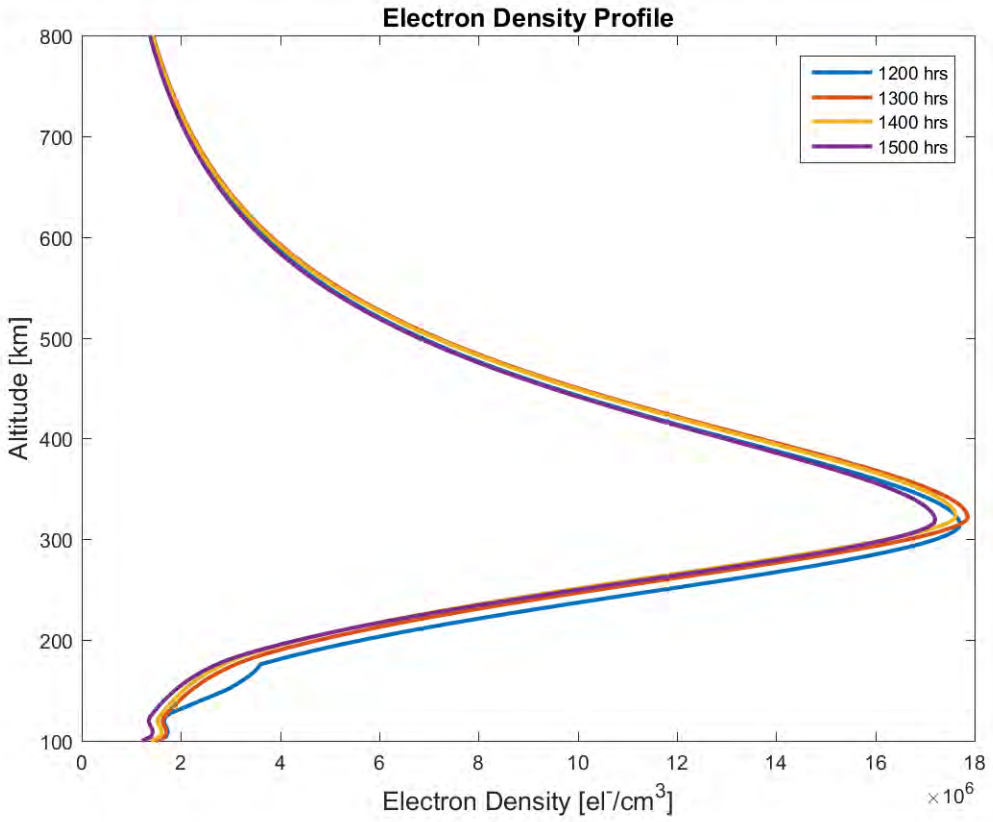

Figure 10. Electron density profile of ionosphere for selected hours on March 13, 1989.

100 kt HANE.

Figures 11 - 14 show the electron density movement for a 100 kt HANE at 200 km and 150 km. For explosions at altitudes of 200 and 150 km the ion debris and electrons from the explosion travel downwards from the explosion point until they are stopped by the Earth's atmosphere ($\approx$ 100 km). For an explosion at 200 km, the Earth's geomagnetic field lines have a greater effect on the electrons produced by the HANE, hence the electrons begin to travel upwards sooner than a 100 kt HANE located at 150 km.

For the HANE located at 150 km, most of the explosion debris travels downward, preventing the electron debris from dispersing along the Earth's geomagnetic lines until 10 sec after detonation. Figure 14 shows at a burst point altitude of 150 km, the maximum electron density remains $\leq 10^9 \frac{el^-}{cm^3}$ until just after 3 min. For a burst height of 200 km the electron densities drop to $10^8 \frac{el^-}{cm^3}$ shortly after 1 min then and reduces to $\leq 10^7 \frac{el^-}{cm^3}$. At 6 min after the HANE, the electron densities for a 200 km burst height reach a height of $\approx$3000 km. For a burst height of 150 km the electron densities reach a height of $\approx$2500 km. Thus, a 50 km explosion height difference results in a 500 km altitude difference after 6 min. This difference is a result of the majority of the electrons and ion debris traveling down towards the Earth for a 150 km HANE and the Earth's geomagnetic lines having a greater effect on the 200 km HANE because the atmosphere is less dense at 200 km than at 150 km.

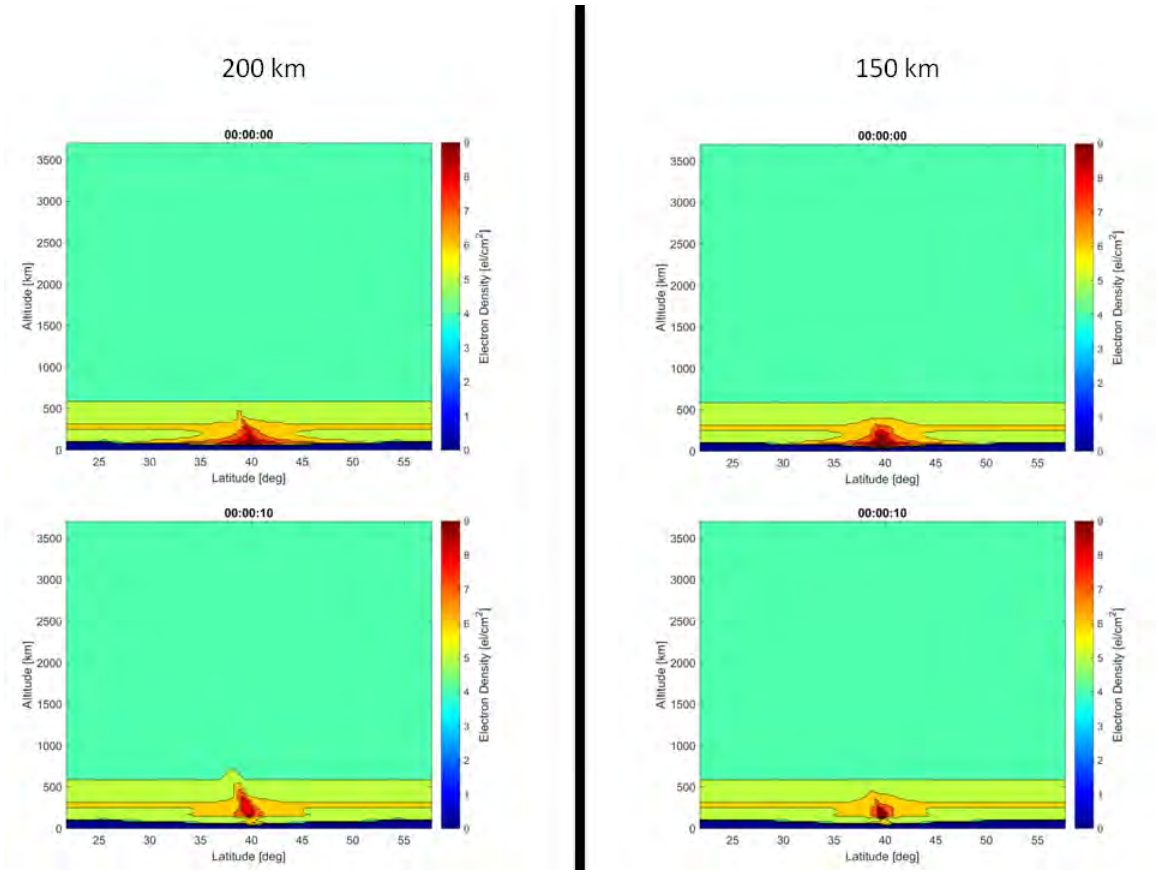

Figure 11. Comparison of electron densities produced by a 100 kt yield HANE at 200 km and 150 km, 00:00:00 - 00:00:10.

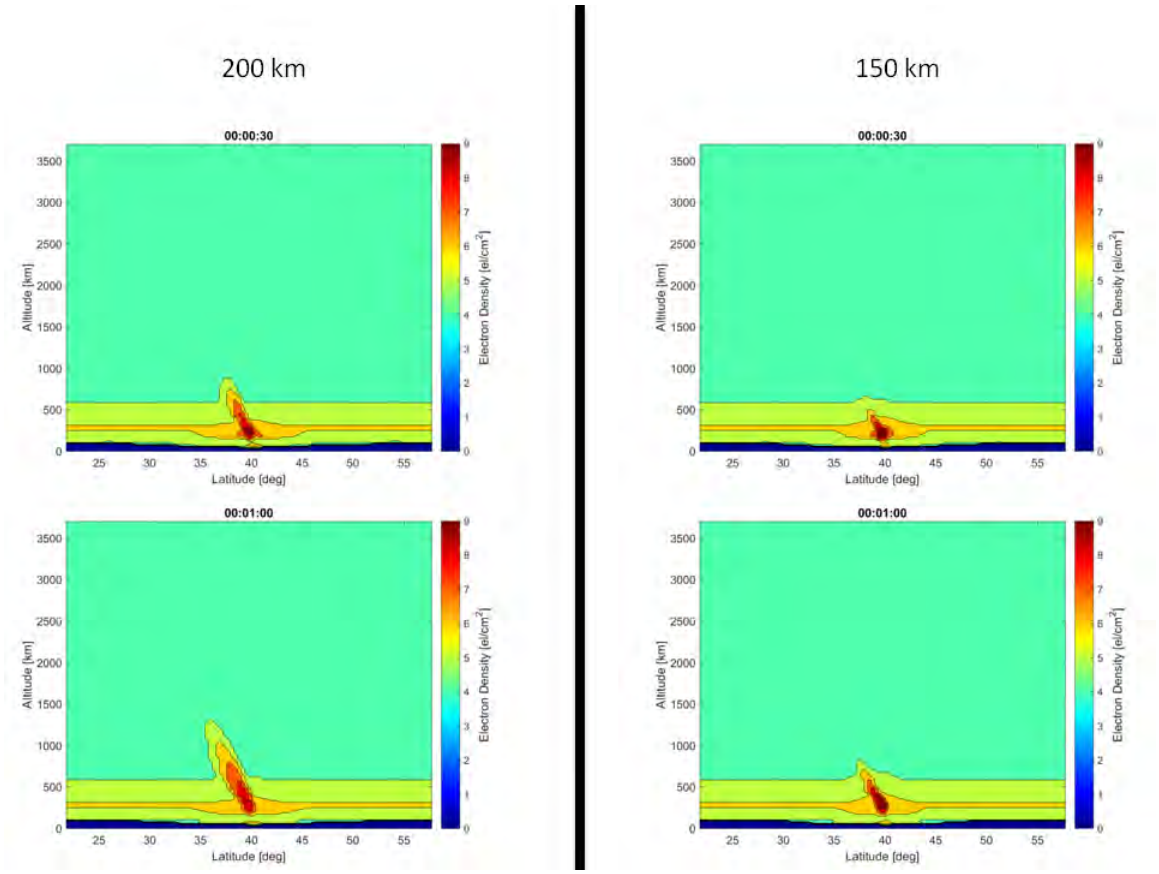

Figure 12. Comparison of electron densities produced by a 100 kt yield HANE at 200 km and 150 km, 00:00:30 - 00:01:00.

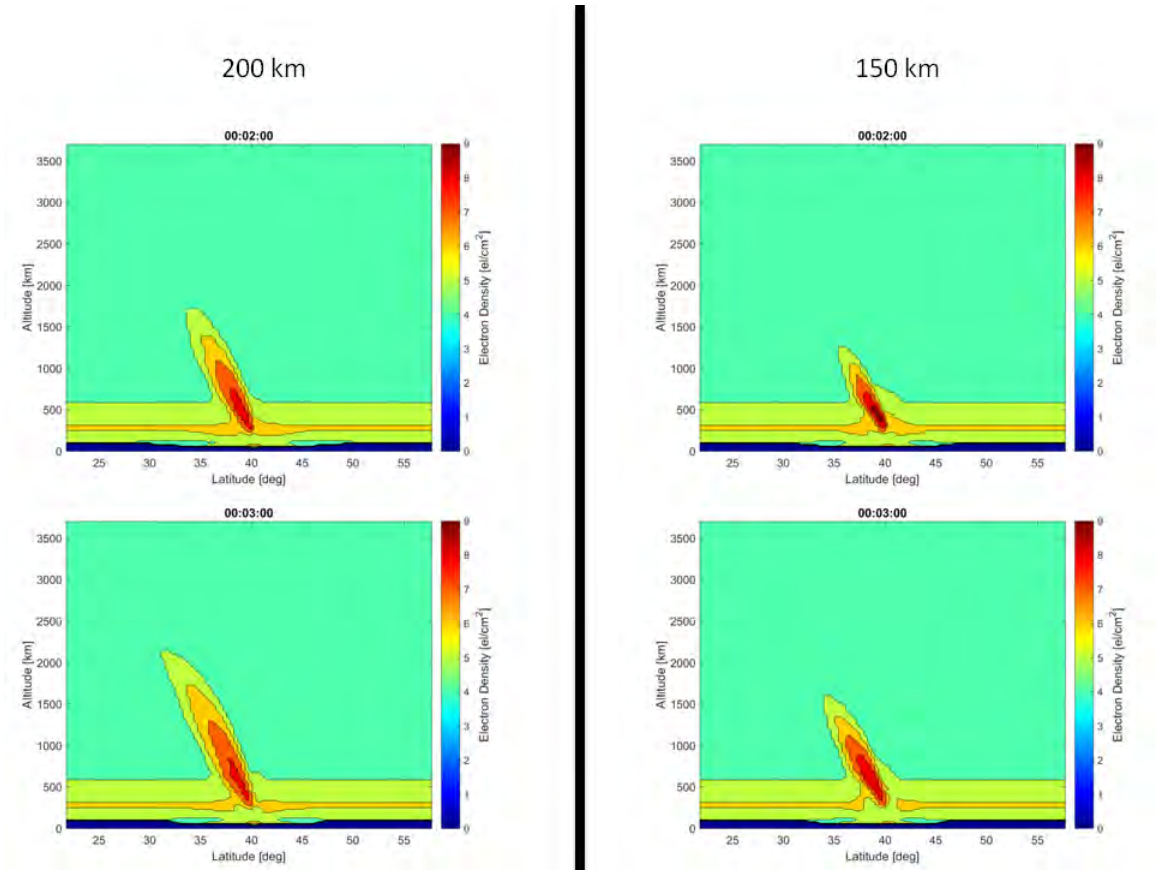

Figure 13. Comparison of electron densities produced by a 100 kt yield HANE at 200 km and 150 km, 00:02:00 - 00:03:00.

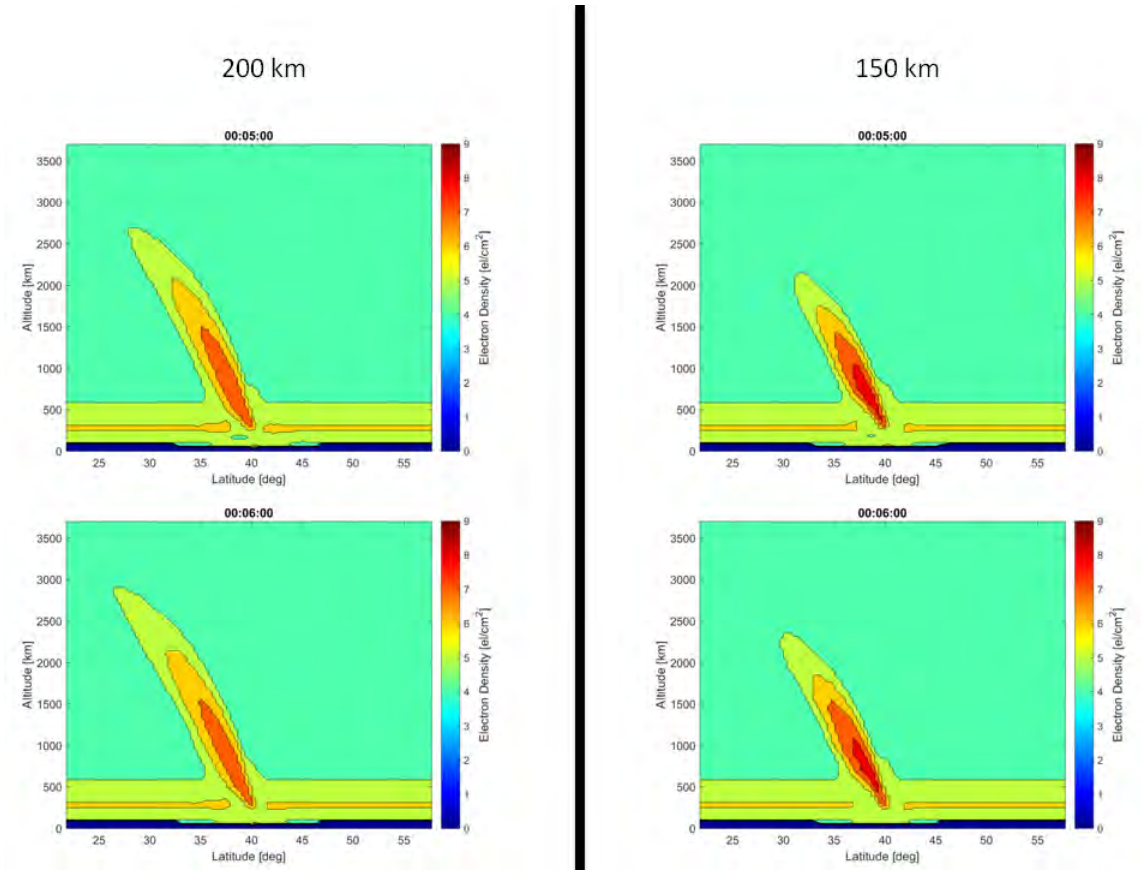

Figure 14. Comparison of electron densities produced by a 100 kt yield HANE at 200 km and 150 km, 00:05:00 - 00:06:00.

500 kt HANE.

Figures 15 and 18 show the electron density movement for a 500 kiloton HANE at 200 km and 150 km. For the 500 kiloton at 200 km HANE, the electrons travel down towards the Earth and upwards along the Earth's geomagnetic lines. The Earth's geomagnetic lines do not affect the 500 kiloton HANE at 150 km until after the majority of electrons travel downwards toward the Earth and begin to rise after the electrons and ion debris are stopped by the Earth's atmosphere (at $\approx$ 100 km).

The main difference between a HANE at 200 km and one at 150 km is the time it takes the electrons to spread themselves out along the Earth's magnetic field lines. The movement of the electrons from the 500 kiloton HANE located at 200 km is dominated by the Earth's magnetic field lines earlier due to less air pressure (directly after detonation as opposed to 30 sec after detonation) than the 500 kiloton HANE located at 150 km (where the air pressure is greater, therefore limiting electron movement). As a result the electrons densities for the 500 kiloton HANE at 150 km remain $\approx 10^9 \frac{el^-}{cm^3}$ until 5 min after detonation. On the other hand, electron densities decrease to $\approx 10^8 \frac{el^-}{cm^3}$ for a 500 kiloton HANE at 200 km, 3 min after detonation. Figure **??** shows that the electrons from a 500 kt HANE located at 200 km reach an altitude $>$ 4000 km 6 min after the HANE and the electrons from a 500 kt HANE located at 150 km reaches a height $\approx$ 4000 km after 6 min after the HANE.

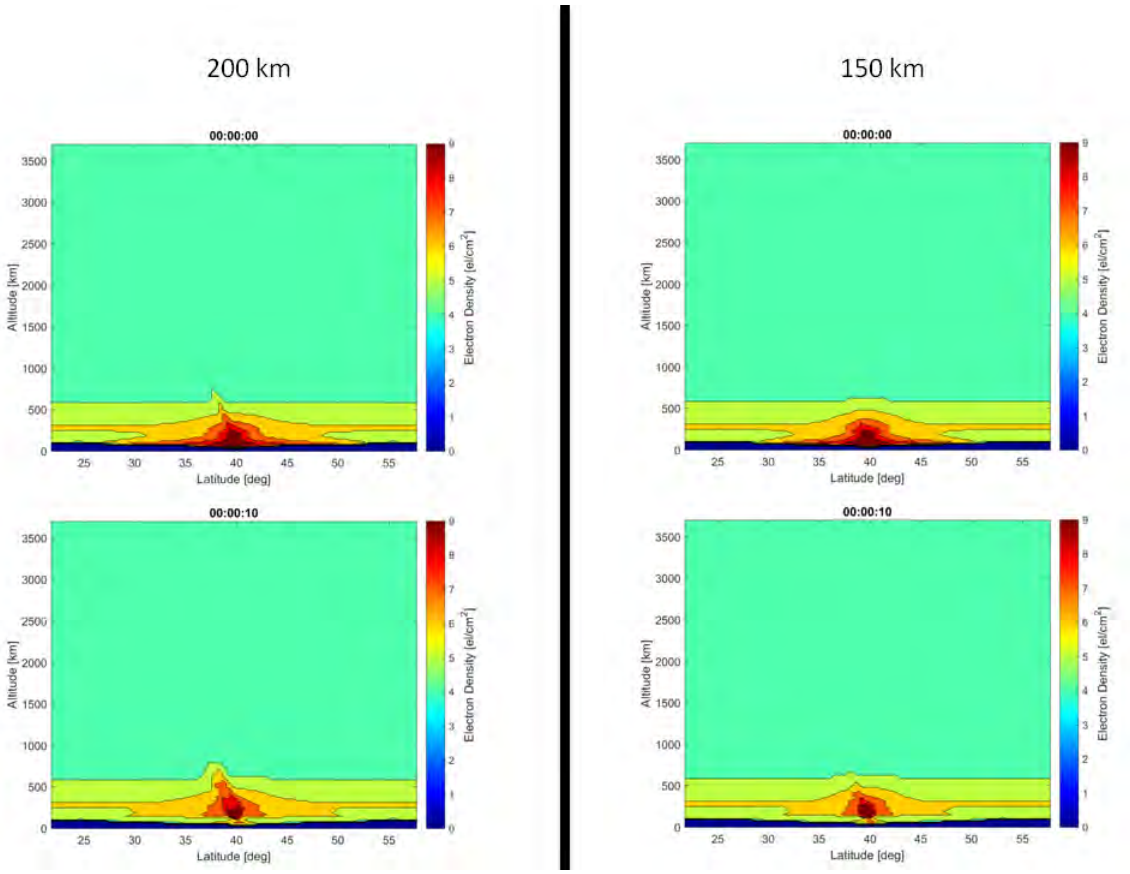

Figure 15. Comparison of electron densities produced by a 500 kt yield HANE at 200 km and 150 km, 00:00:00 - 00:00:10.

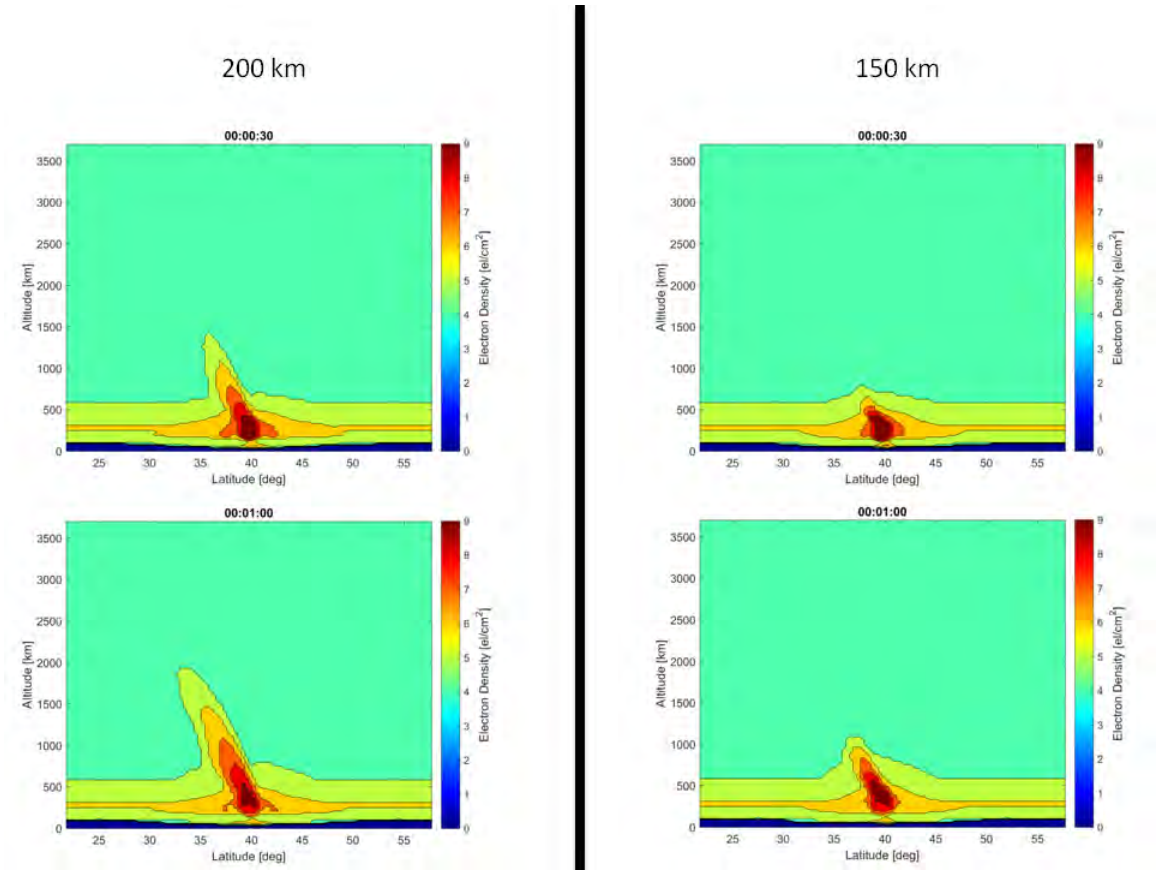

Figure 16. Comparison of electron densities produced by a 500 kt yield HANE at 200 km and 150 km, 00:00:30 - 00:01:00.

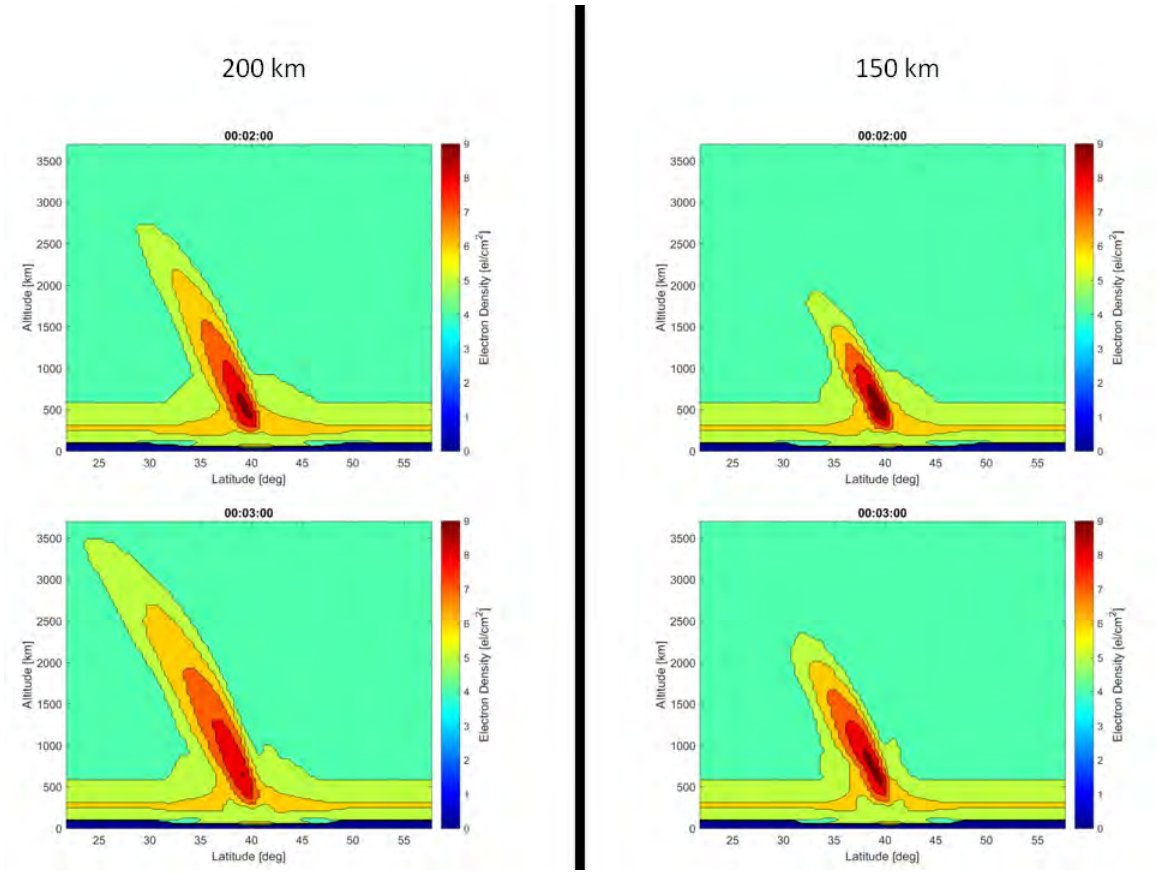

Figure 17. Comparison of electron densities produced by a 500 kt yield HANE at 200 km and 150 km, 00:02:00 - 00:03:00.

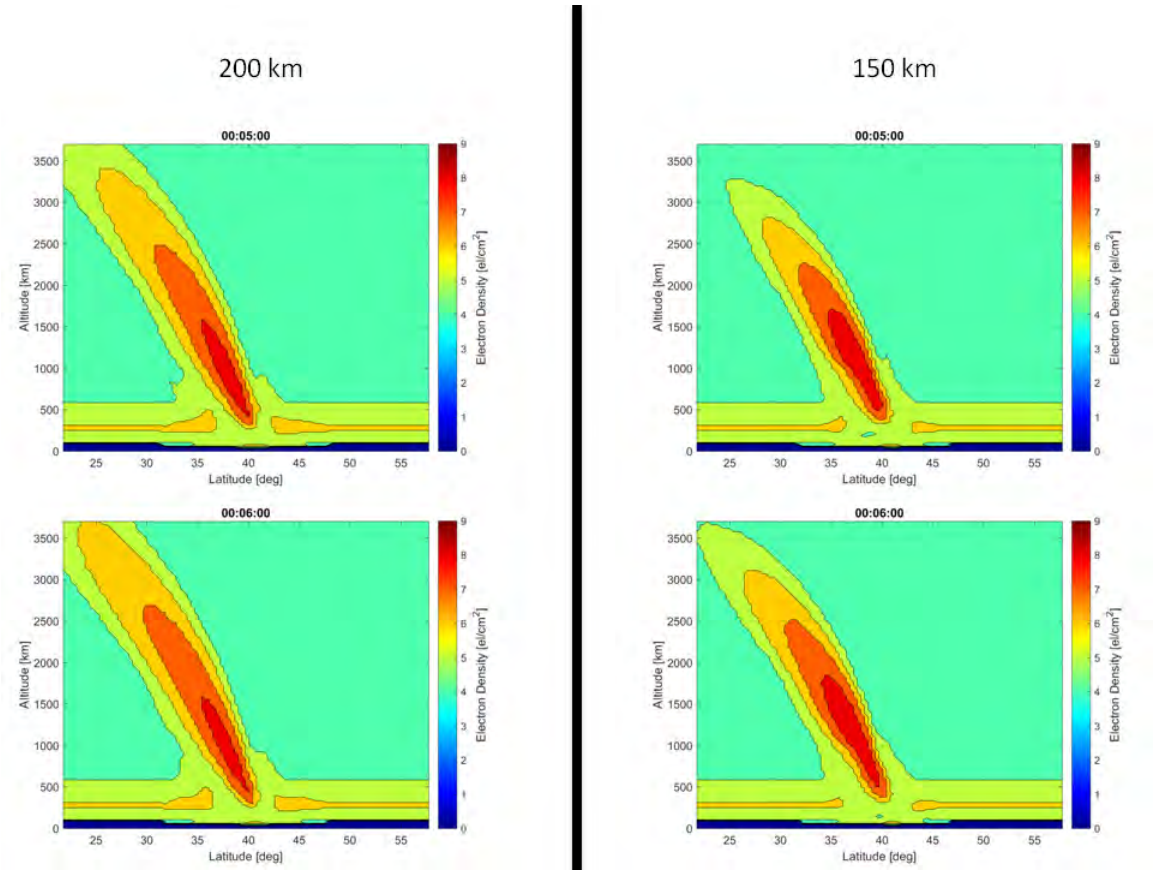

Figure 18. Comparison of electron densities produced by a 500 kt yield HANE at 200 km and 150 km, 00:05:00 - 00:06:00.

1 Mt HANE.

Figures 19 - 22 show the electron density for 1 Mt HANE at 200 km and 150 km. Directly after the 1 Mt HANE at 200 km, the electrons and ion debris travel downward toward the Earth and upward along the Earth's geomagnetic lines. For the 200 km HANE, the Earth's geomagnetic lines have greater effect on the initial electron movement, due to less air pressure, than the 150 km located HANE. The majority of the electron and ion debris from the 1 Mt HANE located at 150 km travel downwards. The Earth's geomagnetic lines have little effect on the the electron movement until 10 sec after the explosion, when the electrons begin to rise after being stopped in their downward travel from the Earth's atmosphere. The electron densities are higher for a longer period of time for the 150 km 1 Mt HANE since the movement of the electron debris is not affected by the Earth's geomagnetic lines until after it begins to rise after it is stopped by the Earth's atmosphere.

2 Mt HANE.

The results from the 2 Mt HANE simulation at 200 km and 150 km can be seen in figures 23 - 26. The Earth's geomagnetic lines have a greater effect initially on the 200 km 2 Mt HANE than the 150 km 2 Mt HANE. As can be seen in figure 23, directly after the 2 Mt HANE, the electrons travel downward toward the Earth for both the 200 km and 150 km HANE, but the 200 km also has electrons traveling upward, away from the Earth, along the Earth's geomagnetic lines. At 10 sec the Earth's geomagnetic lines clearly have a greater effect on the electron debris of the 200 km 2 Mt HANE than the 150 km 2 Mt HANE. The difference of 50 km allows the electrons from the 200 km 2 Mt HANE to spread out sooner than the 150 km HANE. As a result, after 6 min, the electron density levels are much lower for the 200 km HANE than the 150 km HANE.

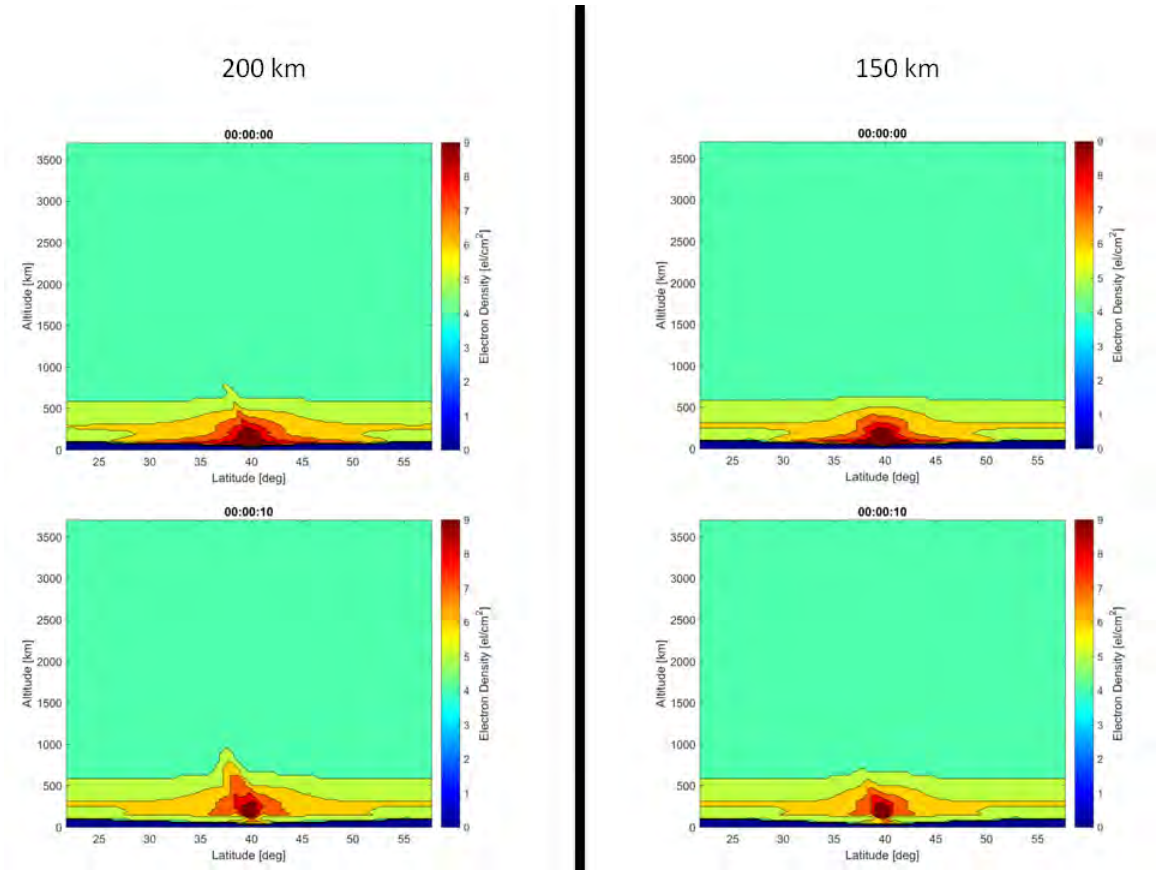

Figure 19. Comparison of electron densities produced by a 1 Mt yield HANE at 200 km and 150 km, 00:00:00 - 00:00:10.

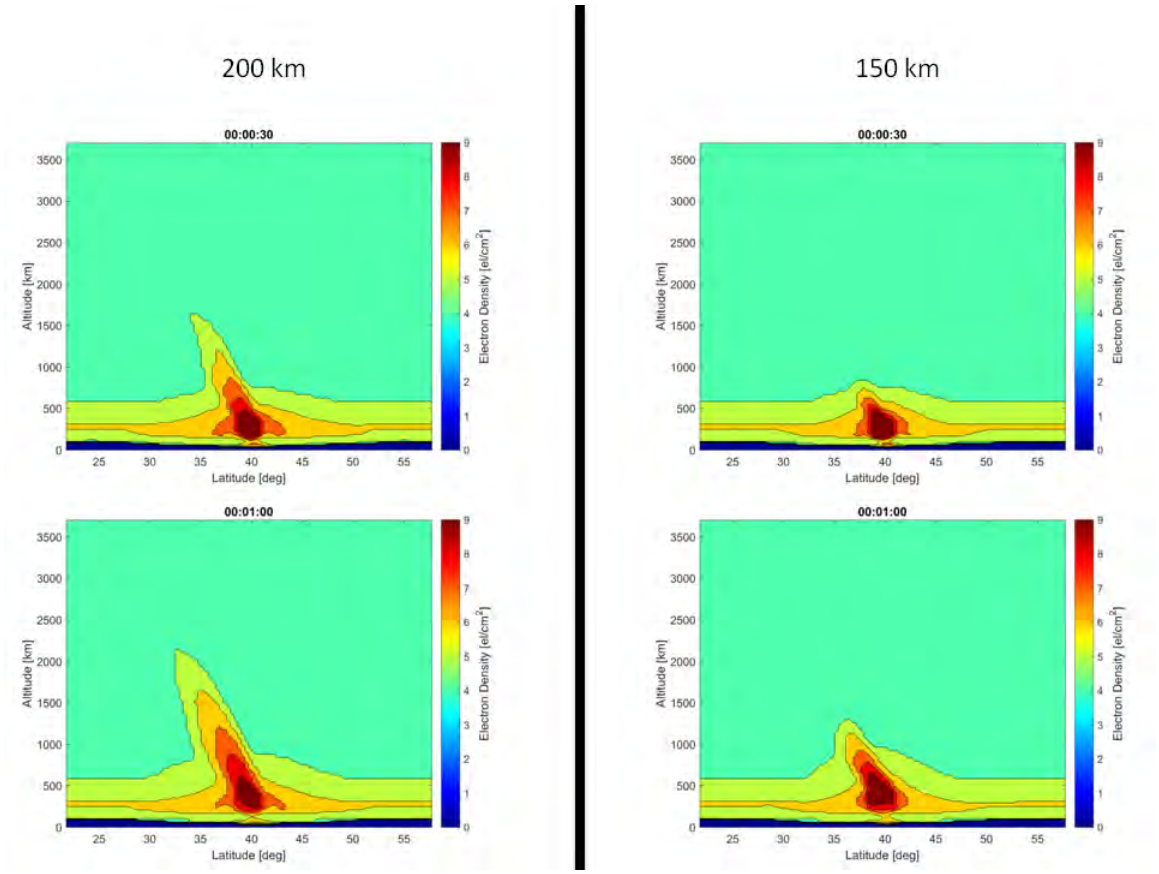

Figure 20. Comparison of electron densities produced by a 1 Mt yield HANE at 200 km and 150 km, 00:00:30 - 00:01:00.

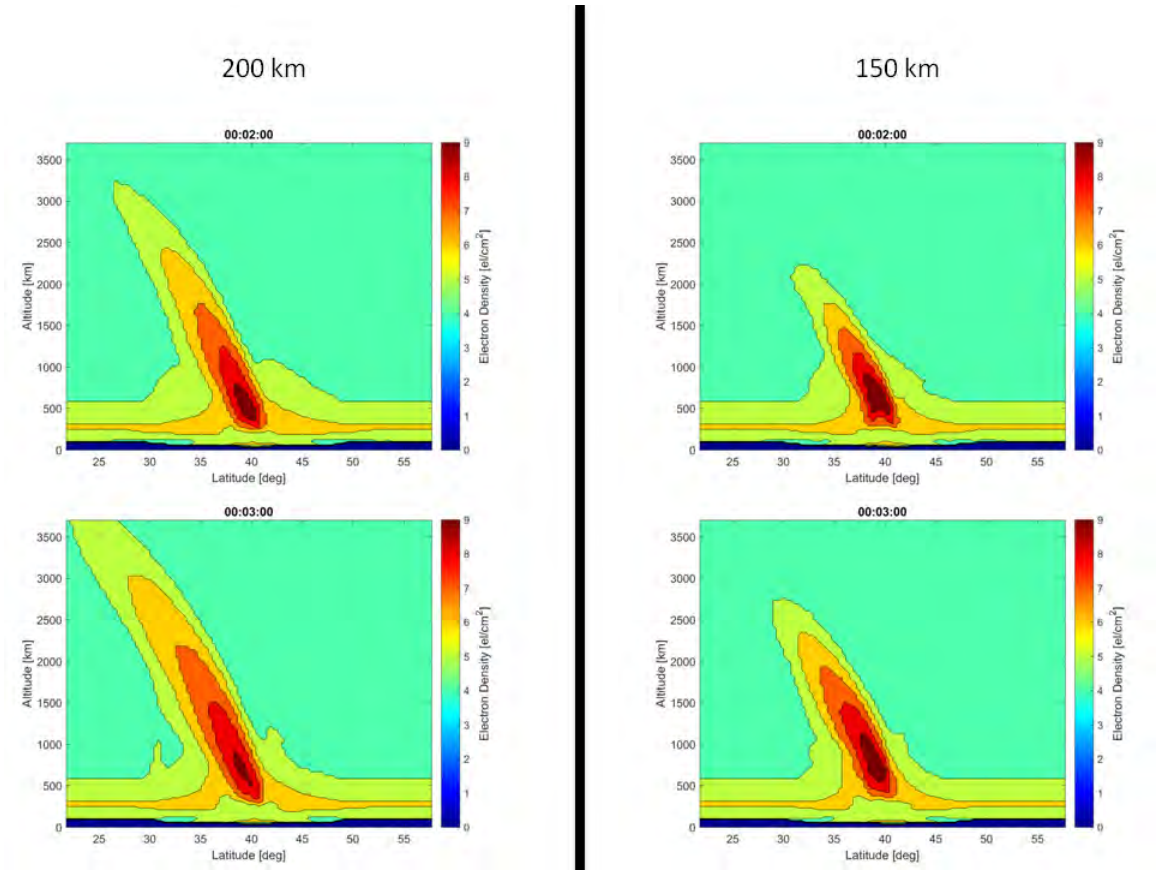

Figure 21. Comparison of electron densities produced by a 1 Mt yield HANE at 200 km and 150 km, 00:02:00 - 00:03:00.

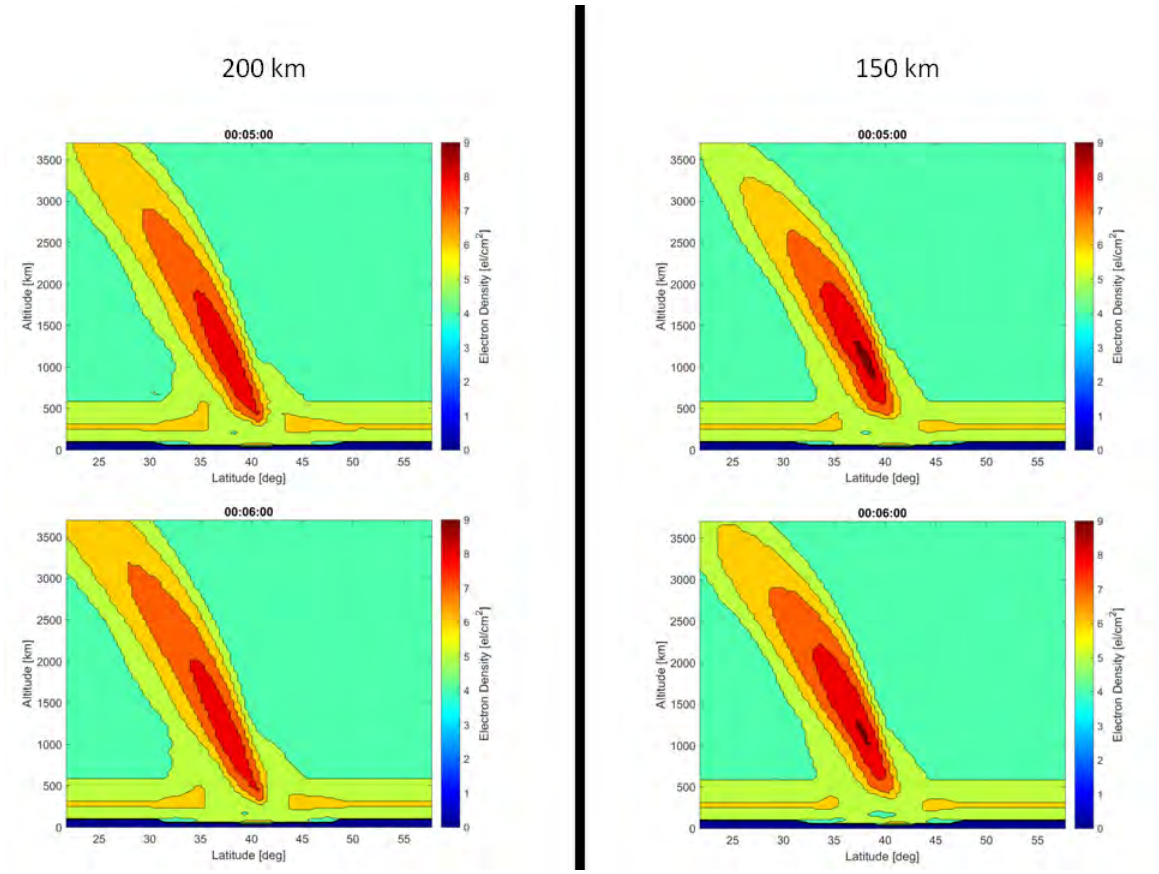

Figure 22. Comparison of electron densities produced by a 1 Mt yield HANE at 200 km and 150 km, 00:05:00 - 00:06:00.

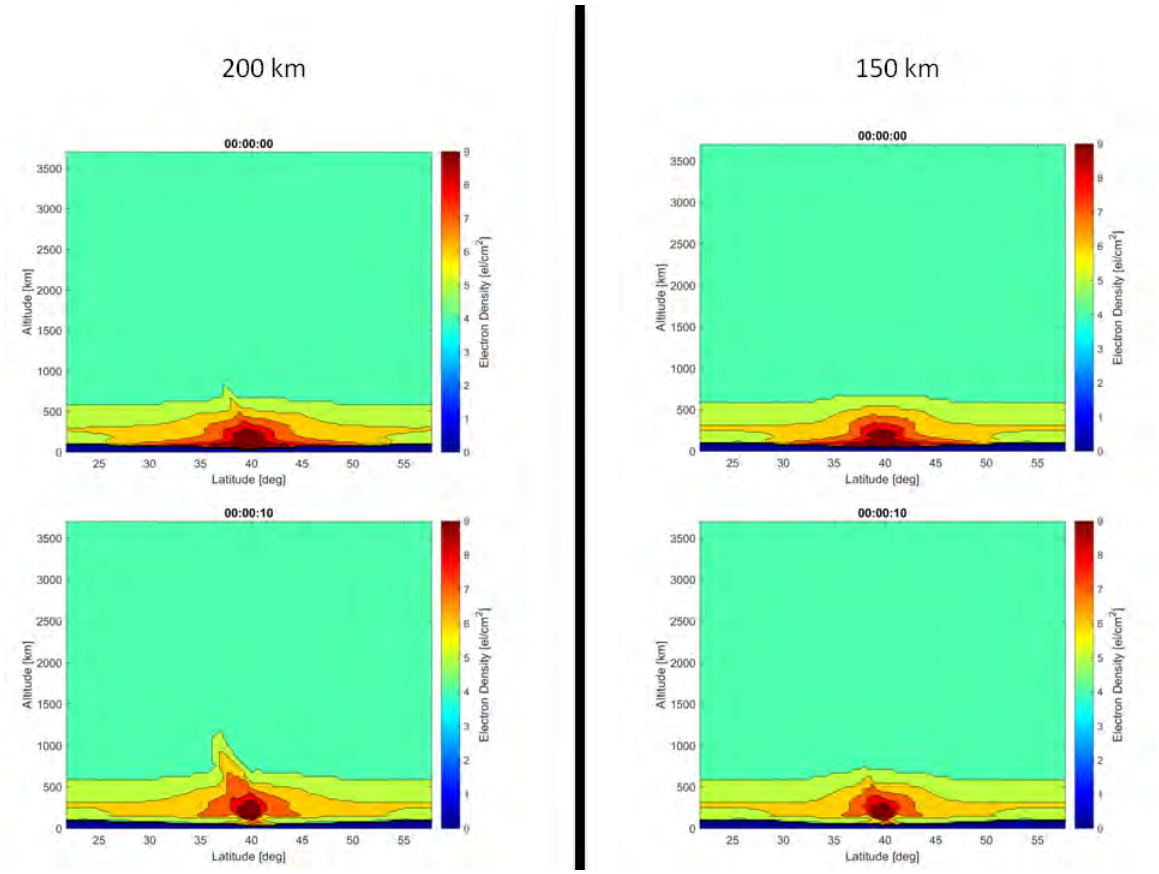

Figure 23. Comparison of electron densities produced by a 2 Mt yield HANE at 200 km and 150 km, 00:00:00 - 00:00:10.

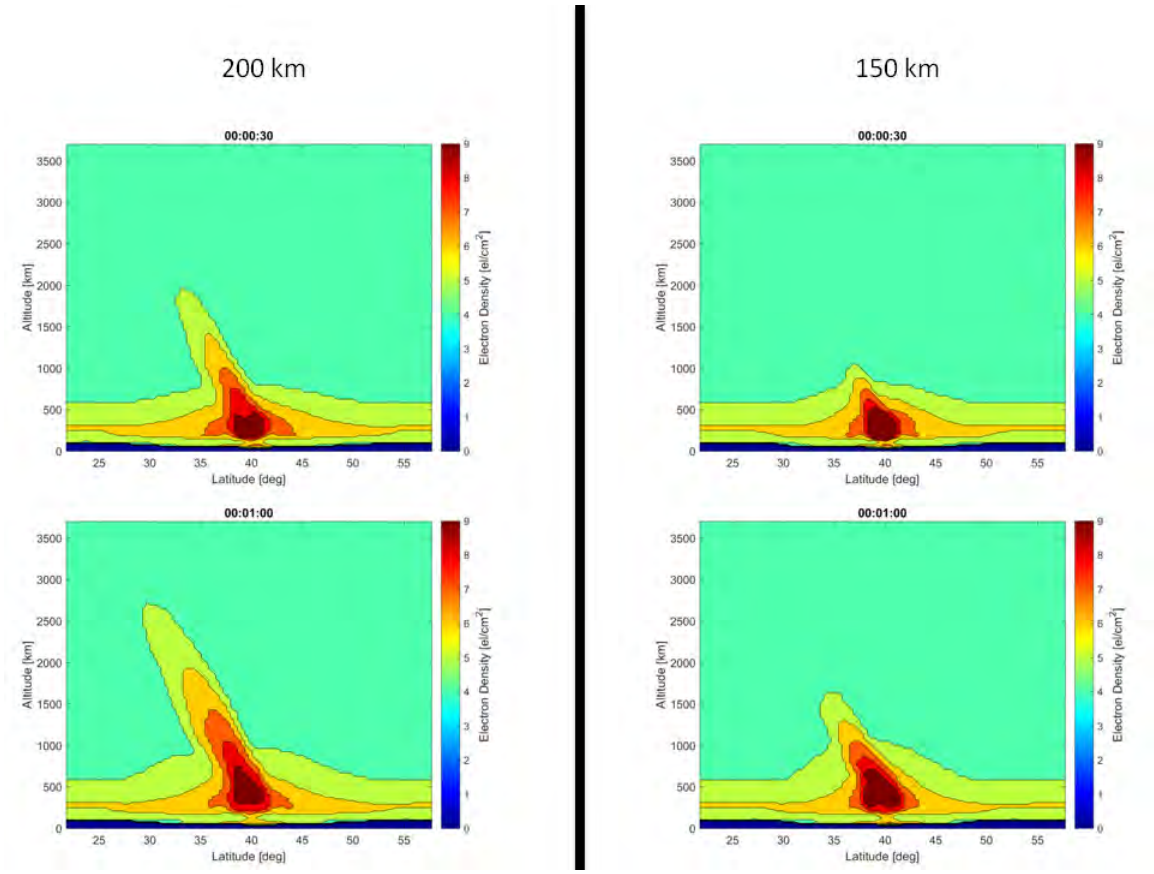

Figure 24. Comparison of electron densities produced by a 2 Mt yield HANE at 200 km and 150 km, 00:00:30 - 00:01:00.

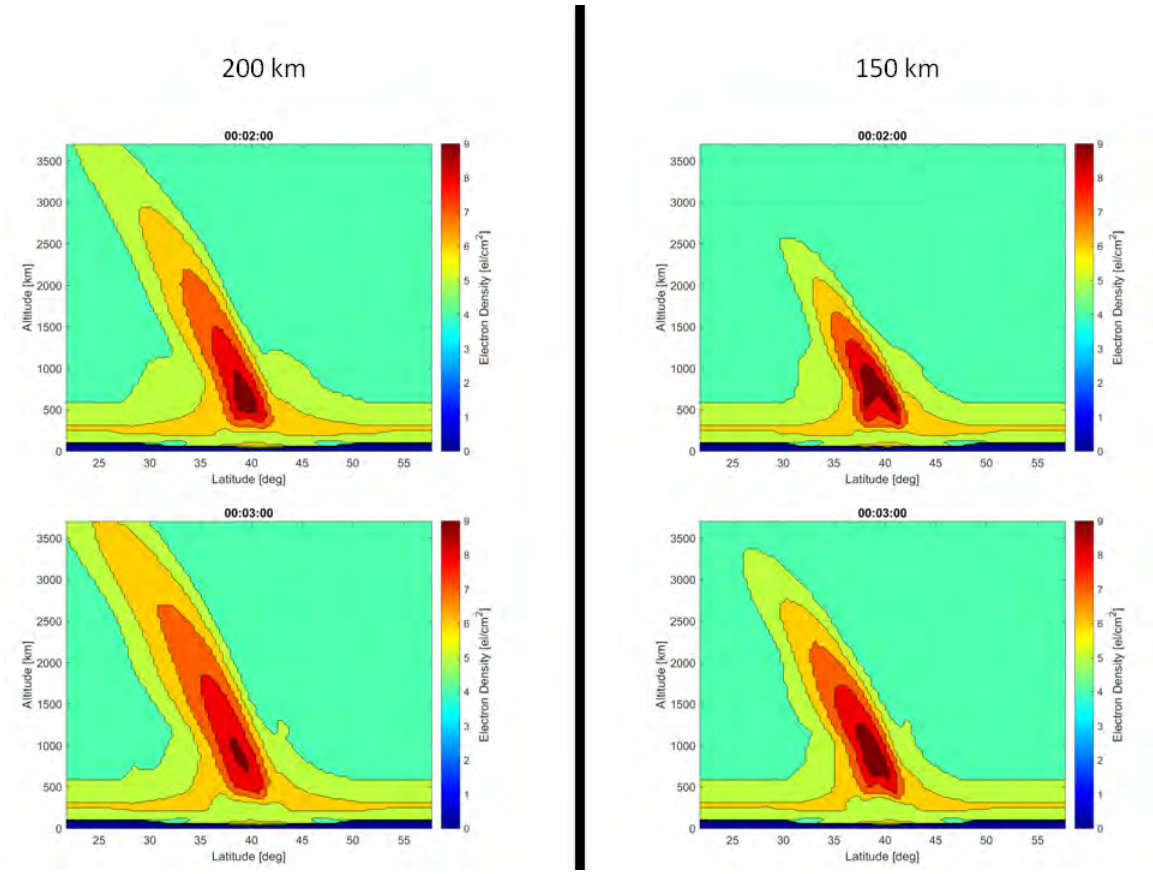

Figure 25. Comparison of electron densities produced by a 2 Mt yield HANE at 200 km and 150 km, 00:05:00 - 00:06:00.

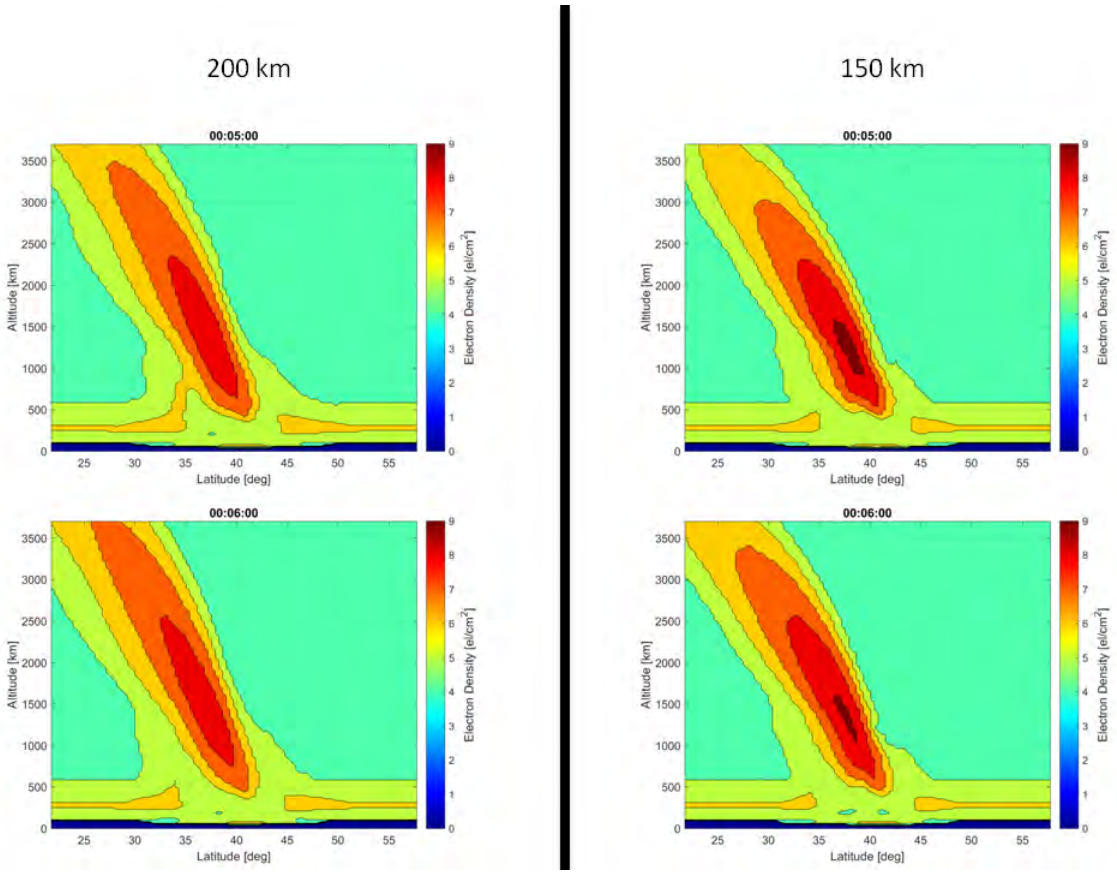

Figure 26. Comparison of electron densities produced by a 2 Mt yield HANE at 200 km and 150 km, 00:05:00 - 00:06:00.

5 Mt HANE.

Figures 27 - 30 show the electron density movement for a 5 Mt HANE at 200 km and 150 km. Similar to the lower yield HANE's previously discussed, the electron debris movement from the 5 Mt HANE at 200 km is dominated by the Earth's geomagnetic lines. At 10 sec, the geomagnetic lines clearly have a greater effect on the electron debris from the 200 km 5 Mt HANE than the 150 km 5 Mt HANE. Thirty seconds after the 5 Mt HANE at 150 km, the Earth's geomagnetic lines have a dominant effect on the electrons, and the electrons move along the geomagnetic lines as the electron debris rises up from the Earth. As a result, the electron densities of the 150 km HANE are high for a longer period of time compared to the electron densities of th 200 km HANE. Figure 30 shows at a burst point altitude of 150 km, the maximum electron density remains $\geq 10^9 \frac{el^-}{cm^3}$ after 6 mins, and that the electron density from the 200 km burst point is $\leq 10^8 \frac{el^-}{cm^3}$ for the same time frame.

4.4 Verification Results

This section will present the results obtained from the verification of the SSFM algorithm. Results from both the phase screen and propagation steps will presented.

Propagation Verification.

To verify that the propagation algorithm produced numerically accurate results, a plane wave $E(x, z, \omega) = 1$ was propagated through a Gaussian lens described in (27) located at $z = 0$. Figures 31 and 32 show the results of the verification test of the SSFM. The Gaussian lens from (27) had a half-width set to the wavelength (λ) of $E(x, z, \omega)$. The Gaussian lens is acts focusing lens (the top left plot in figure 31 is a plot of the Gaussian lens). The focal length of the lens found from (28) is 0.3142λ (or $\frac{F}{\lambda} = 0.3142$). The length of the x-direction was set to $\frac{x}{\lambda} = 20$ and the results of

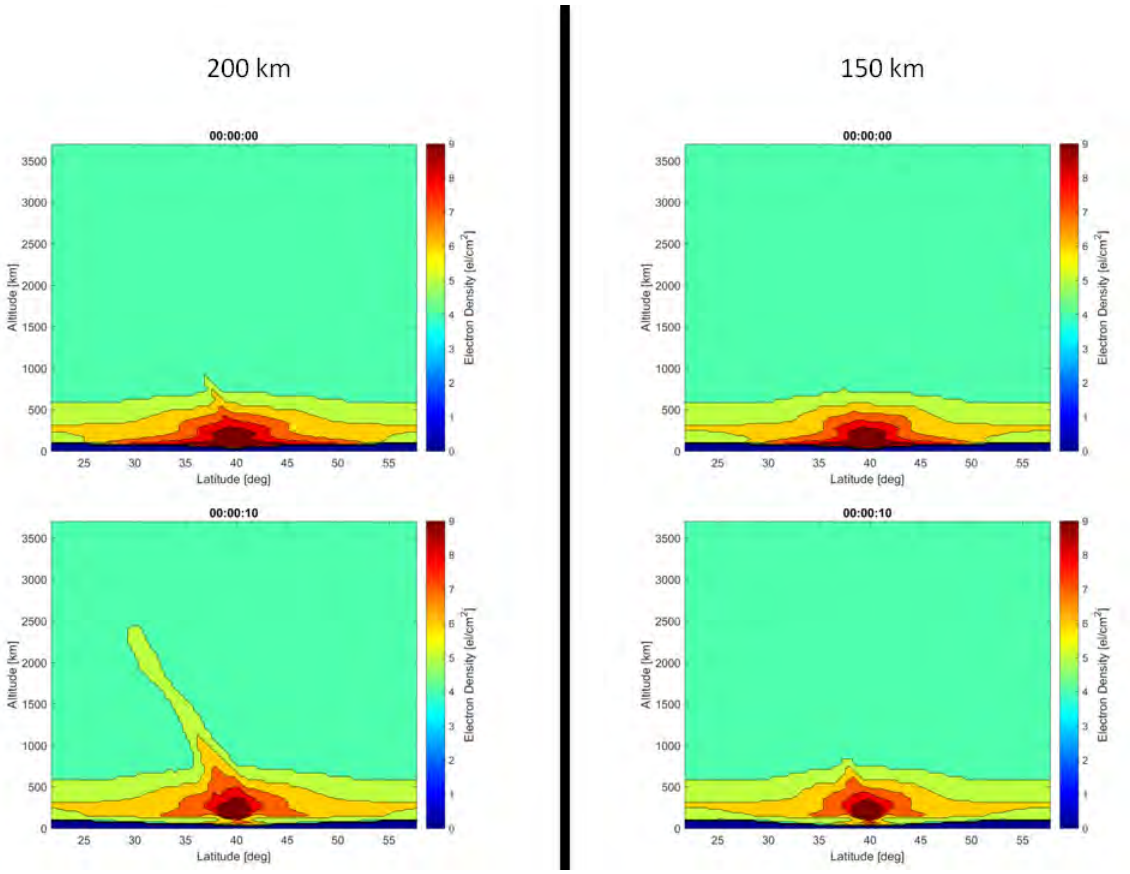

Figure 27. Comparison of electron densities produced by a 5 Mt yield HANE at 200 km and 150 km, 00:00:00 - 00:00:10.

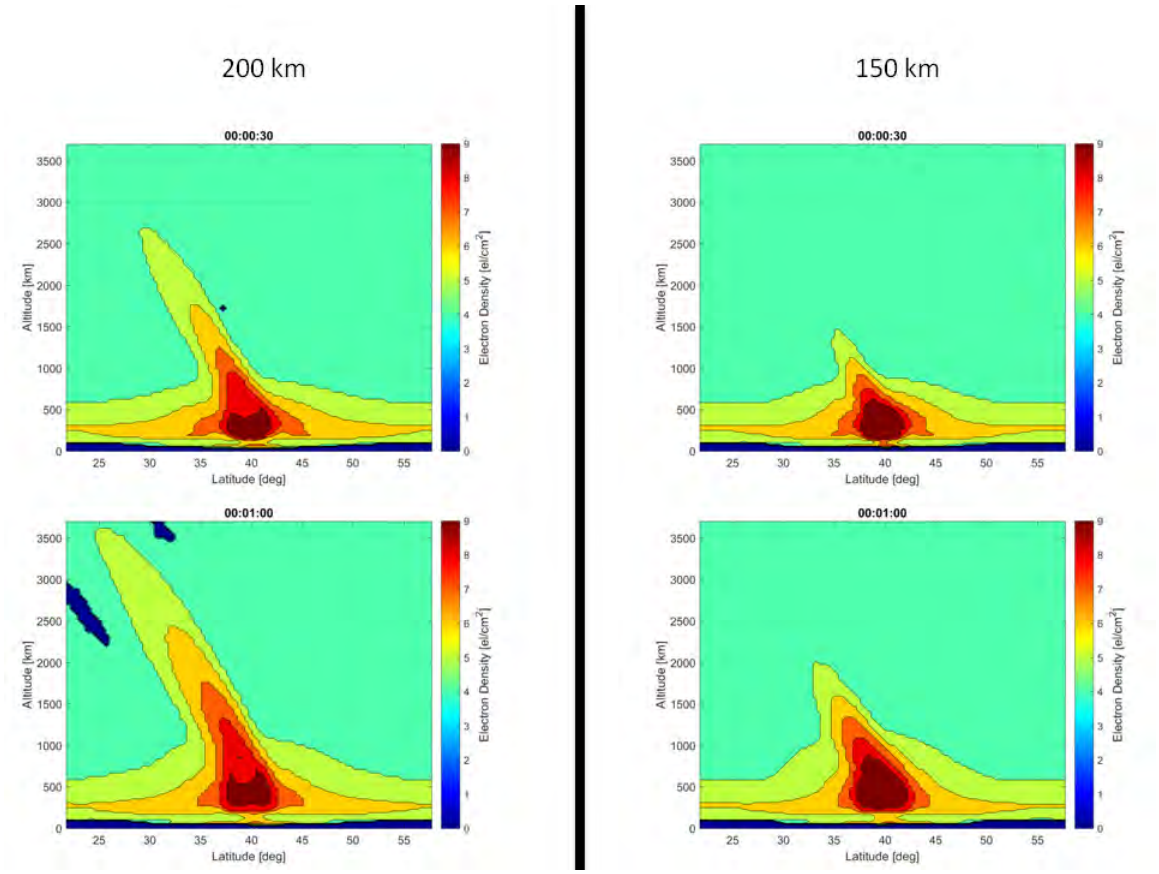

Figure 28. Comparison of electron densities produced by a 5 Mt yield HANE at 200 km and 150 km, 00:00:30 - 00:01:00.

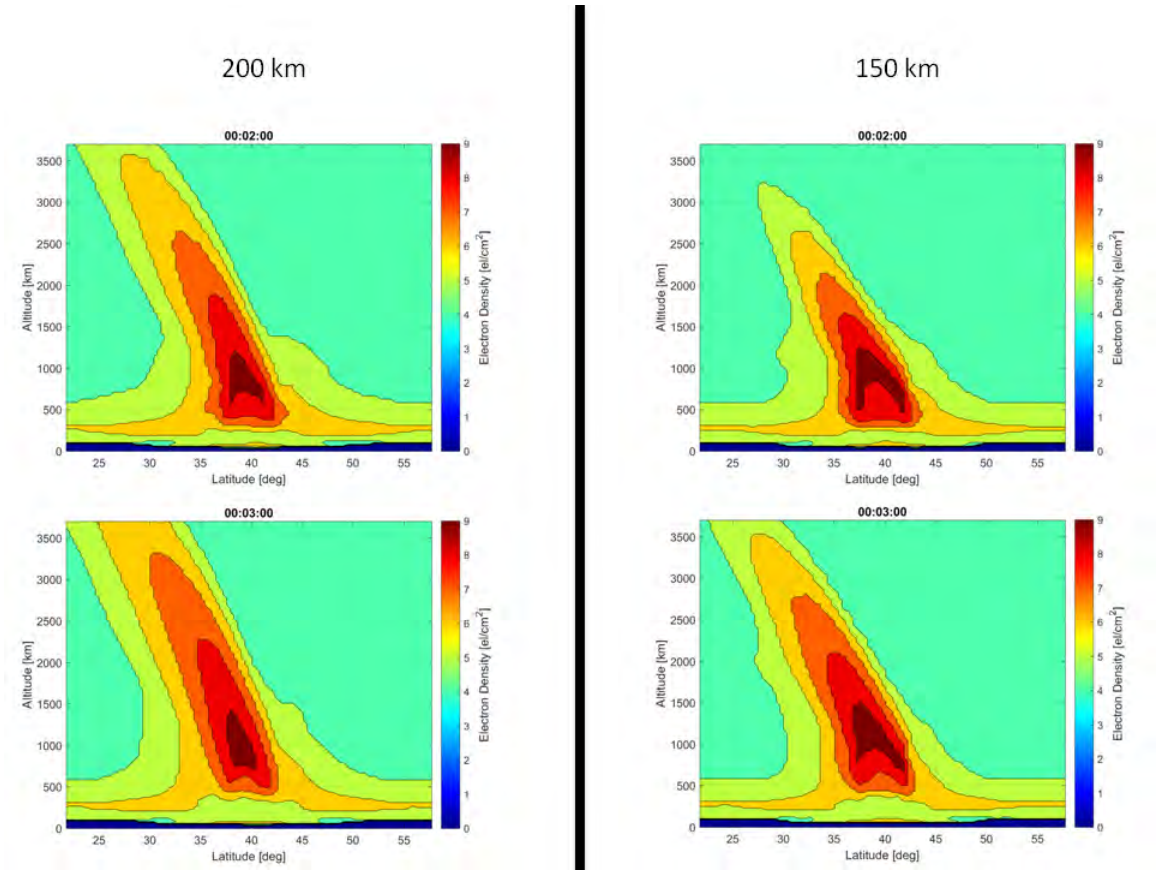

Figure 29. Comparison of electron densities produced by a 5 Mt yield HANE at 200 km and 150 km, 00:02:00 - 00:03:00.

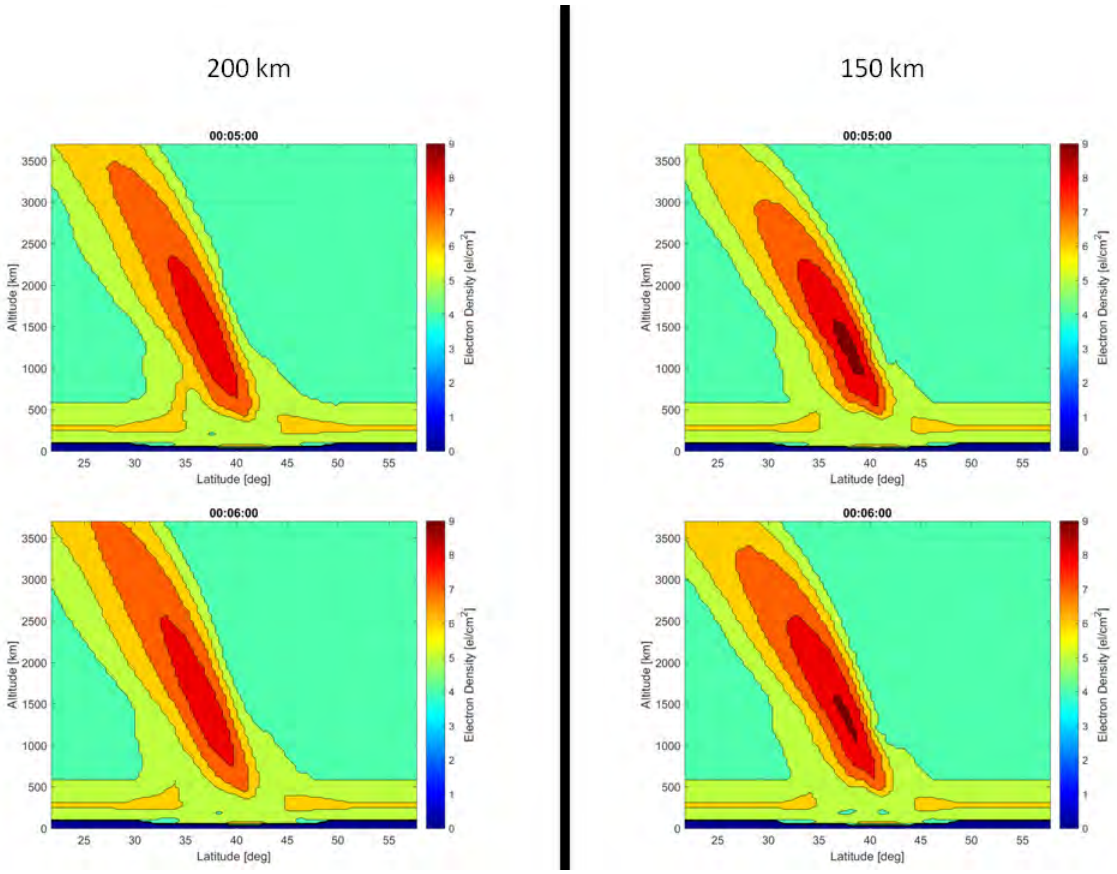

Figure 30. Comparison of electron densities produced by a 5 Mt yield HANE at 200 km and 150 km, 00:05:00 - 00:06:00.

the plane wave passing through the Gaussian lens were observed at $\frac{z}{\lambda} = 0.3$, $\frac{z}{\lambda} = 0.5$, and $\frac{z}{\lambda} = 10$.

The left hand side of figure 31 shows the results of the SSFM for a given distance from the Gaussian lens ($\frac{z}{\lambda} = 0.3$, $\frac{z}{\lambda} = 0.5$, and $\frac{z}{\lambda} = 10$). The right side of figure 31 shows the theoretical results for the solution to the Fresnel-Kirchoff Integral for a Gaussian lens. When comparing the two plots, at distances of $\frac{z}{\lambda} = 0.3$ and $\frac{z}{\lambda} = 0.5$ the numerical results on the left match the theoretical results on the right. For the case of $\frac{z}{\lambda} = 10$ (in figure 31), the numerical results break down when compared to the theoretical results. This is a result of the diffracting waves exiting the MPS grid and re-entering on the other side. These numerical errors show that propagation conditions from (22) and (25) must be used to prevent edge scattering from corrupting the numerical results. Figure 32 clearly shows that for $\frac{z}{\lambda} = 0.3$ the numerical results agree with the theoretical Thus, the propagation portion of the SSFM code has been verified that it will produce numerically accurate results.

Power Spectral Density Verification.

In order to verify that the phase screen portion of the code is computing numerically accurate results, a random ideal Gaussian phase screen from (26) is compared to a numerically randomly generated phase screen created from (20). Here $\sigma_\phi^2 = 10$ radians, and both phase screens were generated using the same random numbers. Also, a total of 10 screens were generated and averaged together for both the Gaussian phase screen and the numerical phase screen, respectively. The number of grid points for this verification were 2^{12} or 2,048. Figure 33 is a comparison of the ideal Gaussian phase screen with that of the numerically generated phase screen. The figure shows that the numerically generated phase screen generally follows the ideal Gaussian with a root mean square error of 0.051.

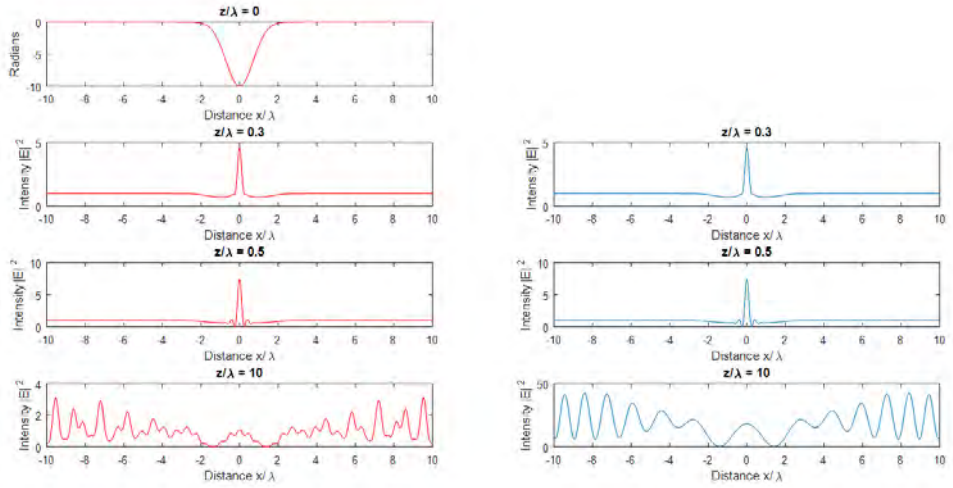

Figure 31. Analysis of MPS numerical and theoretical results.

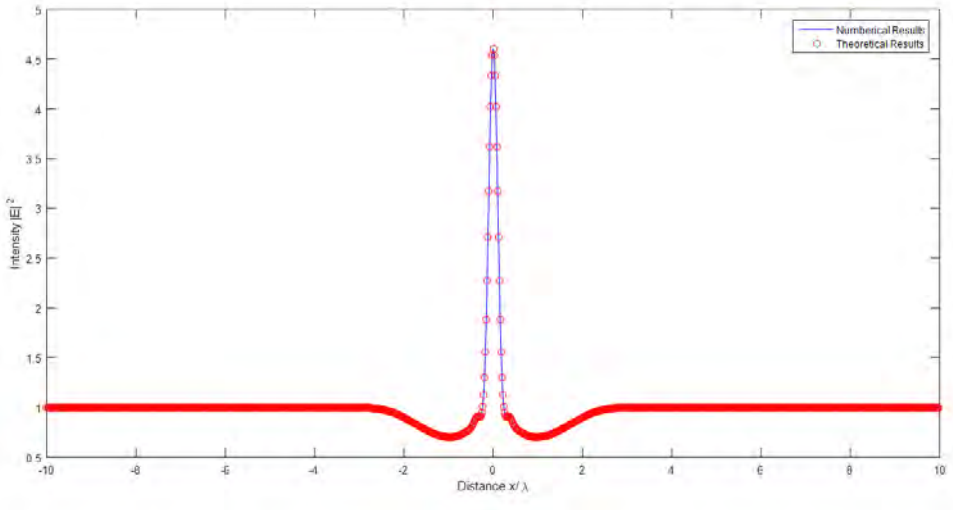

Figure 32. Agreement between numerical and theoretical MPS results at propagation distance $z/\lambda = 0.3$.

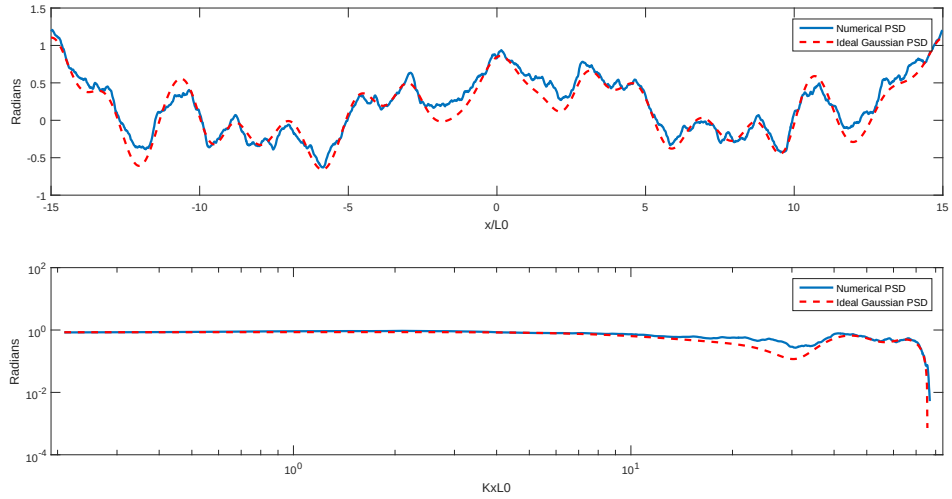

Figure 33. Comparison of an ideal Gaussian phase screen to a numerically generated phase screen.

Central Limit Theorem Verification.

In order to verify that the numerical results of the simulation run were an accurate representation of a given scenario, each scenario was run 100 times. The distribution of the data was calculated from (31). Figure 34 shows the distribution of a given scenario. The figure shows that after 100 runs of a given scenario, the data is distributed normally, with the standard deviation of 1.136×10^{-13} (MATLAB precision is 10^{-16}).

4.5 Propagation Results

This section presents the propagation loss results for the natural ionosphere and from HANE's with yields of 100 kt, 500 kt, 1 Mt, 2 Mt, and 5 Mt. The propagation loss from a natural ionosphere will be presented first. Next, the results from propagation loss are also given for the aforementioned yields at heights of 150 km and 200 km. First the loss from the natural ionosphere will be presented and discussed. Finally,

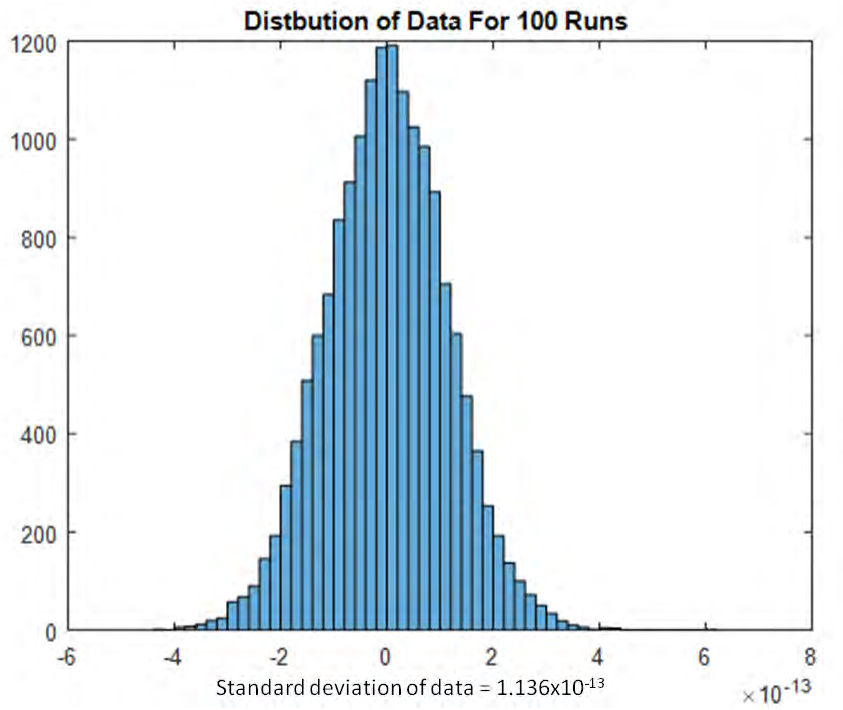

Figure 34. Data distribution of 100 runs for a given scenario.

the absorption loss that was calculated from the GSCENARIO software suite will be presented alongside the amplitude scintillation loss results that were calculated from the SSFM algorithm.

Natural Ionosphere Loss.

The naturally occurring ionosphere contributes little loss from amplitude scintillation. The max signal loss from figure 35 corresponds with the electron density profile of figure 10 and shows that maximum scintillation loss occurs from 1300-1400 hrs Zulu, for 40 GHz, when the F-layer is at its peak. Figure 35 also shows that the maximum loss experienced in a given channel was 0.025 db. Thus, the natural ionosphere provided negligible loss to signals with frequencies between 40 - 110 GHz.

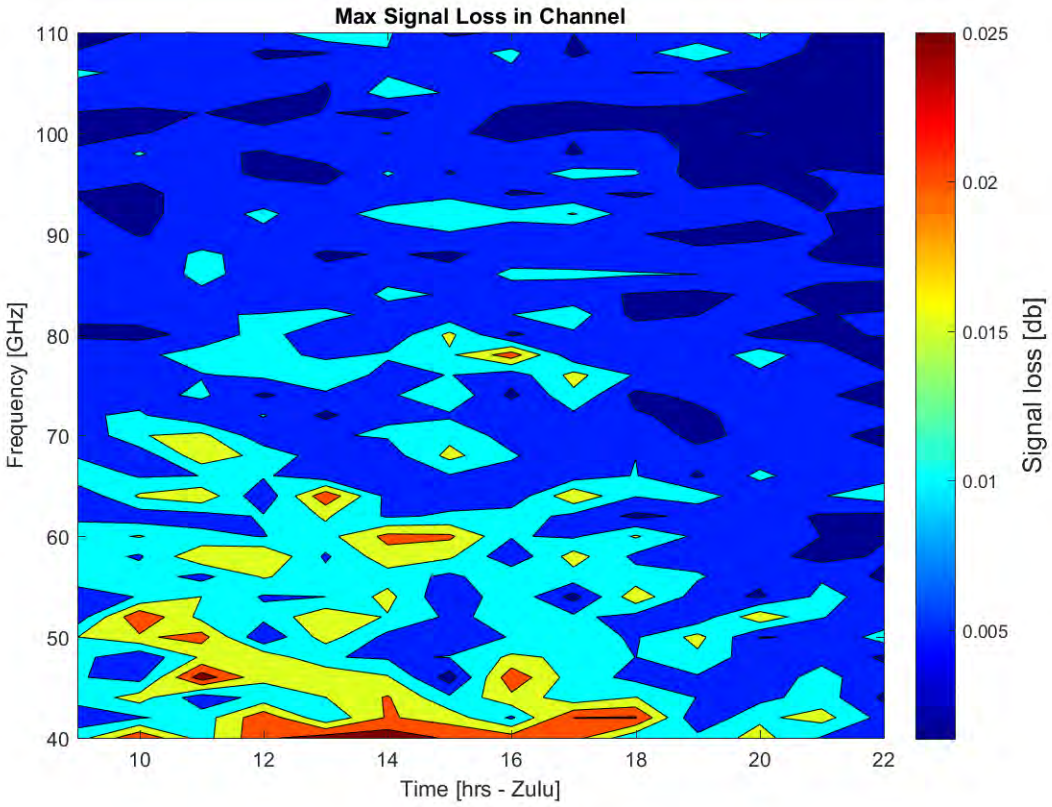

Figure 35. Maximum signal loss from the natural ionosphere.

Absorption Loss.

Tables 1 - 10 represent the maximum total absorption loss expected from the HANEs used in this research. The maximum absorption loss was calculated from GSCENARIO from the total integrated debris content above a given HANE location. Each absorption value is the maximum total absorption loss expected ≈100 km to 5000 km above the Earth's surface. Therefore, tables 1 - 10 represent total integrated absorption loss.

Absorption From a 100 kt HANE.

Table 1. Max absorption from ion debris for a 100 kt HANE located at 150 km.

	Max Absorption (dB)						
	40 GHz	50 GHz	60 GHz	70 GHz	80 GHz	90 GHz	100 GHz
0 sec	1280	826	577	426	327	259	210
1 sec	1.1	0.7	0.5	0.4	0.3	0.2	0.2
3 sec	1.0	0.6	0.4	0.3	0.2	0.2	0.1
10 sec	0.5	0.3	0.2	0.2	0.1	0.1	0.0
20 sec	0.4	0.2	0.1	0.1	0.0	0.0	0.0
30 sec	0.3	0.2	0.1	0.0	0.0	0.0	0.0
40 sec	0.2	0.1	0.0	0.0	0.0	0.0	0.0
50 sec	0.1	0.1	0.0	0.0	0.0	0.0	0.0
60 sec	0.1	0.0	0.0	0.0	0.0	0.0	0.0
90 sec	0.0	0.0	0.0	0.0	0.0	0.0	0.0

Tables 1 and 2 show the maximum absorption of an EM wave through an ion debris after a HANE at 150 km and 200 km, respectively. It can be seen from both tables 1 and 2 that the majority of absorption effects will occur immediately following a HANE and then become negligible within seconds afterwards (10 secs at 150 km and 1 sec for 200 km burst altitudes at 40 GHz). Only an EM wave above 40 GHz will see a significant impact from absorption directly after the HANE.

Table 2. Max absorption from ion debris for a 100 kt HANE located at 200 km.

	Max Absorption (dB)						
	40 GHz	50 GHz	60 GHz	70 GHz	80 GHz	90 GHz	100 GHz
0 sec	455	293	204	150	115	91.3	74.1
1 sec	0.7	0.4	0.3	0.2	0.2	0.1	0.1
3 sec	0.3	0.2	0.1	0.1	0.1	0.1	0.1
10 sec	0.1	0.1	0.1	0.0	0.0	0.0	0.0
20 sec	0.1	0.0	0.0	0.0	0.0	0.0	0.0
30 sec	0.0	0.0	0.0	0.0	0.0	0.0	0.0

Absorption From a 500 kt HANE.

The data in tables 3 and 4 show the total maximum Blackout occurs directly after the initial explosion with a steep drop in absorption loss for both altitudes. Comparing tables 3 and 4, more absorption is expected from a HANE located at 150 km above the Earth's surface than a HANE located at 200 km above the Earth's surface. The absorption becomes negligible after 2 min from a 150 km HANE and after 40 secs from a 200 km HANE operating at 40 GHz. At a frequency of 100 GHz, the total absorption becomes negligible after 20 secs for a HANE at 150 km and after 10 secs for a HANE at 200 km.

Absorption From a 1 Mt HANE.

The maximum total absorption loss from a 1 Mt HANE at a height of 150 km and 200 km is displayed in tables 5 and 6. The maximum absorption is significantly higher for a 1 Mt HANE than a 500 kt HANE. Operating at 40 GHz, absorption becomes insignificant after 2 min for both a HANE located at 150 km and 200 km. As frequency is increased, total absorption loss becomes less of a concern. At 100 GHz, absorption becomes negligible after ≈40 secs after a HANE located at 150 km and 200 km.

Table 3. Max absorption from ion debris for a 500 kt HANE located at 150 km.

Max Signal Loss (dB)							
	40 GHz	50 GHz	60 GHz	70 GHz	80 GHz	90 GHz	100 GHz
0 secs	6230.0	4020.0	2810.0	2070.0	1590.0	1260.0	1020.0
1 sec	8.1	5.1	3.5	2.5	1.9	1.5	1.2
3 sec	10.6	6.6	4.5	3.2	2.4	1.9	1.5
10 sec	4.4	2.8	1.9	1.3	1.0	0.8	0.6
20 sec	1.6	1.0	0.6	0.5	0.3	0.3	0.2
30 sec	0.9	0.6	0.4	0.3	0.2	0.2	0.1
40 sec	0.6	0.3	0.2	0.2	0.1	0.1	0.1
50 sec	0.5	0.3	0.2	0.1	0.1	0.1	0.1
60 sec	0.5	0.3	0.2	0.1	0.1	0.1	0.1
90 sec	0.6	0.4	0.3	0.2	0.1	0.1	0.1
120 sec	0.4	0.2	0.2	0.1	0.1	0.1	0.1

Table 4. Max absorption from ion debris for a 500 kt HANE located at 200 km.

Max Absorption (dB)							
	40 GHz	50 GHz	60 GHz	70 GHz	80 GHz	90 GHz	100 GHz
0 sec	2380	1530	1070	790	606	480	390
1 sec	2.3	1.4	1.0	0.7	0.5	0.4	0.3
3 sec	3.4	2.1	1.4	1.0	0.8	0.6	0.5
10 sec	3.0	1.9	1.3	0.9	0.7	0.5	0.4
20 sec	0.7	0.4	0.3	0.2	0.2	0.1	0.1
30 sec	0.3	0.2	0.1	0.1	0.1	0.1	0.0
40 sec	0.2	0.1	0.1	0.1	0.0	0.0	0.0
50 sec	0.1	0.1	0.1	0.0	0.0	0.0	0.0
60 sec	0.1	0.1	0.1	0.0	0.0	0.0	0.0
90 sec	0.1	0.0	0.0	0.0	0.0	0.0	0.0
120 sec	0.0	0.0	0.0	0.0	0.0	0.0	0.0

Table 5. Max absorption from ion debris for a 1 Mt HANE located at 150 km.

	Max Absorption (dB)						
	40 GHz	50 GHz	60 GHz	70 GHz	80 GHz	90 GHz	100 GHz
0 sec	12300	7940	5540	4090	3140	2480	2010
1 sec	31.3	19.5	13.2	9.6	7.2	5.6	4.5
3 sec	45.5	28.3	19.2	13.8	10.4	8.1	6.5
10 sec	18.3	11.3	7.7	5.5	4.1	3.2	2.5
20 sec	4.8	3.0	2.0	1.4	1.1	0.8	0.7
30 sec	2.5	1.5	1.0	0.7	0.5	0.4	0.3
40 sec	1.3	0.8	0.5	0.4	0.3	0.2	0.1
50 sec	0.7	0.4	0.3	0.2	0.1	0.1	0.0
60 sec	0.7	0.4	0.2	0.1	0.0	0.0	0.0
90 sec	0.6	0.2	0.1	0.0	0.0	0.0	0.0
120 sec	0.3	0.1	0.0	0.0	0.0	0.0	0.0

Table 6. Max absorption from ion debris for a 1 Mt HANE located at 200 km.

	Max Absorption (dB)						
	40 GHz	50 GHz	60 GHz	70 GHz	80 GHz	90 GHz	100 GHz
0 sec	4810	3110	2170	1600	1230	973	7900
1 sec	11.3	7.1	4.8	3.5	2.6	2.1	1.6
3 sec	14.1	8.8	6.0	4.3	3.2	2.5	2.0
10 sec	8.2	5.1	3.4	2.5	1.8	1.4	1.1
20 sec	1.7	1.1	0.7	0.5	0.4	0.3	0.2
30 sec	0.9	0.6	0.4	0.3	0.2	0.2	0.1
40 sec	0.6	0.4	0.2	0.2	0.1	0.1	0.1
50 sec	0.4	0.2	0.2	0.1	0.1	0.0	0.0
60 sec	0.3	0.2	0.1	0.1	0.1	0.0	0.0
90 sec	0.2	0.1	0.1	0.0	0.0	0.0	0.0
120 sec	0.2	0.1	0.1	0.0	0.0	0.0	0.0

Absorption From a 2 Mt HANE.

Tables 7 and 8 show the total maximum absorption loss for a 2 Mt HANE located at 150 km and 200 km, respectively. For a 2 MtHANE, there is a significant difference in maximum total absorbtion loss between the different HANE locations. A 2 Mt HANE located a 150 km will have longer absorption effects than a 2 Mt HANE located at 200 km. For a 2 Mt HANE located at 150 km the total absorption loss remains strong for frequencies from 40 GHz - 100 GHz until $\approx$ 30 secs after the explosion. For a 2 Mt HANE at 200 km, the absorbtion loss is $\approx$ 90% less than the same size yield HANE located at 150 km. The reason the 2 Mt exploded at 150 km HANE causes more total absorption loss is because electrons have less room to spread after the explosion. This can be observed in figures 23 and 26. In figure 23 the electrons only travel $\approx$ 50 km before they are stopped by the Earth's atmosphere, thus the electron density remains higher until the electrons begin to spread themselves out along the Earth's magnetic field lines.

Table 7. Max absorption from ion debris for a 2 Mt HANE located at 150 km.

	Max Absorption (dB)						
	40 GHz	50 GHz	60 GHz	70 GHz	80 GHz	90 GHz	100 GHz
0 sec	25000	16100	11200	8270	6350	5030	4080
1 sec	143.0	88.5	59.9	43.1	32.4	25.2	20.2
3 sec	211.0	131.0	88.4	63.5	47.7	37.1	29.6
10 sec	106.0	65.4	44.1	31.6	23.7	18.4	14.6
20 sec	24.5	15.1	10.2	7.3	5.4	4.2	3.3
30 sec	8.6	5.3	3.6	2.5	1.9	1.5	1.2
40 sec	3.0	1.9	1.2	0.9	0.7	0.5	0.4
50 sec	1.6	1.0	0.7	0.5	0.4	0.3	0.2
60 sec	0.9	0.6	0.4	0.3	0.2	0.2	0.1
90 sec	0.7	0.4	0.2	0.0	0.0	0.0	0.0
120 sec	0.4	0.2	0.0	0.0	0.0	0.0	0.0

Table 8. Max absorption from ion debris for a 2 Mt HANE located at 200 km.

	Max Absorption (dB)						
	40 GHz	50 GHz	60 GHz	70 GHz	80 GHz	90 GHz	100 GHz
0 sec	9590	6180	4320	3180	2440	1940	1570
1 sec	23.0	14.3	9.7	7.0	5.3	4.1	3.3
3 sec	25.4	15.8	10.7	7.7	5.8	4.5	3.6
10 sec	4.5	2.8	1.9	1.4	1.0	0.8	0.6
20 sec	1.1	0.7	0.5	0.3	0.2	0.2	0.2
30 sec	0.5	0.3	0.2	1.5	0.1	0.1	0.1
40 sec	0.3	0.2	0.1	0.1	0.1	0.1	0.0
50 sec	0.2	0.1	0.1	0.1	0.0	0.0	0.0
60 sec	0.2	0.1	0.1	0.1	0.0	0.0	0.0
90 sec	0.1	0.1	0.1	0.0	0.0	0.0	0.0
120 sec	0.1	0.1	0.0	0.0	0.0	0.0	0.0

Absorption From a 5 Mt HANE.

A 5 Mt HANE located at an altitude of 150 km will have greater total absorption loss than a 5 Mt HANE located at 200 km. Table 9 shows that the total maximum absorption will be a major contributing factor until 90 secs after a 5 Mt HANE at 150 km. For a 5 Mt HANE at 200 km (see table 10), the total maximum absorption loss is significant until $\approx$ 60 secs after the HANE. Again, the absorption is dependent on the frequency of the EM wave (see equation (2)). Therefore, as the frequency of the EM wave increases, the power loss from absorption decreases. For a HANE at 150 km the maximum total absorption loss will be negligible for frequencies 70 GHz and above $\approx$ 90 secs after the HANE. The maximum total absorption loss will be negligible for frequencies 80 GHz and above $\approx$ 50 sec after a HANE at 200 km.

Total Absorption Trend.

Tables (1 - 10) all show a similar trend, that within $\approx$ 1 min after a HANE the total absorption from the ion debris will drop to levels that are negligible. This is a result of the ions and electrons dispersing along the Earth's magnetic field lines.

Table 9. Max absorption from ion debris for a 5 Mt HANE located at 150 km.

	Max Absorption (dB)						
	40 GHz	50 GHz	60 GHz	70 GHz	80 GHz	90 GHz	100 GHz
0 sec	61100	39200	27300	20100	15400	12200	9910
1 sec	644.0	394.0	265.0	190.0	142.0	111.0	88.2
3 sec	676.0	416.0	280.0	201.0	151.0	117.0	93.3
10 sec	341.0	210.0	142.0	102.0	76.2	59.0	47.0
20 sec	61.0	37.7	25.4	18.2	13.6	10.5	8.4
30 sec	19.6	12.0	8.1	5.8	4.3	3.3	2.7
40 sec	7.5	4.6	3.1	2.2	1.7	1.3	1.0
50 sec	3.7	2.3	1.5	1.1	0.8	0.6	0.5
60 sec	1.9	1.2	0.8	0.6	0.4	0.3	0.1
90 sec	1.0	0.6	0.4	0.3	0.0	0.0	0.0
120 sec	0.7	0.3	0.0	0.0	0.0	0.0	0.0

Table 10. Max absorption from ion debris for a 5 Mt HANE located at 200 km.

	Max Absorption (dB)						
	40 GHz	50 GHz	60 GHz	70 GHz	80 GHz	90 GHz	100 GHz
0 sec	24500	15800	11000	8140	6350	4950	4020
1 sec	97.4	60.3	40.8	29.4	22.1	17.2	13.8
3 sec	120	74.4	50.3	36.2	27.2	21.1	16.9
10 sec	17.2	10.7	7.2	5.1	3.8	3.0	2.4
20 sec	5.9	3.6	2.4	1.7	1.3	1.0	0.8
30 sec	2.3	1.4	1.0	0.7	0.5	0.4	0.3
45 sec	0.7	0.5	0.4	0.2	0.2	0.2	0.1
60 sec	0.4	0.3	0.2	0.1	0.1	0	0
75 sec	0.3	0.2	0.1	0	0	0	0
90 sec	0.3	0	0	0	0	0	0
120 sec	0.2	0	0	0	0	0	0

These tables also show that in most cases, absorption will be the dominant effect until $\approx$ 1 min after a HANE, after which amplitude scintillation will become the dominant effect.

Signal Loss from Amplitude Scintillation.

Signal Loss From 100 kt.

Amplitude scintillation is the significant contributor to signal loss after absorption effects have dropped off. For the case of a 100 kt HANE, figure 36 show that most scintillation loss will occur from 3 secs to $\approx$ 100 secs after the burst (200 km) and from 3 sec to $\approx$ 175 secs after the burst (150 km). The frequencies most affected by amplitude scintillation from a 100 kt HANE at 150 km and 200 km are $\approx$ 60 GHz and below. Comparing the plots from figure 36 it can be seen that the scintillation loss is more significant at a lower altitude 100 kt HANE, but overall the scintillation loss from a 100 kt HANE is minimal.

Signal Loss From 500 kt.

The maximum signal loss from a 500 kt HANE located at 150 km produces at least 1 db of signal loss until $\approx$ 275 secs after the initial burst (see figure 37). Most of the stronger scintillation effects (4 - 2.5 db loss) will occur for frequencies below 50 GHz and last for $\approx$ 150 secs. Frequencies as high as 110 GHz can see loss ($\lesssim$ 1 db) up to $\approx$ 60 sec after the initial explosion.

For a 500 kt HANE located at 200 km, signal loss from scintillation greater than 1 db tapers off at $\approx$ 200 secs after the HANE (see figure 37). Similar to the 500 kt HANE located at 150 km, the frequencies 50 GHz and below experience stronger scintillation effects (4 - 2.5 db loss) than the higher frequencies.

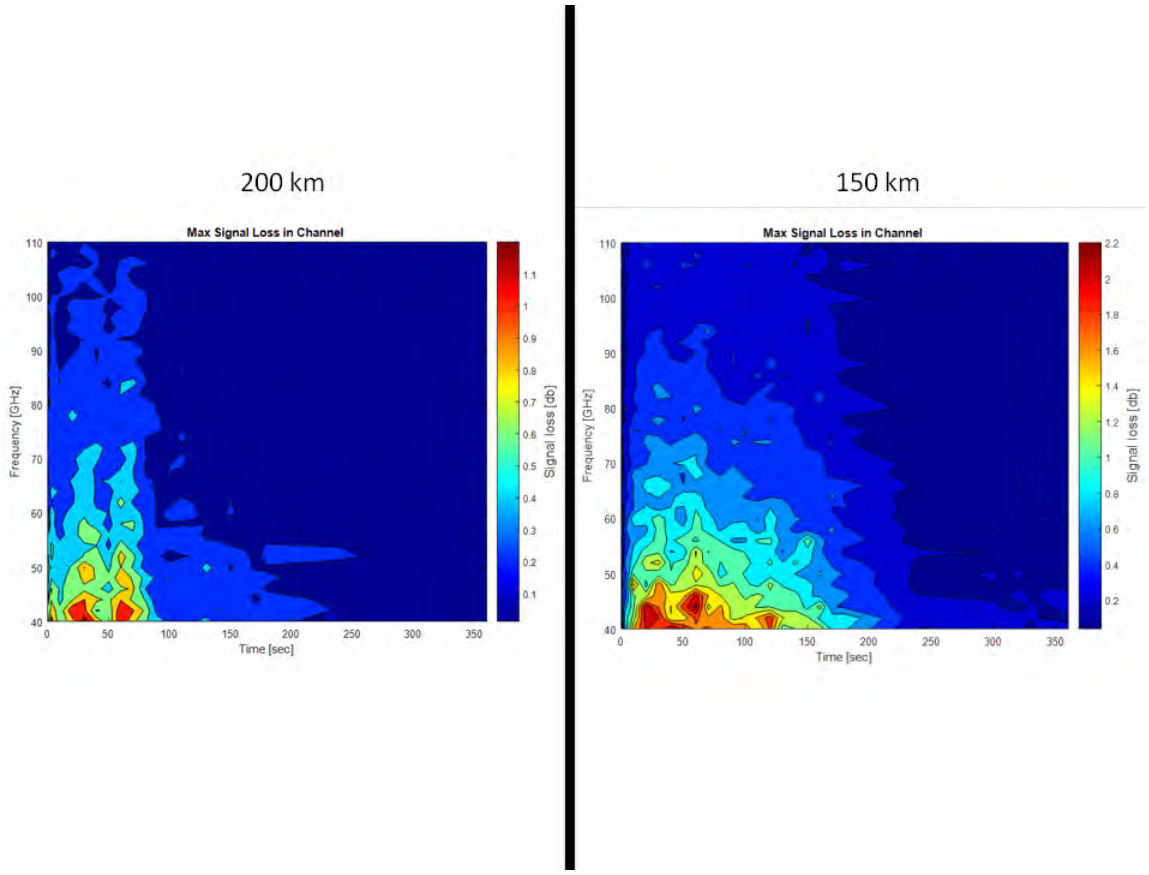

Figure 36. Comparison of maximum signal loss in a given channel from a 100 kt yield HANE at 200 km and 150 km.

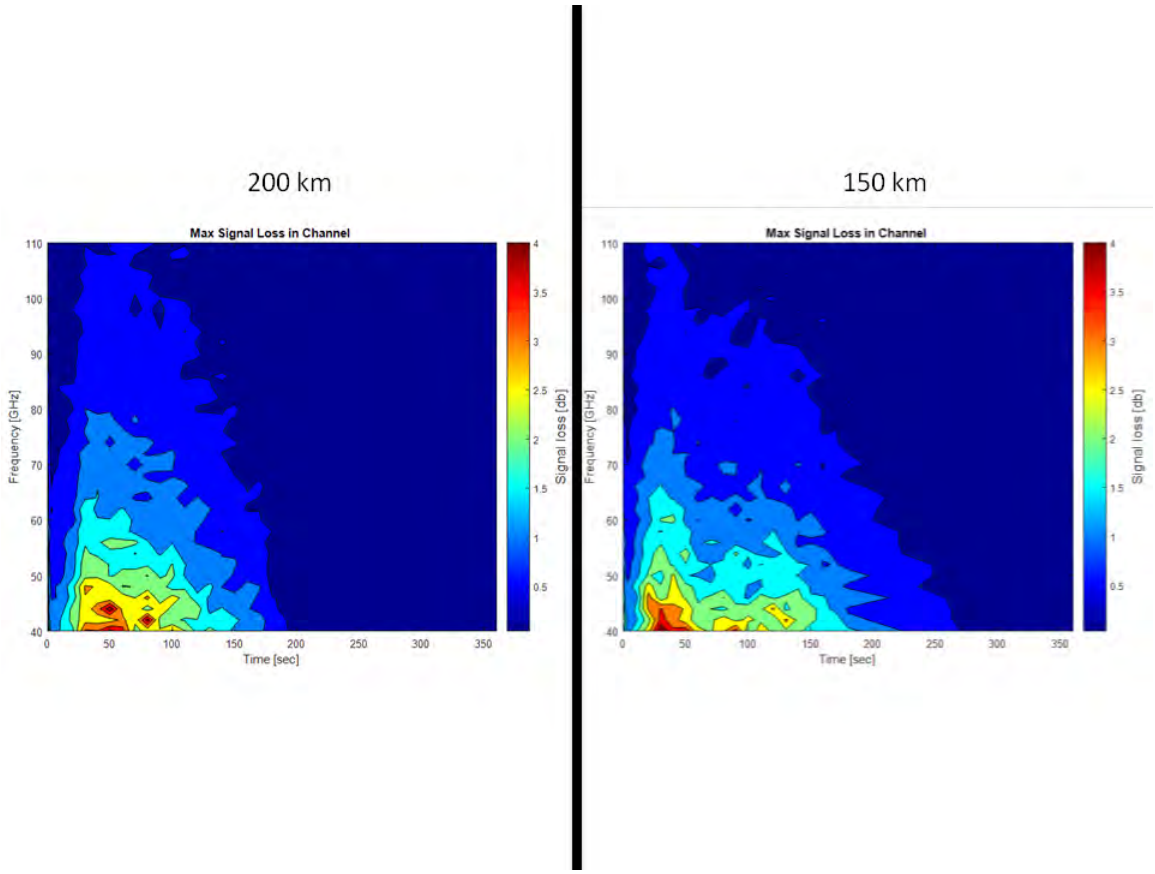

Figure 37. Comparison of maximum signal loss in a given channel from a 500 kt yield HANE at 200 km and 150 km.

Signal Loss From 1 Mt.

Figure 38 displays the maximum signal loss for a 1 Mt HANE located at 150 km and 200 km respectively. At both altitudes, the maximum signal loss is ≈ 5 db which occurs around ≈ 50 secs (at 40 GHz) for both HANE altitudes. Comparing tables 5 and 6 with figure 38, the absorption loss has dropped off to allow scintillation loss to be the dominant loss at 50 secs (at 40 GHz) after the HANE's at 150 km and 200 km.

Figure 38 also shows that after the maximum of 5 db loss occurs (at 40 GHz), the scintillation loss drops to ≈ 2 db and rises to ≈ 3 db, 100 secs after the HANE for both altitudes. After 300 secs, the scintillation loss drops off (for 40 GHz) to negligible levels.

For a 1 Mt HANE at 150 km, significant scintillation loss (≈ 1 db) can impact signals up to 90 GHz in the first 100 secs after a 1 Mt HANE and up to 70 GHz, 200 secs after a 1 Mt HANE. A 1 Mt HANE at 200 km can cause significant scintillation loss (≈ 1 db) for frequencies below 90 GHz in the first 100 secs after a HANE.

Signal Loss From 2 Mt.

The maximum loss in a channel from scintillation after a 2 Mt HANE located at 150 km and 200 km is displayed in figure 39. Comparing figure 39 with table 7, it can be seen that the dominating loss (at 40 GHz) will be from absorption until 60 secs after the 150 km HANE. For the time frame of 120 - 260 secs after a 2 Mt HANE at 150 km there is a distinct window of loss from scintillation. Scintillation loss will drop to ≈ 1 db (at 40 GHz) after 70 secs, rise to ≈ 3.5 db (at 40 GHz) after 120 secs after the 2 Mt HANE, and last until 260 secs after the 2 Mt HANE. During this scintillation loss window (120 - 260 secs after a HANE at 150 km) frequencies below 70 GHz can have a loss up to 1 db.

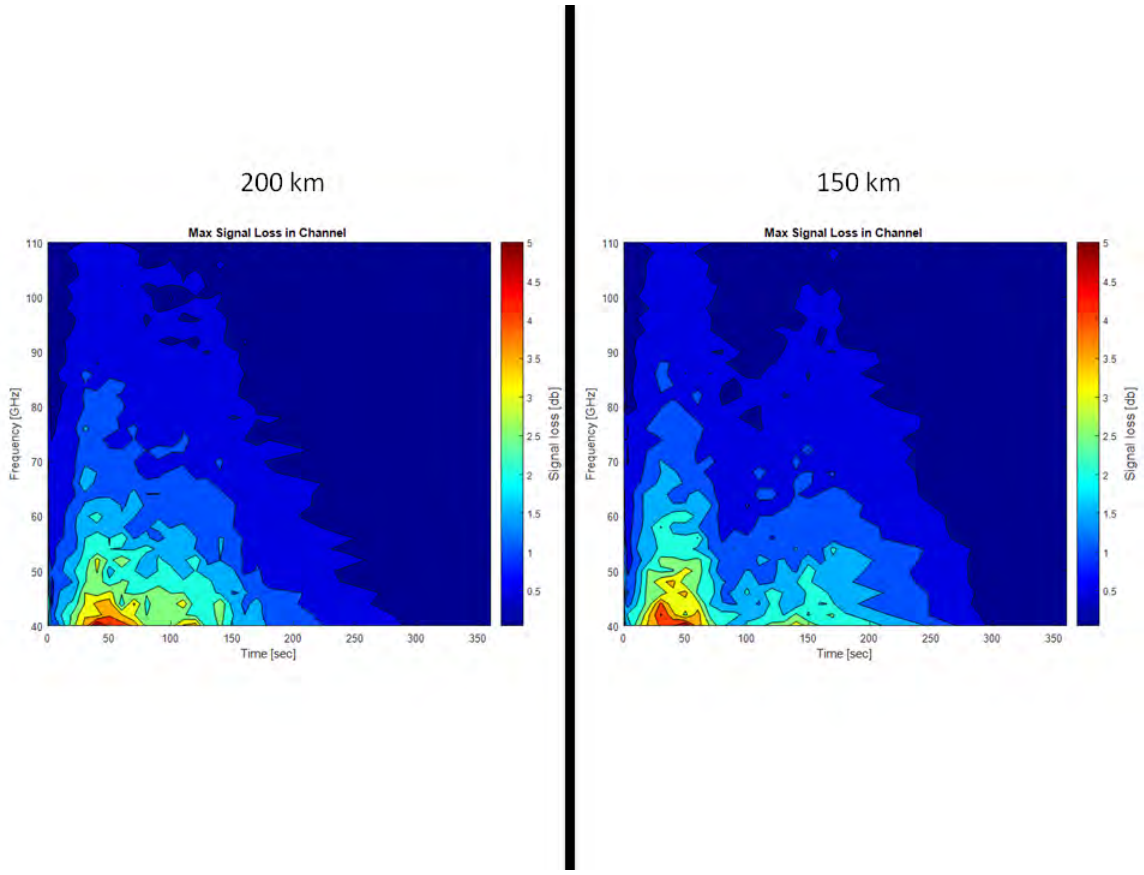

Figure 38. Comparison of maximum signal loss in a given channel from a 1 Mt yield HANE at 200 km and 150 km.

For a 2 Mt HANE located at 200 km, the absorption loss drops to less than 1 db (at 40 GHz) 30 secs after the HANE (see table 8), while scintillation loss peaks to 3.5 db (at 40 GHz) 40 secs after the HANE (see figure 39). The scintillation loss will dip to $\approx$ 2 db (at 40 GHz) 70 secs after the HANE at 200 km, rise to $\approx$ 3 db (at 40 GHz) 140 secs after the HANE at 200 km, and drop off to negligible levels 240 secs after the HANE at 200 km. Frequencies below 80 GHz have a loss up to 1 db from 140 to 240 secs after a HANE at 200km.

Signal Loss From 5 Mt.

For a 5 Mt HANE located at a height of 150 km, absorption loss dominates signal loss at 40 GHz until $\approx$ 50 secs after the HANE when absorption loss is 3.7 db (at 40 GHz) and scintillation loss is $\approx$ 5 db (see table 9 and figure 40). By 120 secs after the HANE at 150 km, the absorption loss drops to below 1 db (at 40 GHz). After absorption loss declines, a scintillation loss window occurs at 180 secs after the HANE, for signals between 40 - 50 GHz, and lasts until approximately 330 secs after the HANE. During this scintillation window, losses of up to $\approx$ 4 db can occur for signals between 40 - 50 GHz. Also, during the scintillation window, signal losses of up to $\approx$ 1 db can occur for signals up to $\approx$ 70 GHz.

As shown in table 10, absorption loss decreases to less than 1 db, 45 secs after a 5 Mt HANE located at 200km, at which time amplitude scintillation loss still remains $\approx$ 2.5 db for signals between 40 - 50 GHz (see figure 40). The scintillation loss drops to 1.5 db 80 secs after the HANE and then rises again 10 secs later, creating a scintillation loss window, and then the loss becomes $<$ 2.5 db after 240 secs after the explosion. Signals of frequencies between $\approx$ 60 - 110 GHz experience signal loss less than 1 db from a 5 Mt HANE located at 200 km.

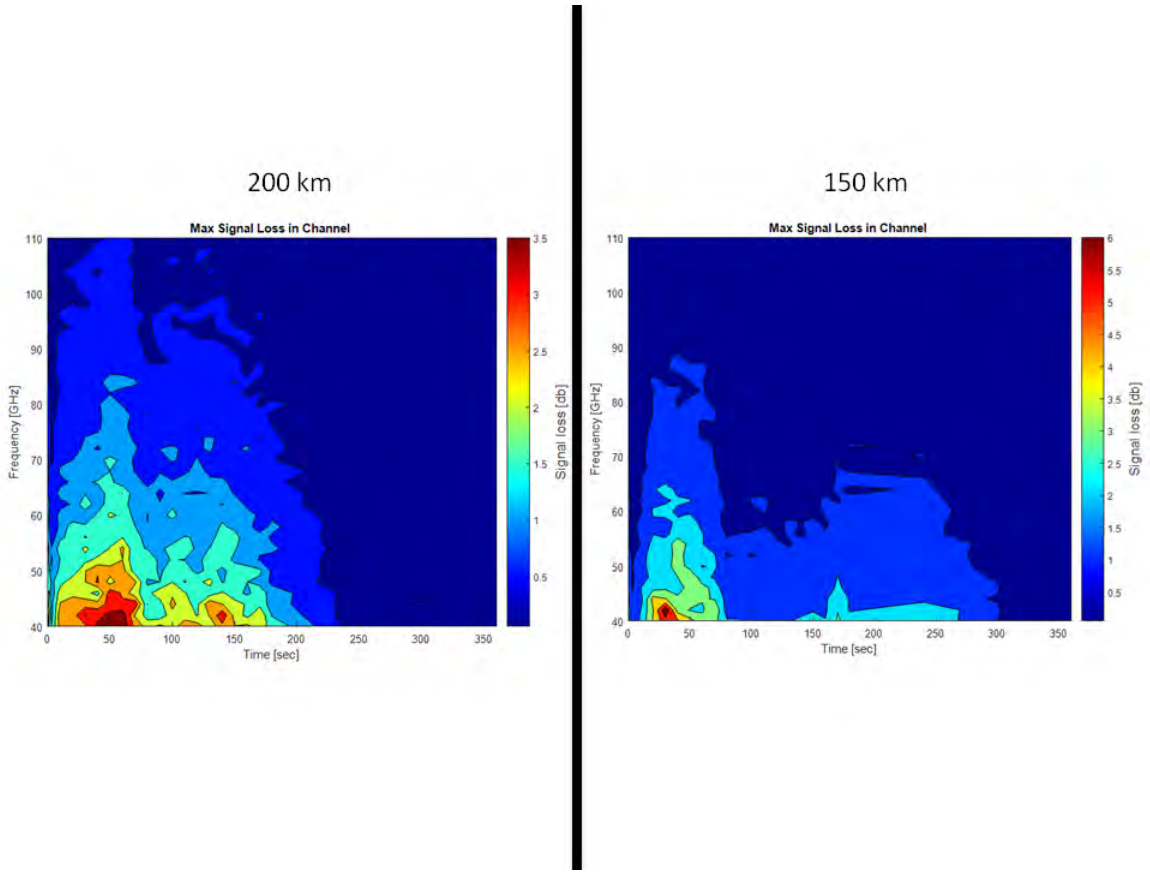

Figure 39. Comparison of maximum signal loss in a given channel from a 2 Mt yield HANE at 200 km and 150 km.

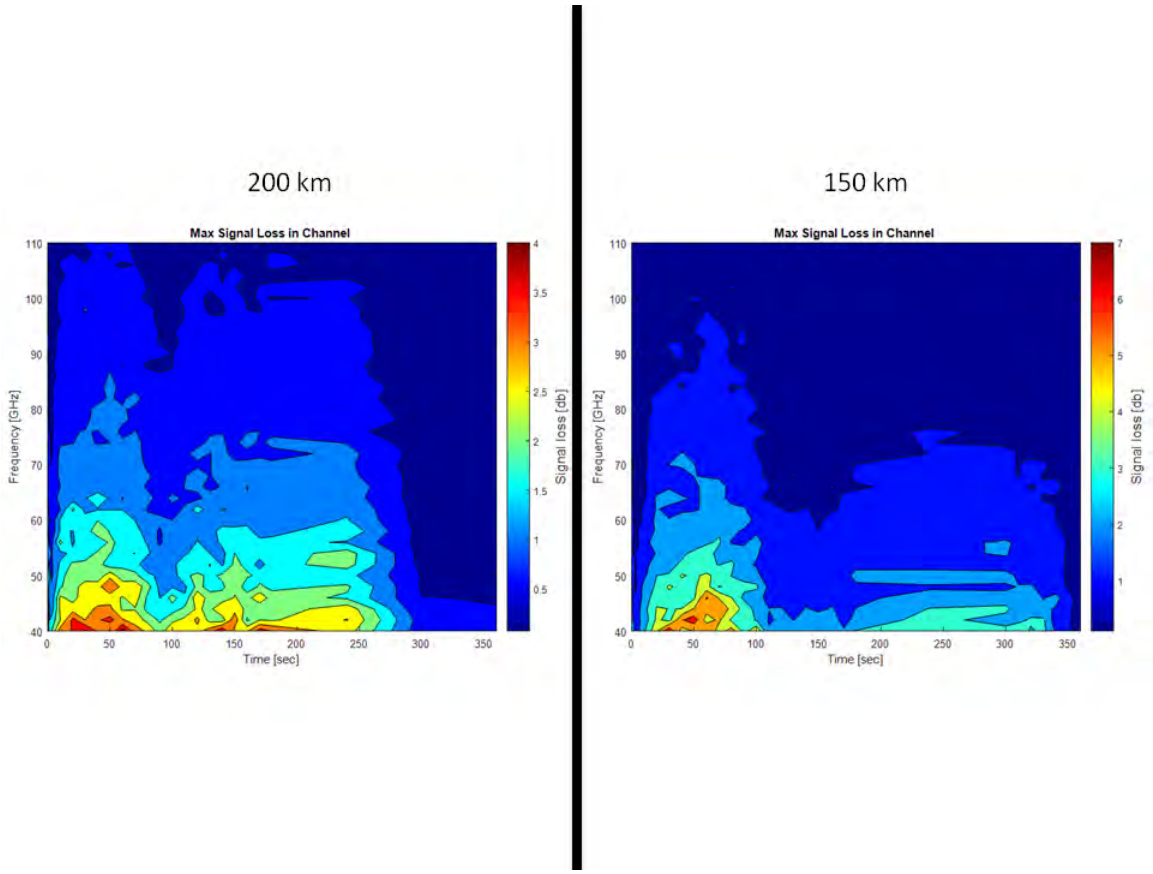

Figure 40. Comparison of maximum signal loss in a given channel from a 5 Mt yield HANE at 200 km and 150 km.

Total Amplitude Scintillation Loss Trend.

Figures 36 - 40 show that after a 5 Mt HANE an amplitude scintillation loss window will occur after the initial scintillation loss drops. This scintillation window is due to the electron distribution after the 5 Mt HANE. The greatest loss from scintillation occurs after the HANE since the electron density is high ($\geq 10^9 \frac{el^-}{cm^3}$), see figures 11 - 30). The decrease in scintillation loss occurs after the electrons begin to spread out along the magnetic lines. The scintillation loss window (clearly show in figure 39) occurs when the electrons create multiple layers of varying electron densities (figure 25), after the electrons have started to spread along the Earth's magnetic field lines.

Another trend that can be seen from figures 36 - 40 is that different frequencies experience different total power loss. For example, figure 40 shows that from 160 to 300 secs after a 5 Mt HANE at 150 km, signals at 50 GHz show greater loss then signals at 48 GHz for the same time frame.

4.6 Conclusion

In conclusion, the scenario of a natural ionosphere and a HANE disturbed ionosphere produces different results. The electron content from the natural ionosphere is at least three orders of magnitude less than the HANE disturbed environment ($10^6 \frac{el^-}{cm^3}$ compared to $10^9 \frac{el^-}{cm^3}$). Thus, as can be seen by comparing the results, the natural ionosphere will have negligible effects on frequencies for 40 - 110 GHz. In the case of the ionosphere disturbed by a HANE, the primary signal loss will come from absorption, but this loss quickly fades as time progresses during the worse case scenario (5 Mt located at 150 km) of absorption loss up to 2 min after a HANE. Interestingly, once the absorption loss drops off, an amplitude scintillation loss window appears and can provide signal loss of $\approx$ 3-4 db.

In summary the results show that high frequencies (70 - 110 GHz) are less effected by both absorption and amplitude scintillation loss. Even in the lower frequencies (40 - 60 GHz), the loss from scintillation is not very significant (3-4 db) and will have minimal to no effects on the lower frequencies 5 mins after the initial HANE (worse case scenario, i.e. 5 MT located at 150 km).

V. Conclusion

5.1 Introduction

The final chapter gives concluding remarks and provides suggestions for further research. The concluding remarks section addresses the overall conclusions of the research and places them in the context of SATCOM. The future work section offers ideas to extend the research to include loss for different antenna types and ionospheric effects on a modulated wide-band signal.

5.2 Loss from the Ionosphere

This research has focused on ionosphere propagation of EM waves in the V and W bands (40 - 110 GHz). What this research has shown is that the natural ionosphere will have little, if any, effect on these frequencies of EM waves. This is a result of the density of electrons that naturally occur in the ionosphere. The question that was investigated was what loss would occur if the electron content in the ionosphere was artificially increased due to from a HANE. The answer produced from this investigation is that loss would primarily come from absorption from the ions and electrons released from the explosion. Amplitude scintillation would cause some loss ($\leq$ 10 db), but only for frequencies below 60 GHz. Frequencies above 60 GHz would have little loss from amplitude scintillation ($\leq$ 1 db).

Signal loss after a HANE is dependent on the yield of the HANE and the frequency of the EM wave. The worst case scenario would be an EM wave transmitted at 40 GHz after a 5 Mt HANE located at 150 km. The down time from absorption would be less than 120 secs after the HANE, and while the down time from amplitude scintillation would be less than 300 secs after the HANE. The electron density of the ionosphere 300 secs after a 5 Mt HANE decreases because the electrons spread themselves along

the Earth's geomagnetic field lines. EM waves at frequencies above 60 GHz do not experience the same amount of loss as the lower operational frequencies. Therefore, after absorption loss declines, transmitting at frequencies above 60 GHz will mitigate signal loss.

5.3 Suggestions for Further Research

Loss for Specific Antennas.

This research investigated ionosphere loss as a result of amplitude scintillation and absorption after a HANE at varying altitudes and at various yields. In order to better understand the loss for the ionosphere, a plane wave was used in the propagation model. No antenna designs were considered. An extension to this work would be to understand the effects a receiving antenna would have on a received signal, given the same scenarios.

Antennas collect EM energy that is incident upon the antenna and delivers it to the receiver. An antenna in receive mode delivers only the EM energy that is accepted from a narrow range of angles, and while in transmit mode, the antenna transmits an EM wave over a small angular region. When a scintillated EM wave's energy arrives at angles greater than the receiving antenna can accept, the receiver will experience loss from angle scattering due to the antenna and the scintillating medium [36]. Thus, an investigation in the angle scattering loss from an antenna should be investigated.

Non-Earth normal signal loss.

This research was limited to studying signals that were earth normal in direction (in other words, the domain was limited to the area directly above the Earth located transmitter). An important aspect that needs to be researched is propagation directions that are not normal to the earth. Satellites are not stationary and therefore,

the transmit direction is other than normal from the transmitter. As a satellite orbits the earth the transmit path will change. The transmit could contain more nuclear debris or less depending on the location of the satellite. Thus, follow-on research is needed to understand the effects of the HANE environment on a constantly changing transmit path.

Wide-band Signal Effects.

This research has shown that the ionosphere disturbed from a HANE can have effects on signals of different frequencies. For example, a 48 GHz signal may not be affected much by amplitude scintillation while a signal at 50 GHz is affected. Thus, the ionosphere can be frequency selective to frequencies close to (within a $\approx$ 1-2 GHz) a carrier frequency of an EM wave. Wide-band signals that use frequency hopping will not be affected from the frequency selectiveness of the ionosphere since a frequency hopping signal is essentially a narrow-band signal that changes the carrier wave frequency, but a wide-band signal with a spread spectrum, such as code division multiple access (CDMA) would be affected by the ionosphere.

Another aspect of wide band signals that needs to be investigated is the effects of dispersion from the ionosphere. Dispersion is signal distortion caused by the phase velocity of the EM wave being different than the group velocity. Thus, a wide-band signal is susceptible to the dispersion since the signal contains a large amount of frequencies.

5.4 Conclusion

In conclusion, the natural ionosphere signal loss will be negligible for signals in the V and W bands. In an ionosphere that has been artificially disturbed, brought about by a HANE, the worst case scenario is that SATCOM downtime from signal loss

would only occur in the first 300 secs after a HANE. Further research that should be investigated is understanding the loss demonstrated from different receiving antenna and the effects on wide-band signals, such as CDMA.

Appendix A. S4 Scintillation Index Tables

This appendix contains S_4 scintillation indices for the different HANE magnitudes and hieghts that were calculated from the SSFM model.

Table 11. S_4 index values for 100 kt HANE at 200 km

	S_4 Scintillation Index							
	40 GHz	50 GHz	60 GHz	70 GHz	80 GHz	90 GHz	100 GHz	110 GHz
10 sec	0.20	0.16	0.13	0.12	0.10	0.09	0.07	0.07
20 sec	0.22	0.18	0.15	0.13	0.11	0.10	0.10	0.08
30 sec	0.26	0.22	0.17	0.15	0.14	0.11	0.10	0.10
40 sec	0.23	0.19	0.16	0.13	0.11	0.10	0.09	0.08
50 sec	0.18	0.17	0.14	0.12	0.11	0.10	0.09	0.08
60 sec	0.24	0.21	0.16	0.14	0.13	0.12	0.11	0.09
70 sec	0.23	0.19	0.14	0.14	0.13	0.11	0.09	0.08
80 sec	0.17	0.13	0.11	0.10	0.09	0.08	0.07	0.07
90 sec	0.14	0.10	0.10	0.07	0.08	0.06	0.05	0.05
100 sec	0.13	0.11	0.08	0.08	0.07	0.05	0.05	0.05
110 sec	0.12	0.11	0.09	0.07	0.07	0.06	0.05	0.04
120 sec	0.12	0.10	0.09	0.08	0.07	0.06	0.05	0.04
130 sec	0.14	0.10	0.08	0.07	0.06	0.06	0.05	0.05
140 sec	0.11	0.11	0.08	0.07	0.06	0.06	0.05	0.05
150 sec	0.12	0.10	0.09	0.07	0.06	0.06	0.04	0.04
160 sec	0.11	0.09	0.08	0.07	0.05	0.05	0.05	0.05
170 sec	0.11	0.09	0.07	0.06	0.06	0.05	0.04	0.04
180 sec	0.11	0.09	0.07	0.07	0.05	0.05	0.05	0.04
240 sec	0.09	0.07	0.06	0.05	0.05	0.04	0.03	0.03
300 sec	0.04	0.03	0.03	0.02	0.02	0.02	0.02	0.01

Table 12. S_4 index values for 100 kt HANE at 150 km

	S_4 Scintillation Index							
	40 GHz	50 GHz	60 GHz	70 GHz	80 GHz	90 GHz	100 GHz	110 GHz
10 sec	0.08	0.06	0.05	0.03	0.02	0.01	0.01	0.01
20 sec	0.11	0.06	0.05	0.03	0.02	0.02	0.02	0.02
30 sec	0.12	0.06	0.06	0.04	0.03	0.03	0.02	0.02
40 sec	0.12	0.06	0.04	0.03	0.02	0.02	0.01	0.01
50 sec	0.10	0.07	0.04	0.04	0.02	0.02	0.02	0.02
60 sec	0.11	0.07	0.06	0.04	0.04	0.02	0.02	0.01
70 sec	0.10	0.07	0.05	0.03	0.03	0.02	0.01	0.01
80 sec	0.10	0.05	0.04	0.03	0.02	0.02	0.02	0.01
90 sec	0.10	0.06	0.04	0.03	0.02	0.01	0.02	0.01
100 sec	0.10	0.05	0.04	0.03	0.02	0.02	0.02	0.01
110 sec	0.07	0.05	0.03	0.02	0.02	0.01	0.01	0.01
120 sec	0.10	0.05	0.05	0.03	0.02	0.02	0.01	0.01
130 sec	0.06	0.05	0.04	0.02	0.02	0.01	0.01	0.01
140 sec	0.07	0.05	0.03	0.02	0.02	0.01	0.01	0.01
150 sec	0.07	0.04	0.03	0.02	0.02	0.01	0.01	0.01
160 sec	0.07	0.04	0.03	0.02	0.02	0.01	0.01	0.01
170 sec	0.05	0.03	0.02	0.02	0.01	0.01	0.01	0.01
180 sec	0.05	0.03	0.02	0.01	0.01	0.01	0.01	0.01
240 sec	0.01	0.01	0.01	0.00	0.00	0.00	0.00	0.00
300 sec	0.01	0.01	0.01	0.00	0.00	0.00	0.00	0.00

Table 13. S_4 index values for 500 kt HANE at 200 km

	S_4 Scintillation Index							
	40 GHz	50 GHz	60 GHz	70 GHz	80 GHz	90 GHz	100 GHz	110 GHz
10 sec	0.09	0.05	0.03	0.03	0.02	0.02	0.01	0.01
20 sec	0.11	0.07	0.04	0.03	0.03	0.02	0.01	0.02
30 sec	0.24	0.14	0.10	0.07	0.05	0.04	0.04	0.03
40 sec	0.20	0.14	0.09	0.07	0.04	0.03	0.03	0.02
50 sec	0.22	0.12	0.08	0.05	0.04	0.03	0.03	0.03
60 sec	0.22	0.11	0.09	0.06	0.05	0.04	0.03	0.03
70 sec	0.14	0.13	0.08	0.05	0.05	0.04	0.03	0.03
80 sec	0.16	0.13	0.07	0.06	0.04	0.03	0.03	0.03
90 sec	0.18	0.10	0.07	0.07	0.05	0.03	0.03	0.03
100 sec	0.16	0.12	0.07	0.05	0.04	0.03	0.03	0.02
110 sec	0.13	0.08	0.06	0.04	0.04	0.03	0.02	0.02
120 sec	0.13	0.08	0.06	0.05	0.03	0.03	0.02	0.02
130 sec	0.12	0.07	0.05	0.03	0.02	0.02	0.02	0.02
140 sec	0.11	0.07	0.04	0.03	0.03	0.01	0.02	0.01
150 sec	0.07	0.05	0.04	0.02	0.02	0.02	0.01	0.01
160 sec	0.07	0.05	0.04	0.02	0.02	0.01	0.01	0.01
170 sec	0.07	0.04	0.02	0.03	0.01	0.01	0.01	0.01
180 sec	0.03	0.02	0.02	0.01	0.01	0.01	0.01	0.00
240 sec	0.02	0.01	0.01	0.01	0.00	0.00	0.00	0.00
300 sec	0.01	0.01	0.01	0.01	0.00	0.00	0.00	0.00

Table 14. S_4 index values for 500 kt HANE at 150 km

	S_4 Scintillation Index							
	40 GHz	50 GHz	60 GHz	70 GHz	80 GHz	90 GHz	100 GHz	110 GHz
10 sec	0.11	0.08	0.05	0.04	0.03	0.02	0.02	0.01
20 sec	0.16	0.13	0.07	0.07	0.05	0.03	0.02	0.02
30 sec	0.24	0.11	0.11	0.06	0.04	0.04	0.04	0.03
40 sec	0.21	0.16	0.11	0.07	0.06	0.04	0.04	0.02
50 sec	0.20	0.09	0.07	0.05	0.04	0.03	0.02	0.02
60 sec	0.16	0.08	0.06	0.05	0.04	0.02	0.02	0.02
70 sec	0.14	0.08	0.05	0.05	0.03	0.03	0.02	0.02
80 sec	0.15	0.10	0.07	0.06	0.04	0.03	0.02	0.02
90 sec	0.19	0.10	0.06	0.05	0.04	0.04	0.02	0.02
100 sec	0.13	0.11	0.05	0.04	0.05	0.03	0.02	0.02
110 sec	0.17	0.09	0.06	0.06	0.04	0.03	0.03	0.02
120 sec	0.15	0.09	0.07	0.06	0.04	0.03	0.02	0.02
130 sec	0.14	0.08	0.06	0.05	0.04	0.03	0.02	0.02
140 sec	0.13	0.08	0.06	0.05	0.03	0.03	0.02	0.01
150 sec	0.09	0.08	0.07	0.03	0.03	0.02	0.02	0.01
160 sec	0.10	0.06	0.04	0.02	0.02	0.02	0.02	0.01
170 sec	0.10	0.06	0.04	0.03	0.02	0.02	0.01	0.01
180 sec	0.09	0.06	0.03	0.03	0.02	0.02	0.01	0.01
240 sec	0.04	0.02	0.02	0.01	0.01	0.01	0.01	0.00
300 sec	0.01	0.01	0.01	0.00	0.00	0.00	0.00	0.00

Table 15. S_4 index values for 1 Mt HANE at 200 km

	S_4 Scintillation Index							
	40 GHz	50 GHz	60 GHz	70 GHz	80 GHz	90 GHz	100 GHz	110 GHz
10 sec	0.1	0.08	0.05	0.03	0.02	0.02	0.01	0.01
20 sec	0.15	0.09	0.07	0.05	0.04	0.04	0.02	0.02
30 sec	0.21	0.15	0.11	0.07	0.05	0.05	0.04	0.03
40 sec	0.28	0.16	0.11	0.08	0.07	0.04	0.03	0.04
50 sec	0.21	0.11	0.09	0.07	0.06	0.05	0.04	0.03
60 sec	0.25	0.14	0.08	0.07	0.05	0.04	0.03	0.03
70 sec	0.2	0.11	0.09	0.06	0.04	0.05	0.03	0.02
80 sec	0.19	0.1	0.06	0.05	0.04	0.03	0.03	0.02
90 sec	0.19	0.11	0.07	0.05	0.05	0.04	0.03	0.02
100 sec	0.17	0.11	0.06	0.05	0.04	0.03	0.02	0.03
110 sec	0.2	0.09	0.07	0.05	0.04	0.04	0.03	0.02
120 sec	0.19	0.11	0.06	0.05	0.04	0.03	0.02	0.02
130 sec	0.14	0.09	0.06	0.05	0.04	0.03	0.02	0.02
140 sec	0.14	0.1	0.06	0.05	0.04	0.03	0.03	0.02
150 sec	0.11	0.09	0.05	0.04	0.03	0.03	0.02	0.02
160 sec	0.09	0.05	0.05	0.04	0.03	0.02	0.02	0.01
170 sec	0.1	0.06	0.04	0.03	0.02	0.02	0.02	0.01
180 sec	0.08	0.04	0.03	0.03	0.02	0.02	0.01	0.01
240 sec	0.04	0.02	0.02	0.01	0.01	0.01	0.01	0.01
300 sec	0.01	0.01	0.01	0	0	0	0	0

Table 16. S_4 index values for 1 Mt HANE at 150 km

	S_4 Scintillation Index							
	40 GHz	50 GHz	60 GHz	70 GHz	80 GHz	90 GHz	100 GHz	110 GHz
10 sec	0.14	0.08	0.06	0.04	0.03	0.03	0.02	0.02
20 sec	0.22	0.14	0.09	0.06	0.05	0.04	0.03	0.03
30 sec	0.25	0.15	0.10	0.08	0.06	0.05	0.05	0.03
40 sec	0.26	0.16	0.11	0.06	0.07	0.05	0.03	0.03
50 sec	0.28	0.17	0.13	0.07	0.06	0.05	0.04	0.03
60 sec	0.25	0.15	0.10	0.06	0.05	0.04	0.03	0.03
70 sec	0.19	0.10	0.07	0.06	0.04	0.03	0.03	0.02
80 sec	0.12	0.07	0.05	0.03	0.03	0.02	0.02	0.01
90 sec	0.10	0.06	0.05	0.04	0.03	0.03	0.02	0.01
100 sec	0.12	0.08	0.05	0.04	0.03	0.02	0.02	0.01
110 sec	0.15	0.08	0.05	0.04	0.03	0.02	0.02	0.02
120 sec	0.13	0.08	0.05	0.04	0.03	0.02	0.02	0.02
130 sec	0.14	0.09	0.06	0.04	0.03	0.03	0.02	0.02
140 sec	0.20	0.08	0.05	0.06	0.03	0.03	0.03	0.02
150 sec	0.17	0.11	0.06	0.04	0.05	0.03	0.03	0.02
160 sec	0.14	0.10	0.06	0.05	0.04	0.03	0.03	0.02
170 sec	0.16	0.09	0.06	0.04	0.03	0.03	0.02	0.02
180 sec	0.15	0.09	0.06	0.04	0.03	0.02	0.02	0.02
240 sec	0.09	0.04	0.04	0.03	0.02	0.01	0.01	0.01
300 sec	0.02	0.01	0.01	0.01	0.00	0.00	0.00	0.00

Table 17. S_4 index values for 2 Mt HANE at 200 km

	S_4 Scintillation Index							
	40 GHz	50 GHz	60 GHz	70 GHz	80 GHz	90 GHz	100 GHz	110 GHz
10 sec	0.18	0.09	0.06	0.05	0.03	0.03	0.02	0.02
20 sec	0.20	0.10	0.06	0.06	0.04	0.03	0.03	0.03
30 sec	0.20	0.13	0.06	0.06	0.04	0.04	0.03	0.02
40 sec	0.21	0.16	0.10	0.08	0.05	0.04	0.03	0.02
50 sec	0.22	0.16	0.11	0.09	0.06	0.05	0.03	0.03
60 sec	0.23	0.15	0.11	0.08	0.05	0.05	0.04	0.03
70 sec	0.17	0.10	0.08	0.05	0.04	0.03	0.02	0.02
80 sec	0.15	0.09	0.05	0.05	0.03	0.02	0.02	0.02
90 sec	0.15	0.08	0.07	0.05	0.03	0.03	0.02	0.02
100 sec	0.14	0.10	0.08	0.05	0.04	0.03	0.02	0.02
110 sec	0.14	0.09	0.06	0.05	0.03	0.03	0.02	0.02
120 sec	0.16	0.09	0.07	0.05	0.04	0.03	0.03	0.02
130 sec	0.14	0.10	0.07	0.05	0.03	0.03	0.02	0.02
140 sec	0.17	0.08	0.07	0.06	0.03	0.03	0.02	0.03
150 sec	0.15	0.10	0.07	0.04	0.04	0.03	0.02	0.02
160 sec	0.16	0.08	0.06	0.03	0.04	0.02	0.02	0.02
170 sec	0.12	0.08	0.05	0.04	0.02	0.02	0.02	0.01
180 sec	0.10	0.05	0.04	0.03	0.03	0.02	0.01	0.01
240 sec	0.02	0.02	0.01	0.01	0.01	0.00	0.00	0.00
300 sec	0.02	0.01	0.01	0.01	0.00	0.00	0.00	0.00

Table 18. S_4 index values for 2 Mt HANE at 150 km

	S_4 Scintillation Index							
	40 GHz	50 GHz	60 GHz	70 GHz	80 GHz	90 GHz	100 GHz	110 GHz
10 sec	0.13	0.09	0.05	0.04	0.03	0.02	0.02	0.02
20 sec	0.27	0.15	0.11	0.09	0.06	0.04	0.04	0.03
30 sec	0.29	0.16	0.13	0.10	0.07	0.05	0.04	0.03
40 sec	0.33	0.20	0.10	0.08	0.05	0.05	0.04	0.04
50 sec	0.27	0.18	0.11	0.10	0.06	0.05	0.03	0.03
60 sec	0.22	0.12	0.08	0.08	0.06	0.04	0.03	0.03
70 sec	0.18	0.12	0.08	0.05	0.04	0.03	0.03	0.02
80 sec	0.11	0.06	0.04	0.03	0.03	0.02	0.01	0.01
90 sec	0.12	0.05	0.04	0.03	0.03	0.02	0.02	0.01
100 sec	0.08	0.06	0.04	0.04	0.02	0.02	0.01	0.01
110 sec	0.09	0.07	0.06	0.04	0.02	0.02	0.02	0.02
120 sec	0.08	0.07	0.04	0.03	0.03	0.02	0.01	0.01
130 sec	0.11	0.07	0.04	0.04	0.02	0.02	0.02	0.01
140 sec	0.13	0.08	0.05	0.05	0.03	0.02	0.02	0.02
150 sec	0.14	0.09	0.05	0.05	0.03	0.02	0.02	0.01
160 sec	0.12	0.08	0.06	0.04	0.03	0.02	0.02	0.02
170 sec	0.17	0.09	0.07	0.05	0.03	0.03	0.03	0.02
180 sec	0.16	0.11	0.06	0.05	0.03	0.03	0.02	0.02
240 sec	0.16	0.09	0.07	0.05	0.04	0.03	0.03	0.02
300 sec	0.05	0.04	0.03	0.02	0.01	0.01	0.01	0.01

Table 19. S_4 index values for 5 Mt HANE at 200 km

	S_4 Scintillation Index							
	40 GHz	50 GHz	60 GHz	70 GHz	80 GHz	90 GHz	100 GHz	110 GHz
10 sec	0.17	0.11	0.09	0.06	0.05	0.03	0.03	0.03
20 sec	0.2	0.13	0.09	0.06	0.05	0.03	0.04	0.03
30 sec	0.23	0.13	0.09	0.06	0.05	0.04	0.03	0.03
40 sec	0.19	0.12	0.11	0.08	0.06	0.04	0.03	0.03
50 sec	0.2	0.17	0.1	0.08	0.06	0.04	0.03	0.03
60 sec	0.23	0.13	0.1	0.06	0.06	0.04	0.03	0.03
70 sec	0.17	0.13	0.09	0.08	0.05	0.04	0.03	0.03
80 sec	0.17	0.11	0.06	0.05	0.04	0.03	0.02	0.02
90 sec	0.13	0.08	0.05	0.04	0.03	0.02	0.02	0.01
100 sec	0.14	0.08	0.06	0.04	0.04	0.03	0.02	0.01
110 sec	0.15	0.1	0.07	0.03	0.04	0.03	0.03	0.02
120 sec	0.13	0.12	0.06	0.05	0.03	0.03	0.03	0.03
130 sec	0.17	0.09	0.08	0.05	0.03	0.03	0.02	0.02
140 sec	0.2	0.13	0.07	0.06	0.04	0.03	0.03	0.02
150 sec	0.18	0.11	0.07	0.05	0.04	0.04	0.03	0.02
160 sec	0.16	0.11	0.07	0.06	0.04	0.03	0.02	0.02
170 sec	0.22	0.11	0.06	0.06	0.04	0.03	0.03	0.02
180 sec	0.19	0.1	0.06	0.06	0.05	0.03	0.03	0.02
240 sec	0.17	0.1	0.08	0.06	0.04	0.04	0.03	0.02
300 sec	0.03	0.02	0.01	0.01	0.01	0.01	0	0.01

Table 20. S_4 index values for 5 Mt HANE at 150 km

	S_4 Scintillation Index							
	40 GHz	50 GHz	60 GHz	70 GHz	80 GHz	90 GHz	100 GHz	110 GHz
10 sec	0.18	0.10	0.07	0.04	0.04	0.03	0.03	0.02
20 sec	0.28	0.19	0.14	0.09	0.06	0.05	0.04	0.03
30 sec	0.42	0.17	0.14	0.11	0.07	0.05	0.04	0.04
40 sec	0.35	0.23	0.14	0.13	0.07	0.06	0.04	0.04
50 sec	0.32	0.22	0.12	0.11	0.08	0.04	0.06	0.05
60 sec	0.38	0.25	0.13	0.09	0.07	0.07	0.05	0.04
70 sec	0.30	0.24	0.14	0.10	0.08	0.06	0.05	0.03
80 sec	0.31	0.18	0.13	0.11	0.06	0.05	0.05	0.04
90 sec	0.23	0.16	0.13	0.08	0.05	0.05	0.05	0.04
100 sec	0.27	0.14	0.09	0.07	0.04	0.04	0.04	0.02
110 sec	0.12	0.07	0.06	0.04	0.03	0.02	0.02	0.02
120 sec	0.12	0.08	0.07	0.04	0.03	0.02	0.02	0.02
130 sec	0.15	0.08	0.06	0.04	0.04	0.02	0.02	0.02
140 sec	0.11	0.08	0.07	0.05	0.04	0.03	0.02	0.02
150 sec	0.11	0.08	0.05	0.04	0.03	0.03	0.02	0.02
160 sec	0.13	0.10	0.06	0.05	0.03	0.02	0.02	0.01
170 sec	0.12	0.09	0.06	0.04	0.03	0.02	0.02	0.01
180 sec	0.18	0.13	0.07	0.06	0.03	0.03	0.02	0.02
240 sec	0.20	0.13	0.08	0.06	0.04	0.03	0.03	0.02
300 sec	0.21	0.13	0.08	0.06	0.04	0.03	0.03	0.02

Appendix B. Mean Signal Loss Tables

This appendix contains tables of the mean signal loss for a given channel. The tables include data from all HANE scenarios.

Table 21. Mean signal loss caused by amplitude scintillation for a 100 kt HANE at 200 km

	Mean Signal Loss (dB)							
	40 GHz	50 GHz	60 GHz	70 GHz	80 GHz	90 GHz	100 GHz	110 GHz
10 sec	0.405	0.226	0.159	0.125	0.100	0.082	0.057	0.050
20 sec	0.466	0.308	0.247	0.164	0.111	0.097	0.091	0.065
30 sec	0.648	0.432	0.282	0.220	0.147	0.118	0.108	0.089
40 sec	0.521	0.390	0.287	0.167	0.126	0.101	0.080	0.066
50 sec	0.343	0.275	0.192	0.143	0.117	0.090	0.075	0.058
60 sec	0.582	0.430	0.255	0.216	0.163	0.126	0.114	0.080
70 sec	0.509	0.343	0.219	0.172	0.163	0.111	0.087	0.072
80 sec	0.275	0.180	0.125	0.095	0.077	0.063	0.046	0.042
90 sec	0.186	0.106	0.083	0.055	0.050	0.036	0.028	0.023
100 sec	0.157	0.110	0.069	0.054	0.046	0.028	0.027	0.022
110 sec	0.151	0.099	0.071	0.052	0.044	0.033	0.027	0.021
120 sec	0.150	0.105	0.069	0.053	0.043	0.030	0.023	0.020
130 sec	0.173	0.093	0.076	0.044	0.038	0.033	0.025	0.019
140 sec	0.129	0.091	0.066	0.044	0.038	0.031	0.022	0.021
150 sec	0.146	0.087	0.064	0.050	0.036	0.030	0.020	0.016
160 sec	0.131	0.088	0.061	0.041	0.029	0.030	0.025	0.020
170 sec	0.131	0.091	0.054	0.041	0.033	0.028	0.021	0.017
180 sec	0.125	0.082	0.058	0.050	0.033	0.024	0.021	0.016
240 sec	0.082	0.054	0.036	0.030	0.025	0.019	0.013	0.012
300 sec	0.019	0.011	0.008	0.005	0.005	0.003	0.002	0.002

Table 22. Mean signal loss caused by amplitude scintillation for a 100 kt HANE at 150 km

	Mean Signal Loss (dB)							
	40 GHz	50 GHz	60 GHz	70 GHz	80 GHz	90 GHz	100 GHz	110 GHz
10 sec	0.825	0.617	0.422	0.259	0.184	0.158	0.122	0.101
20 sec	1.065	0.592	0.472	0.323	0.237	0.181	0.190	0.143
30 sec	1.132	0.683	0.457	0.384	0.270	0.239	0.161	0.159
40 sec	1.070	0.596	0.443	0.285	0.229	0.178	0.141	0.120
50 sec	0.903	0.728	0.385	0.346	0.255	0.196	0.159	0.154
60 sec	1.005	0.699	0.504	0.349	0.310	0.207	0.176	0.150
70 sec	0.947	0.649	0.463	0.307	0.286	0.182	0.141	0.120
80 sec	0.883	0.525	0.376	0.284	0.228	0.162	0.127	0.122
90 sec	0.764	0.474	0.380	0.259	0.204	0.157	0.138	0.104
100 sec	0.980	0.516	0.388	0.273	0.206	0.178	0.155	0.121
110 sec	0.670	0.483	0.342	0.230	0.161	0.143	0.132	0.116
120 sec	0.908	0.534	0.403	0.285	0.200	0.169	0.144	0.093
130 sec	0.654	0.489	0.370	0.252	0.178	0.129	0.135	0.091
140 sec	0.636	0.439	0.342	0.228	0.177	0.134	0.106	0.110
150 sec	0.614	0.412	0.271	0.215	0.167	0.123	0.089	0.071
160 sec	0.645	0.396	0.288	0.217	0.168	0.124	0.125	0.072
170 sec	0.510	0.310	0.228	0.173	0.137	0.092	0.085	0.064
180 sec	0.436	0.295	0.192	0.133	0.104	0.071	0.062	0.048
240 sec	0.111	0.071	0.054	0.038	0.027	0.021	0.018	0.015
300 sec	0.100	0.068	0.053	0.035	0.030	0.020	0.013	0.012

Table 23. Mean signal loss caused by amplitude scintillation for a 500 kt HANE at 200 km

	Mean Signal Loss (dB)							
	40 GHz	50 GHz	60 GHz	70 GHz	80 GHz	90 GHz	100 GHz	110 GHz
10 sec	0.863	0.454	0.338	0.271	0.206	0.163	0.123	0.097
20 sec	1.048	0.579	0.387	0.325	0.251	0.182	0.154	0.147
30 sec	2.109	1.280	0.915	0.655	0.539	0.345	0.292	0.278
40 sec	1.753	1.282	0.836	0.676	0.415	0.365	0.290	0.205
50 sec	1.855	1.185	0.767	0.528	0.430	0.345	0.327	0.289
60 sec	1.896	1.043	0.817	0.572	0.506	0.381	0.292	0.264
70 sec	1.380	1.178	0.713	0.467	0.476	0.336	0.278	0.245
80 sec	1.450	1.183	0.699	0.526	0.409	0.333	0.280	0.250
90 sec	1.551	1.029	0.683	0.588	0.410	0.284	0.248	0.227
100 sec	1.412	1.092	0.577	0.532	0.412	0.269	0.260	0.190
110 sec	1.244	0.695	0.543	0.406	0.379	0.296	0.215	0.172
120 sec	1.256	0.806	0.561	0.473	0.265	0.240	0.205	0.157
130 sec	1.085	0.666	0.469	0.356	0.219	0.232	0.187	0.144
140 sec	0.923	0.554	0.395	0.286	0.238	0.150	0.166	0.132
150 sec	0.780	0.476	0.359	0.256	0.194	0.172	0.130	0.114
160 sec	0.726	0.486	0.311	0.201	0.174	0.125	0.108	0.088
170 sec	0.669	0.447	0.260	0.222	0.150	0.136	0.122	0.093
180 sec	0.299	0.204	0.132	0.098	0.079	0.064	0.055	0.049
240 sec	0.167	0.089	0.076	0.056	0.039	0.034	0.023	0.020
300 sec	0.121	0.093	0.061	0.045	0.028	0.025	0.021	0.017

Table 24. Mean signal loss caused by amplitude scintillation for a 500 kt HANE at 150 km

	Mean Signal Loss (dB)							
	40 GHz	50 GHz	60 GHz	70 GHz	80 GHz	90 GHz	100 GHz	110 GHz
10 sec	0.988	0.762	0.467	0.403	0.286	0.249	0.179	0.146
20 sec	1.472	1.175	0.722	0.568	0.457	0.366	0.255	0.228
30 sec	1.903	1.071	0.944	0.655	0.441	0.355	0.330	0.247
40 sec	1.896	1.395	0.988	0.630	0.493	0.365	0.341	0.246
50 sec	1.754	0.946	0.638	0.490	0.394	0.300	0.252	0.236
60 sec	1.377	0.834	0.589	0.458	0.333	0.258	0.223	0.192
70 sec	1.354	0.806	0.572	0.416	0.325	0.283	0.209	0.173
80 sec	1.293	1.039	0.648	0.480	0.393	0.280	0.218	0.191
90 sec	1.490	0.955	0.661	0.494	0.364	0.352	0.229	0.208
100 sec	1.276	0.991	0.557	0.396	0.369	0.261	0.228	0.197
110 sec	1.544	0.980	0.647	0.573	0.401	0.307	0.264	0.227
120 sec	1.459	0.881	0.590	0.492	0.337	0.272	0.217	0.176
130 sec	1.323	0.783	0.575	0.436	0.336	0.267	0.230	0.167
140 sec	1.224	0.755	0.559	0.465	0.284	0.287	0.222	0.163
150 sec	0.963	0.679	0.567	0.340	0.292	0.233	0.179	0.137
160 sec	0.966	0.664	0.409	0.263	0.246	0.186	0.151	0.129
170 sec	0.956	0.565	0.387	0.296	0.209	0.186	0.135	0.138
180 sec	0.873	0.520	0.291	0.277	0.209	0.169	0.127	0.105
240 sec	0.393	0.235	0.164	0.136	0.104	0.072	0.060	0.051
300 sec	0.132	0.096	0.061	0.045	0.032	0.028	0.020	0.016

Table 25. Mean signal loss caused by amplitude scintillation for a 1 Mt HANE at 200 km

	Mean Signal Loss (dB)							
	40 GHz	50 GHz	60 GHz	70 GHz	80 GHz	90 GHz	100 GHz	110 GHz
10 sec	0.989	0.679	0.435	0.335	0.249	0.218	0.132	0.131
20 sec	1.328	0.822	0.674	0.453	0.338	0.325	0.229	0.195
30 sec	1.925	1.334	1.003	0.580	0.518	0.463	0.372	0.297
40 sec	2.109	1.308	0.956	0.814	0.625	0.461	0.358	0.346
50 sec	1.674	1.124	0.905	0.672	0.490	0.460	0.312	0.266
60 sec	2.088	1.275	0.814	0.621	0.468	0.416	0.340	0.275
70 sec	1.716	1.106	0.832	0.579	0.413	0.419	0.323	0.245
80 sec	1.702	0.993	0.629	0.475	0.447	0.303	0.298	0.196
90 sec	1.750	1.007	0.712	0.484	0.386	0.331	0.276	0.194
100 sec	1.532	1.060	0.583	0.467	0.361	0.297	0.233	0.248
110 sec	1.644	0.855	0.699	0.464	0.386	0.362	0.302	0.229
120 sec	1.485	0.945	0.586	0.514	0.371	0.318	0.232	0.169
130 sec	1.246	0.869	0.615	0.486	0.339	0.271	0.201	0.194
140 sec	1.282	0.930	0.613	0.493	0.408	0.291	0.238	0.213
150 sec	1.130	0.805	0.461	0.462	0.271	0.262	0.199	0.160
160 sec	0.870	0.504	0.436	0.361	0.227	0.182	0.182	0.124
170 sec	0.904	0.545	0.373	0.268	0.225	0.212	0.148	0.136
180 sec	0.733	0.458	0.321	0.274	0.200	0.173	0.116	0.119
240 sec	0.456	0.229	0.196	0.118	0.105	0.104	0.065	0.062
300 sec	0.139	0.108	0.067	0.043	0.044	0.030	0.026	0.017

Table 26. Mean signal loss caused by amplitude scintillation for a 1 Mt HANE at 150 km

	Mean Signal Loss (dB)							
	40 GHz	50 GHz	60 GHz	70 GHz	80 GHz	90 GHz	100 GHz	110 GHz
10 sec	1.170	0.803	0.616	0.388	0.294	0.261	0.211	0.187
20 sec	1.876	1.217	0.780	0.615	0.511	0.443	0.308	0.268
30 sec	2.061	1.439	0.915	0.700	0.598	0.450	0.389	0.290
40 sec	2.226	1.315	0.970	0.656	0.582	0.416	0.340	0.280
50 sec	2.391	1.410	1.033	0.710	0.541	0.430	0.363	0.347
60 sec	2.211	1.285	0.881	0.572	0.469	0.424	0.276	0.294
70 sec	1.743	0.986	0.623	0.551	0.421	0.265	0.275	0.211
80 sec	1.096	0.669	0.465	0.337	0.307	0.241	0.182	0.140
90 sec	0.995	0.585	0.475	0.326	0.295	0.265	0.161	0.154
100 sec	1.212	0.778	0.455	0.374	0.273	0.214	0.160	0.133
110 sec	1.225	0.781	0.507	0.367	0.268	0.208	0.201	0.162
120 sec	1.200	0.774	0.530	0.420	0.304	0.240	0.210	0.174
130 sec	1.334	0.876	0.549	0.425	0.325	0.241	0.198	0.169
140 sec	1.713	0.794	0.544	0.508	0.305	0.292	0.237	0.164
150 sec	1.515	0.825	0.613	0.475	0.430	0.301	0.271	0.191
160 sec	1.338	0.903	0.637	0.528	0.396	0.281	0.267	0.186
170 sec	1.405	0.770	0.599	0.389	0.358	0.297	0.209	0.201
180 sec	1.424	0.870	0.564	0.376	0.293	0.241	0.259	0.194
240 sec	0.825	0.465	0.356	0.282	0.209	0.165	0.131	0.097
300 sec	0.179	0.111	0.077	0.056	0.044	0.037	0.027	0.022

Table 27. Mean signal loss caused by amplitude scintillation for a 2 Mt HANE at 200 km

	Mean Signal Loss (dB)							
	40 GHz	50 GHz	60 GHz	70 GHz	80 GHz	90 GHz	100 GHz	110 GHz
10 sec	1.449	0.861	0.547	0.502	0.333	0.276	0.242	0.186
20 sec	1.765	0.990	0.665	0.543	0.376	0.271	0.286	0.223
30 sec	1.860	1.100	0.681	0.579	0.398	0.338	0.270	0.200
40 sec	1.765	1.299	0.920	0.666	0.480	0.352	0.297	0.244
50 sec	1.990	1.438	0.993	0.706	0.527	0.474	0.332	0.294
60 sec	2.084	1.332	0.938	0.743	0.481	0.429	0.355	0.296
70 sec	1.613	0.936	0.755	0.516	0.379	0.336	0.246	0.209
80 sec	1.346	0.847	0.533	0.489	0.323	0.249	0.199	0.155
90 sec	1.420	0.804	0.617	0.463	0.336	0.294	0.212	0.193
100 sec	1.458	0.881	0.671	0.439	0.364	0.306	0.213	0.199
110 sec	1.254	0.871	0.648	0.446	0.340	0.270	0.240	0.226
120 sec	1.487	0.925	0.693	0.494	0.344	0.304	0.234	0.182
130 sec	1.336	0.918	0.629	0.459	0.292	0.326	0.257	0.177
140 sec	1.590	0.868	0.624	0.481	0.336	0.263	0.239	0.208
150 sec	1.336	0.874	0.559	0.389	0.397	0.253	0.213	0.193
160 sec	1.331	0.753	0.577	0.330	0.319	0.219	0.196	0.174
170 sec	1.099	0.706	0.496	0.360	0.268	0.223	0.171	0.130
180 sec	0.826	0.472	0.388	0.282	0.213	0.161	0.130	0.097
240 sec	0.204	0.156	0.097	0.071	0.062	0.042	0.034	0.025
300 sec	0.170	0.122	0.081	0.066	0.045	0.035	0.035	0.025

Table 28. Mean signal loss caused by amplitude scintillation for a 2 Mt HANE at 150 km

	Mean Signal Loss (dB)							
	40 GHz	50 GHz	60 GHz	70 GHz	80 GHz	90 GHz	100 GHz	110 GHz
10 sec	1.241	0.821	0.559	0.443	0.341	0.228	0.196	0.180
20 sec	2.279	1.365	0.977	0.767	0.531	0.421	0.371	0.283
30 sec	2.447	1.465	1.160	0.852	0.626	0.478	0.433	0.304
40 sec	2.522	1.463	0.975	0.644	0.486	0.421	0.354	0.316
50 sec	2.279	1.655	1.026	0.809	0.606	0.523	0.318	0.292
60 sec	1.943	1.187	0.840	0.708	0.540	0.416	0.287	0.279
70 sec	1.504	1.077	0.733	0.507	0.449	0.320	0.278	0.235
80 sec	0.857	0.542	0.416	0.253	0.239	0.163	0.149	0.131
90 sec	0.990	0.531	0.387	0.301	0.242	0.181	0.142	0.116
100 sec	0.822	0.624	0.385	0.397	0.260	0.201	0.138	0.131
110 sec	0.940	0.672	0.509	0.371	0.278	0.197	0.190	0.155
120 sec	0.837	0.647	0.456	0.294	0.259	0.182	0.147	0.105
130 sec	1.062	0.679	0.467	0.335	0.243	0.233	0.186	0.147
140 sec	1.136	0.745	0.467	0.446	0.311	0.214	0.170	0.151
150 sec	1.296	0.754	0.461	0.401	0.299	0.232	0.162	0.152
160 sec	1.145	0.694	0.601	0.377	0.318	0.206	0.195	0.168
170 sec	1.459	0.870	0.632	0.456	0.320	0.259	0.249	0.173
180 sec	1.489	1.013	0.629	0.431	0.329	0.302	0.230	0.183
240 sec	1.382	0.922	0.678	0.472	0.347	0.300	0.252	0.178
300 sec	0.571	0.435	0.262	0.192	0.153	0.123	0.116	0.068

Table 29. Mean signal loss caused by amplitude scintillation for a 5 Mt HANE at 200 km

	Mean Signal Loss (dB)							
	40 GHz	50 GHz	60 GHz	70 GHz	80 GHz	90 GHz	100 GHz	110 GHz
10 sec	1.523	1.037	0.757	0.587	0.458	0.324	0.250	0.231
20 sec	1.788	1.243	0.879	0.543	0.440	0.337	0.349	0.270
30 sec	1.984	1.215	0.750	0.533	0.464	0.420	0.310	0.261
40 sec	1.688	1.193	0.996	0.704	0.552	0.408	0.343	0.274
50 sec	1.895	1.296	0.949	0.721	0.511	0.432	0.281	0.287
60 sec	1.839	1.292	0.853	0.559	0.497	0.384	0.312	0.262
70 sec	1.517	1.195	0.722	0.697	0.439	0.369	0.295	0.247
80 sec	1.522	1.054	0.558	0.508	0.396	0.304	0.213	0.185
90 sec	1.147	0.684	0.435	0.352	0.236	0.198	0.169	0.144
100 sec	1.165	0.851	0.522	0.380	0.286	0.211	0.210	0.151
110 sec	1.408	0.808	0.614	0.380	0.383	0.281	0.280	0.204
120 sec	1.122	1.003	0.631	0.473	0.352	0.289	0.247	0.217
130 sec	1.527	0.869	0.729	0.415	0.336	0.305	0.208	0.208
140 sec	1.640	1.074	0.713	0.607	0.410	0.296	0.282	0.179
150 sec	1.641	1.029	0.695	0.517	0.448	0.351	0.259	0.229
160 sec	1.312	1.047	0.695	0.544	0.415	0.280	0.232	0.204
170 sec	1.747	1.071	0.635	0.507	0.391	0.299	0.248	0.194
180 sec	1.586	1.009	0.645	0.599	0.423	0.303	0.269	0.200
240 sec	1.503	1.017	0.772	0.534	0.386	0.323	0.304	0.220
300 sec	0.327	0.187	0.145	0.105	0.087	0.066	0.049	0.047

Table 30. Mean signal loss caused by amplitude scintillation for a 5 Mt HANE at 150 km

	Mean Signal Loss (dB)							
	40 GHz	50 GHz	60 GHz	70 GHz	80 GHz	90 GHz	100 GHz	110 GHz
10 sec	1.559	0.929	0.675	0.454	0.384	0.299	0.227	0.216
20 sec	2.184	1.755	1.286	0.830	0.592	0.560	0.399	0.354
30 sec	3.039	1.641	1.314	0.878	0.608	0.499	0.424	0.367
40 sec	2.851	1.846	1.261	1.060	0.629	0.522	0.404	0.389
50 sec	2.704	1.893	1.108	0.969	0.719	0.458	0.558	0.396
60 sec	2.963	1.936	1.192	0.890	0.694	0.608	0.505	0.418
70 sec	2.502	1.911	1.255	0.904	0.744	0.575	0.506	0.350
80 sec	2.531	1.576	1.163	0.909	0.630	0.530	0.417	0.388
90 sec	2.032	1.469	1.100	0.779	0.537	0.505	0.449	0.298
100 sec	2.058	1.165	0.858	0.601	0.461	0.376	0.345	0.263
110 sec	1.155	0.663	0.543	0.396	0.304	0.234	0.198	0.165
120 sec	1.110	0.687	0.534	0.414	0.302	0.232	0.210	0.165
130 sec	1.310	0.798	0.601	0.405	0.312	0.239	0.191	0.158
140 sec	1.042	0.773	0.591	0.404	0.375	0.286	0.187	0.164
150 sec	1.111	0.739	0.475	0.376	0.308	0.265	0.172	0.156
160 sec	1.174	0.787	0.607	0.496	0.275	0.228	0.193	0.147
170 sec	1.176	0.870	0.595	0.387	0.338	0.235	0.216	0.145
180 sec	1.492	0.923	0.614	0.453	0.325	0.291	0.203	0.181
240 sec	1.562	1.100	0.764	0.546	0.423	0.329	0.251	0.219
300 sec	1.765	1.123	0.796	0.550	0.425	0.336	0.293	0.251

Appendix C. Maximum Signal Loss Tables

This appendix contains tables of the maximum signal loss for a given channel. The tables include data from all HANE scenarios.

Table 31. Maximum signal loss in channel for a 100 kt HANE located at 150 km.

	Max Signal Loss (db)							
	40 GHz	50 GHz	60 GHz	70 GHz	80 GHz	90 GHz	100 GHz	110 GHz
0 sec	2.2	1.0	0.9	0.8	0.4	0.5	0.5	0.3
1 sec	0.4	0.4	0.2	0.1	0.1	0.1	0.1	0.1
3 sec	0.8	0.5	0.4	0.2	0.4	0.2	0.2	0.1
10 sec	1.6	1.2	1.0	0.5	0.4	0.3	0.3	0.4
20 sec	2.0	1.1	0.9	0.6	0.4	0.4	0.3	0.5
30 sec	1.8	1.1	1.2	0.8	0.5	0.6	0.3	0.3
40 sec	2.3	1.0	0.8	0.8	0.5	0.4	0.3	0.2
50 sec	2.0	1.2	0.7	0.8	0.4	0.3	0.3	0.3
60 sec	1.8	1.5	1.1	0.8	0.7	0.4	0.3	0.2
70 sec	1.8	1.4	0.9	0.5	0.5	0.4	0.3	0.2
80 sec	1.7	0.9	0.6	0.5	0.4	0.3	0.3	0.3
90 sec	1.8	1.1	0.7	0.6	0.5	0.4	0.4	0.2
100 sec	1.8	1.0	0.8	0.5	0.4	0.3	0.3	0.3
110 sec	1.4	1.0	0.6	0.4	0.4	0.4	0.3	0.3
120 sec	1.8	0.9	1.0	0.6	0.6	0.4	0.3	0.3
130 sec	1.1	0.9	0.6	0.5	0.6	0.3	0.3	0.2
140 sec	1.2	0.8	0.6	0.4	0.4	0.4	0.2	0.3
150 sec	1.4	0.7	0.6	0.4	0.3	0.3	0.3	0.2
160 sec	1.3	0.8	0.5	0.5	0.3	0.2	0.2	0.2
170 sec	1.0	0.7	0.5	0.3	0.2	0.3	0.2	0.1
180 sec	0.8	0.6	0.3	0.3	0.3	0.2	0.3	0.1
240 sec	0.2	0.2	0.1	0.1	0.2	0.1	0.1	0.1
300 sec	0.2	0.2	0.1	0.1	0.1	0.1	0.1	0.1

Table 32. Maximum signal loss in channel for a 100 kt HANE located at 200 km.

	Max Signal Loss (db)							
	40 GHz	50 GHz	60 GHz	70 GHz	80 GHz	90 GHz	100 GHz	110 GHz
0 sec	1.2	0.7	0.5	0.3	0.3	0.2	0.2	0.1
1 sec	0.7	0.6	0.4	0.3	0.2	0.2	0.2	0.1
3 sec	1.1	0.5	0.5	0.3	0.2	0.3	0.2	0.1
10 sec	0.6	0.5	0.3	0.3	0.2	0.2	0.2	0.2
20 sec	0.9	0.6	0.5	0.3	0.3	0.2	0.2	0.1
30 sec	1.3	1.0	0.6	0.6	0.4	0.3	0.2	0.2
40 sec	0.9	0.7	0.4	0.4	0.3	0.2	0.2	0.2
50 sec	0.7	0.6	0.4	0.3	0.2	0.3	0.2	0.2
60 sec	1.2	0.8	0.5	0.3	0.3	0.3	0.3	0.2
70 sec	0.9	0.6	0.5	0.5	0.3	0.4	0.3	0.1
80 sec	0.6	0.3	0.3	0.2	0.4	0.2	0.2	0.2
90 sec	0.5	0.2	0.2	0.1	0.2	0.1	0.1	0.1
100 sec	0.3	0.2	0.3	0.2	0.2	0.1	0.1	0.1
110 sec	0.4	0.3	0.2	0.3	0.2	0.2	0.1	0.1
120 sec	0.4	0.2	0.2	0.1	0.1	0.1	0.1	0.1
130 sec	0.4	0.5	0.1	0.2	0.1	0.1	0.1	0.1
140 sec	0.3	0.3	0.2	0.1	0.1	0.1	0.1	0.1
150 sec	0.3	0.2	0.2	0.1	0.1	0.1	0.1	0.1
160 sec	0.3	0.3	0.2	0.1	0.1	0.1	0.1	0.1
170 sec	0.3	0.2	0.2	0.1	0.1	0.1	0.1	0.1
180 sec	0.2	0.2	0.1	0.2	0.1	0.1	0.1	0.1
240 sec	0.2	0.1	0.1	0.1	0.1	0.1	0.0	0.1
300 sec	0.1	0.1	0.0	0.0	0.0	0.1	0.0	0.0

Table 33. Maximum signal loss in channel for a 500 kt HANE located at 150 km.

	Max Signal Loss (db)							
	40 GHz	50 GHz	60 GHz	70 GHz	80 GHz	90 GHz	100 GHz	110 GHz
0 sec	2.2	1.9	1.0	0.9	0.7	0.6	0.4	0.4
1 sec	1.7	1.1	1.0	0.6	0.4	0.4	0.3	0.3
3 sec	1.2	0.8	0.5	0.5	0.3	0.3	0.2	0.2
10 sec	1.9	1.3	0.8	0.8	0.4	0.4	0.3	0.2
20 sec	2.7	2.0	1.3	1.3	0.9	0.5	0.4	0.4
30 sec	4.5	1.7	2.1	1.1	0.8	0.7	0.7	0.5
40 sec	3.6	2.6	2.1	1.4	1.0	0.6	0.6	0.5
50 sec	3.9	1.5	1.3	0.9	0.7	0.6	0.4	0.4
60 sec	2.7	1.3	1.0	1.0	0.7	0.4	0.4	0.4
70 sec	2.4	1.3	1.0	0.8	0.6	0.5	0.4	0.3
80 sec	2.8	1.8	1.2	1.0	0.8	0.5	0.4	0.4
90 sec	3.8	1.6	1.1	0.9	0.7	0.7	0.3	0.3
100 sec	2.0	1.8	0.9	0.8	0.9	0.5	0.4	0.4
110 sec	2.7	1.4	1.1	1.0	0.7	0.5	0.5	0.4
120 sec	2.3	1.7	1.3	1.0	0.7	0.5	0.4	0.3
130 sec	2.4	1.3	1.0	0.7	0.6	0.5	0.4	0.3
140 sec	2.3	1.5	1.0	1.1	0.5	0.5	0.3	0.3
150 sec	1.5	1.4	1.4	0.6	0.5	0.4	0.3	0.3
160 sec	1.6	1.1	0.7	0.4	0.4	0.3	0.3	0.3
170 sec	1.7	1.1	0.8	0.6	0.3	0.4	0.3	0.2
180 sec	1.6	1.2	0.6	0.6	0.4	0.3	0.2	0.2
240 sec	0.8	0.5	0.3	0.2	0.2	0.1	0.1	0.1
300 sec	0.2	0.2	0.1	0.1	0.1	0.0	0.0	0.0

Table 34. Maximum signal loss in channel for a 500 kt HANE located at 200 km.

	Max Signal Loss (db)							
	40 GHz	50 GHz	60 GHz	70 GHz	80 GHz	90 GHz	100 GHz	110 GHz
0 sec	3.7	2.1	1.2	1.0	0.6	0.5	0.6	0.5
1 sec	2.0	1.2	1.0	0.7	0.5	0.4	0.4	0.4
3 sec	1.1	0.7	0.5	0.4	0.3	0.3	0.2	0.2
10 sec	1.5	0.8	0.8	0.5	0.4	0.3	0.3	0.2
20 sec	1.9	1.4	0.8	0.6	0.5	0.4	0.3	0.4
30 sec	3.6	2.3	1.8	1.2	1.0	0.7	0.7	0.5
40 sec	3.5	2.4	1.6	1.4	0.8	0.6	0.5	0.4
50 sec	4.1	2.0	1.5	1.0	0.9	0.6	0.7	0.5
60 sec	3.7	2.1	1.8	1.1	0.9	0.7	0.7	0.6
70 sec	2.4	2.3	1.4	0.8	0.8	0.7	0.5	0.5
80 sec	2.6	2.5	1.1	1.2	0.8	0.7	0.6	0.5
90 sec	2.5	1.9	1.2	1.3	1.0	0.7	0.5	0.5
100 sec	3.1	2.1	1.3	1.0	0.7	0.6	0.5	0.3
110 sec	2.5	1.4	1.1	0.8	0.7	0.7	0.5	0.5
120 sec	1.8	1.4	1.2	0.9	0.5	0.5	0.4	0.3
130 sec	2.1	1.1	0.8	0.6	0.4	0.4	0.3	0.3
140 sec	1.9	1.3	0.8	0.6	0.5	0.3	0.4	0.2
150 sec	1.3	0.9	0.7	0.4	0.6	0.3	0.3	0.3
160 sec	1.3	0.9	0.7	0.4	0.3	0.3	0.2	0.2
170 sec	1.2	0.7	0.5	0.5	0.3	0.3	0.3	0.2
180 sec	0.6	0.4	0.3	0.2	0.2	0.2	0.1	0.1
240 sec	0.3	0.2	0.2	0.2	0.1	0.1	0.1	0.1
300 sec	0.2	0.2	0.1	0.1	0.1	0.1	0.1	0.1

Table 35. Maximum signal loss in channel for a 1 Mt HANE located at 150 km.

	Max Signal Loss (db)							
	40 GHz	50 GHz	60 GHz	70 GHz	80 GHz	90 GHz	100 GHz	110 GHz
0 sec	3.1	1.6	1.2	1.0	0.7	0.9	0.5	0.3
1 sec	2.2	1.8	0.8	0.6	0.5	0.4	0.5	0.4
3 sec	1.6	0.9	0.7	0.5	0.4	0.3	0.3	0.2
10 sec	2.7	1.5	1.2	0.7	0.5	0.6	0.5	0.5
20 sec	3.6	2.6	1.7	1.1	1.0	0.8	0.8	0.5
30 sec	4.1	2.4	1.9	1.6	1.0	0.8	0.9	0.5
40 sec	4.5	2.5	2.3	1.1	1.3	0.8	0.8	0.5
50 sec	5.1	3.3	2.5	1.3	0.9	0.8	0.8	0.6
60 sec	3.7	2.8	1.8	0.9	1.0	0.8	0.6	0.6
70 sec	2.9	1.9	1.3	1.2	0.8	0.5	0.6	0.5
80 sec	2.1	1.1	0.8	0.6	0.5	0.5	0.3	0.4
90 sec	1.7	1.2	0.9	0.7	0.6	0.6	0.4	0.3
100 sec	2.1	1.5	0.9	0.9	0.6	0.4	0.3	0.3
110 sec	2.4	1.4	1.0	0.7	0.5	0.4	0.4	0.3
120 sec	2.6	1.4	1.0	0.7	0.6	0.4	0.4	0.3
130 sec	2.8	1.7	1.2	0.8	0.6	0.5	0.4	0.4
140 sec	3.2	1.4	1.0	1.1	0.6	0.7	0.5	0.3
150 sec	2.9	2.3	1.2	0.8	0.8	0.7	0.5	0.5
160 sec	2.4	1.8	1.1	0.9	0.8	0.5	0.5	0.4
170 sec	2.4	1.7	1.2	0.6	0.6	0.5	0.7	0.4
180 sec	2.4	1.7	1.1	0.7	0.6	0.6	0.4	0.4
240 sec	1.6	0.9	0.7	0.5	0.4	0.4	0.3	0.3
300 sec	0.4	0.3	0.2	0.2	0.1	0.1	0.1	0.0

Table 36. Maximum signal loss in channel for a 1 Mt HANE located at 200 km.

	Max Signal Loss (db)							
	40 GHz	50 GHz	60 GHz	70 GHz	80 GHz	90 GHz	100 GHz	110 GHz
0 secs	2.77	1.74	1.45	1.25	0.74	0.84	0.58	0.38
1 sec	2.05	1.20	0.91	0.75	0.55	0.48	0.34	0.37
3 sec	1.47	1.06	0.63	0.55	0.35	0.28	0.39	0.24
10 sec	1.50	1.41	0.86	0.59	0.48	0.39	0.33	0.30
20 sec	2.82	1.93	1.29	0.89	0.83	0.64	0.51	0.37
30 sec	3.66	2.41	1.91	1.40	1.01	0.79	0.70	0.54
40 sec	5.31	3.04	2.22	1.25	1.21	0.73	0.59	0.60
50 sec	4.31	1.74	1.69	1.33	1.12	0.83	0.69	0.49
60 sec	4.29	2.35	1.51	1.43	1.09	0.75	0.67	0.48
70 sec	3.87	2.03	1.55	1.00	0.80	0.95	0.59	0.40
80 sec	2.85	1.57	1.12	0.92	0.66	0.56	0.56	0.44
90 sec	2.96	2.04	1.47	0.98	0.90	0.71	0.44	0.33
100 sec	2.75	2.14	1.03	0.75	0.63	0.54	0.51	0.47
110 sec	3.58	1.74	1.16	0.94	0.84	0.68	0.42	0.42
120 sec	3.84	2.02	1.02	0.88	0.66	0.51	0.49	0.36
130 sec	2.01	1.70	1.30	0.89	0.74	0.49	0.49	0.38
140 sec	2.61	1.79	1.09	1.10	0.82	0.54	0.52	0.40
150 sec	1.89	1.66	1.05	0.66	0.66	0.57	0.39	0.35
160 sec	1.56	0.82	0.78	0.77	0.78	0.46	0.33	0.24
170 sec	2.00	1.05	0.87	0.54	0.45	0.44	0.35	0.31
180 sec	1.34	0.88	0.56	0.47	0.34	0.34	0.33	0.22
240 sec	0.88	0.45	0.40	0.27	0.21	0.21	0.19	0.16
300 sec	0.41	0.25	0.16	0.11	0.19	0.08	0.07	0.23

Table 37. Maximum signal loss in channel for a 2 Mt HANE located at 150 km.

	Max Signal Loss (db)							
	40 GHz	50 GHz	60 GHz	70 GHz	80 GHz	90 GHz	100 GHz	110 GHz
0 sec	3.6	1.6	1.3	0.9	0.7	0.7	0.5	0.5
1 sec	1.8	1.3	1.1	0.7	0.5	0.5	0.4	0.3
3 sec	1.2	1.0	0.7	0.4	0.3	0.3	0.2	0.2
10 sec	2.3	1.6	0.8	0.8	0.6	0.4	0.4	0.7
20 sec	4.1	2.5	2.2	1.4	1.0	0.7	0.9	0.5
30 sec	5.6	2.7	2.4	1.8	1.4	0.9	0.8	0.6
40 sec	5.1	3.4	1.7	1.5	0.9	0.9	0.8	0.8
50 sec	4.4	2.7	1.8	2.0	1.2	0.9	0.6	0.5
60 sec	3.4	1.9	1.5	1.6	1.2	0.8	0.7	0.6
70 sec	3.3	2.1	1.4	1.0	0.8	0.7	0.5	0.5
80 sec	2.1	1.3	0.7	0.6	0.5	0.3	0.3	0.2
90 sec	2.1	1.1	0.8	0.6	0.5	0.4	0.3	0.2
100 sec	1.4	1.2	0.8	0.8	0.4	0.4	0.3	0.2
110 sec	1.6	1.1	1.1	0.7	0.4	0.5	0.4	0.3
120 sec	1.5	1.3	0.7	0.7	0.5	0.5	0.5	0.3
130 sec	1.8	1.4	0.7	0.6	0.4	0.4	0.4	0.4
140 sec	2.3	1.5	0.7	1.0	0.5	0.4	0.3	0.3
150 sec	2.3	1.7	0.8	0.8	0.6	0.5	0.4	0.3
160 sec	2.0	1.6	1.1	0.8	0.6	0.5	0.5	0.3
170 sec	3.1	1.9	1.3	1.0	0.6	0.5	0.5	0.3
180 sec	2.6	1.6	1.0	0.9	0.6	0.7	0.5	0.3
240 sec	2.9	1.5	1.4	1.0	0.8	0.6	0.5	0.4
300 sec	0.9	0.8	0.4	0.4	0.3	0.3	0.2	0.2

Table 38. Maximum signal loss in channel for a 2 Mt HANE located at 200 km.

	Max Signal Loss (db)							
	40 GHz	50 GHz	60 GHz	70 GHz	80 GHz	90 GHz	100 GHz	110 GHz
0 secs	3.45	1.91	1.52	1.11	0.93	0.63	0.65	0.51
1 sec	1.89	1.60	1.03	0.75	0.67	0.53	0.36	0.42
3 sec	1.52	1.02	0.60	0.43	0.32	0.33	0.34	0.21
10 sec	2.70	1.66	1.19	0.88	0.61	0.61	0.42	0.39
20 sec	3.00	1.60	1.12	1.00	0.93	0.55	0.48	0.47
30 sec	2.92	2.47	1.12	1.05	0.66	0.74	0.52	0.52
40 sec	3.60	2.94	1.61	1.36	0.96	0.68	0.69	0.46
50 sec	3.99	2.71	2.08	1.65	1.14	0.95	0.66	0.54
60 sec	3.87	2.71	1.91	1.38	0.98	0.82	0.85	0.64
70 sec	2.87	1.74	1.32	0.89	0.75	0.68	0.46	0.46
80 sec	2.28	1.83	0.99	0.89	0.58	0.42	0.43	0.35
90 sec	2.62	1.40	1.26	0.89	0.53	0.53	0.41	0.43
100 sec	2.27	1.82	1.69	1.04	0.59	0.61	0.41	0.45
110 sec	2.78	1.74	1.13	0.93	0.64	0.58	0.39	0.53
120 sec	2.74	1.36	1.35	1.02	0.86	0.65	0.48	0.37
130 sec	2.14	1.64	1.47	0.83	0.57	0.66	0.40	0.39
140 sec	2.88	1.40	1.40	1.00	0.67	0.62	0.50	0.52
150 sec	2.51	1.70	1.20	0.72	0.82	0.43	0.38	0.37
160 sec	2.62	1.63	1.28	0.64	0.64	0.46	0.39	0.33
170 sec	2.22	1.61	0.89	0.88	0.44	0.40	0.42	0.25
180 sec	1.84	0.90	0.91	0.51	0.59	0.29	0.29	0.28
240 sec	0.37	0.29	0.24	0.15	0.15	0.13	0.13	0.09
300 sec	0.36	0.31	0.20	0.22	0.14	0.14	0.15	0.12

Table 39. Maximum signal loss in channel for a 5 Mt HANE located at 150 km.

	Max Signal Loss (db)							
	40 GHz	50 GHz	60 GHz	70 GHz	80 GHz	90 GHz	100 GHz	110 GHz
0 sec	2.5	2.0	1.3	1.2	0.7	0.7	0.4	0.4
1 sec	2.7	1.9	1.2	0.9	0.9	0.5	0.4	0.2
3 sec	1.3	1.0	0.5	0.4	0.4	0.3	0.3	0.2
10 sec	2.9	1.8	1.1	0.8	0.6	0.6	0.5	0.6
20 sec	4.9	3.0	2.3	1.5	1.2	0.9	0.8	0.6
30 sec	7.1	3.1	2.0	2.0	1.4	1.0	0.8	0.8
40 sec	4.6	4.1	2.5	2.2	1.3	1.1	0.7	0.8
50 sec	5.0	3.8	2.1	2.0	1.6	0.8	1.1	0.9
60 sec	6.1	4.2	2.1	1.5	1.2	1.4	1.0	0.7
70 sec	4.5	3.6	2.0	1.8	1.5	1.1	0.8	0.7
80 sec	5.5	3.0	2.3	2.0	1.2	0.9	0.9	0.8
90 sec	3.6	2.7	2.5	1.2	1.0	0.9	0.9	0.7
100 sec	4.9	2.3	1.7	1.3	1.1	0.8	0.7	0.5
110 sec	2.1	1.2	1.1	0.7	0.6	0.5	0.4	0.3
120 sec	2.2	1.4	1.3	0.9	0.6	0.4	0.5	0.3
130 sec	2.7	1.2	1.2	0.8	0.7	0.4	0.4	0.3
140 sec	2.3	1.3	1.2	0.8	0.6	0.5	0.4	0.4
150 sec	2.0	1.5	0.9	0.8	0.6	0.5	0.3	0.3
160 sec	2.3	1.8	1.2	0.9	0.6	0.4	0.4	0.3
170 sec	2.1	1.4	1.3	0.7	0.7	0.4	0.4	0.3
180 sec	3.1	2.4	1.2	1.0	0.5	0.5	0.4	0.5
240 sec	3.3	2.5	1.6	1.0	0.8	0.6	0.5	0.4
300 sec	3.5	2.3	1.3	1.1	0.8	0.8	0.8	0.5

Table 40. Maximum signal loss in channel for a 5 Mt HANE located at 200 km.

	Max Signal Loss (db)							
	40 GHz	50 GHz	60 GHz	70 GHz	80 GHz	90 GHz	100 GHz	110 GHz
0 secs	2.83	1.89	1.28	1.09	0.95	0.69	0.55	0.43
1 sec	1.95	1.74	1.06	0.69	0.48	0.45	0.35	0.26
3 sec	1.97	0.9	0.67	0.5	0.47	0.29	0.22	0.26
10 sec	3.27	1.78	1.56	1.14	0.89	0.75	0.62	0.49
20 sec	3.53	2.37	1.6	1.22	0.87	0.72	0.65	0.47
30 sec	4.11	2.27	1.69	1	0.92	0.75	0.63	0.53
40 sec	3.43	2.11	1.98	1.42	1.08	0.77	0.58	0.49
50 sec	2.93	2.87	1.9	1.49	1.03	0.8	0.52	0.63
60 sec	4.3	2.13	1.79	1.04	1.06	0.7	0.57	0.53
70 sec	3.23	2.14	1.49	1.44	0.88	0.82	0.56	0.46
80 sec	2.92	1.64	1.17	0.84	0.81	0.62	0.46	0.37
90 sec	2.25	1.38	1.1	0.56	0.52	0.57	0.31	0.26
100 sec	2.92	1.27	1	0.77	0.72	0.5	0.39	0.37
110 sec	2.96	1.88	1.27	0.6	0.82	0.52	0.6	0.44
120 sec	2.81	2.16	1.05	0.85	0.74	0.53	0.66	0.48
130 sec	3.28	1.85	1.42	0.99	0.64	0.52	0.36	0.46
140 sec	3.97	2.11	1.28	1.07	0.76	0.57	0.56	0.44
150 sec	2.76	2.05	1.25	1.1	0.7	0.65	0.65	0.51
160 sec	2.95	2.08	1.25	1.15	0.76	0.55	0.46	0.44
170 sec	3.76	1.87	1.11	1.13	0.73	0.51	0.53	0.38
180 sec	3.51	1.62	1.23	1.1	0.82	0.58	0.48	0.42
240 sec	2.73	1.66	1.53	1.09	0.78	0.66	0.52	0.45
300 sec	0.67	0.47	0.28	0.23	0.27	0.24	0.11	0.14

Bibliography

1. NASA, "http://www.nasa.gov/sites/default/files/styles/full_width_feature/public/images/463940m layers2_full.jpg?itok=oB1Fx8Le. Accessed Aug 22, 2016." [Online]. Available: http://www.nasa.gov/sites/default/files/styles/full{_}width{_}feature/public/images/463940main{_}atmosphere-layers2{_}full.jpg?itok=oB1Fx8Le

2. Boston College: Institute for Scientific Research, "http://www.bc.edu/content/dam/files/research_sites/isr/png/ISR_Rettererfig1a.png. Accesssed Jul 29, 2016." 2016. [Online]. Available: http://www.bc.edu/research/isr/spaceweatherforecasting.html

3. R. Middlestead, R. LeLevier, and M. Smith, "Satellite Crosslink Communications Vulnerability in a Nuclear Environment," *IEEE Journal on Selected Areas in Communications*, vol. 5, no. 2, pp. 138–145, feb 1987. [Online]. Available: http://ieeexplore.ieee.org/lpdocs/epic03/wrapper.htm?arnumber=1146532

4. S. Glasstone and P. J. Dolan, "The Effects of Nuclear Weapons," 1977. [Online]. Available: https://www.fourmilab.ch/etexts/www/effects/

5. L. J. Ippolito, "Radio propagation for space communications systems," *Proceedings of the IEEE*, vol. 69, no. 6, pp. 697–727, 1981.

6. R. Schunk and A. Nagy, *Ionospheres: physics, plasma physics, and chemistry*. Cambridge university press, 2009.

7. K. Davies, *Ionospheric radio*. IET, 1990, no. 31.

8. International Telecommunications Union - Radiocommunications, "http://www.itu.int/pub/R-REC. Accessed Aug 23, 2016." [Online]. Available: http://www.itu.int/pub/R-REC

9. D. L. Knepp, "Multiple Phase-Screen Calculation of the Temporal Behavior of Stochastic Waves," *Proceedings of the IEEE*, vol. 71, no. 6, pp. 722–737, 1983.

10. ——, "Multiple phase screen calculation of two-way spherical wave propagation in the ionosphere," *Radio Science*, vol. 51, no. 4, pp. 259–270, apr 2016. [Online]. Available: http://doi.wiley.com/10.1002/2015RS005915

11. C. Grimault, "A multiple phase screen technique for electromagnetic wave propagation through random ionospheric irregularities," *Radio Science*, vol. 33, no. 3, pp. 595–605, 1998.

12. D. L. Knepp and L. J. Nickisch, "Multiple phase screen calculation of wide bandwidth propagation," *Radio Science*, vol. 44, no. 1, feb 2009. [Online]. Available: http://onlinelibrary.wiley.com/doi/10.1029/2008RS004054/fullhttp://doi.wiley.com/10.1029/2008RS004054

13. C. L. Rino, "A power law phase screen model for ionospheric scintillation: 1. Weak scatter," *Radio Science*, vol. 14, no. 6, pp. 1135–1145, 1979.

14. J. A. Secan, R. M. Bussey, E. J. Fremouw, and S. Basu, "An improved model of equatorial scintillation," *Radio Science*, vol. 30, no. 3, pp. 607–617, 1995.

15. ——, "Highlatitude upgrade to the Wideband ionospheric scintillation model," *Radio Science*, vol. 32, no. 4, pp. 1567–1574, 1997.

16. M. C. Kelley, *The Earth's Ionosphere: Plasma Physics & Electrodynamics*. Academic press, 2009, vol. 96.

17. S. J. Bauer, "Correlations between tropospheric and ionospheric parameters," *Geofisica pura e applicata*, vol. 40, no. 1, pp. 235–240, 1958.

18. P. Bernhardt and W. Scales, "Ionospheric chemical releases," oct 1990. [Online]. Available: http://www.osti.gov/scitech/biblio/7275613

19. P. Krueger and J. Weitzen, "DBPSK signalling rates that maximize the performance of 60 GHz crosslinks in a doubly dispersive channel," in *IEEE Conference on Military Communications*. IEEE, 1990, pp. 339–343. [Online]. Available: http://ieeexplore.ieee.org/lpdocs/epic03/wrapper.htm?arnumber=117438

20. S. Matsushita, "On artificial geomagnetic and ionospheric storms associated with high-altitude explosions," *Journal of Geophysical Research*, vol. 64, no. 9, pp. 1149–1161, sep 1959. [Online]. Available: http://onlinelibrary.wiley.com/doi/10.1029/JZ064i009p01149/abstract

21. W. S. Knapp and K. Schwartz, "Aids for the Study of Electromagnetic Blackout," feb 1975. [Online]. Available: http://oai.dtic.mil/oai/oai?verb=getRecord{\&}metadataPrefix=html{\&}identifier=ADA010228

22. L. J. Nickisch and P. M. Franke, "Finite-difference time-domain solution of Maxwell's equations for the dispersive ionosphere," *IEEE Antennas and Propagation Magazine*, vol. 34, no. 5, pp. 33–39, 1992.

23. Y. Yu, J. Niu, and J. J. Simpson, "A 3-D global earth-ionosphere FDTD model including an anisotropic magnetized plasma ionosphere," *IEEE Transactions on Antennas and Propagation*, vol. 60, no. 7, pp. 3246–3256, 2012.

24. J. E. Allnutt, "Satellite-to-ground radiowave propagation-Theory, practice and system impact at frequencies above 1 GHz," *Stevenage Herts England Peter Peregrinus Ltd IEE Electromagnetic Waves Series*, vol. 29, 1989.

25. K. C. Yeh and C.-H. Liu, "Radio wave scintillations in the ionosphere," *Proceedings of the IEEE*, vol. 70, no. 4, pp. 324–360, 1982.

26. P. L. Dyson, J. P. McClure, and W. B. Hanson, "In situ measurements of the spectral characteristics of F region ionospheric irregularities," *Journal of Geophysical Research*, vol. 79, no. 10, pp. 1497–1502, 1974.

27. A. D. R. Phelps and R. C. Sagalyn, "Plasma density irregularities in the highlatitude top side ionosphere," *Journal of Geophysical Research*, vol. 81, no. 4, pp. 515–523, 1976.

28. D. L. Knepp, "Propagation of wide bandwidth signals through strongly turbulent ionized media," Tech. Rep., 1982.

29. M. Levy, *Parabolic equation methods for electromagnetic wave propagation*. IET, 2000, no. 45.

30. University of Alabama in Huntsville, "http://www.math.uah.edu/stat/sample/CLT.html." [Online]. Available: http://www.math.uah.edu/stat/sample/CLT.html

31. Mathworks, "http://www.mathworks.com/products/matlab/?s_tid=hp_fp_ml. Accessed Aug 22, 2016." [Online]. Available: http://www.mathworks.com/products/matlab/?s{_}tid=hp{_}fp{_}ml

32. T/ICT4D, "NeQuick model. http://t-ict4d.ictp.it/nequick2. Accessed Aug 22, 2016." [Online]. Available: http://t-ict4d.ictp.it/nequick2

33. W. White, G. Bullock, P. Edwardson, and E. Witt, "SCENARIO User Manual," *MRC/NSH-R-92-005-R2*, 2000.

34. P. Edwardson and C. Lauer, "Modeling HANE Impacts on RF Propagation with GSCENARIO and PRPSIM," *The Dispatch*, vol. 3, no. 4, pp. 2–4, 2014. [Online]. Available: http://www.dtra.mil/Portals/61/Documents/dispatch-v3-i4-web-2.pdf

35. H. Zell, "The Day the Sun Brought Darkness. http://www.nasa.gov/topics/earth/features/sun_darkness.html. Accessed Nov 7, 2016." 2015. [Online]. Available: http://www.nasa.gov/topics/earth/features/sun{_}darkness.html

36. D. L. Knepp, "Aperture Antenna Effects After Propagation Through Strongly Disturbed Random Media," *IEEE Transactions on Antennas and Propagation*, vol. 33, no. 10, pp. 1074–1084, 1985.

REPORT DOCUMENTATION PAGE

Form Approved
OMB No. 0704–0188

1. REPORT DATE *(DD–MM–YYYY)*	2. REPORT TYPE	3. DATES COVERED *(From — To)*
23–03–2017	Master's Thesis	Sept 2015 — Mar 2017

4. TITLE AND SUBTITLE

Satellite Communications in the V and W Band:
Natural and Artificial Scintillation Effects

5a. CONTRACT NUMBER

5b. GRANT NUMBER

5c. PROGRAM ELEMENT NUMBER

6. AUTHOR(S)

Smith, David A, Capt, USAF

5d. PROJECT NUMBER

5e. TASK NUMBER

5f. WORK UNIT NUMBER

7. PERFORMING ORGANIZATION NAME(S) AND ADDRESS(ES)

Air Force Institute of Technology
Graduate School of Engineering and Management (AFIT/EN)
2950 Hobson Way
WPAFB OH 45433-7765

8. PERFORMING ORGANIZATION REPORT NUMBER

AFIT-ENG-MS-17-M-070

9. SPONSORING / MONITORING AGENCY NAME(S) AND ADDRESS(ES)

Air Force Research Laboratory: Information Directorate
26 Electronic Parkway
Rome, NY 13441-4514
DSN 587-7418, COMM 315-330-7418
Email: heather.dussault.1@us.af.mil

10. SPONSOR/MONITOR'S ACRONYM(S)

11. SPONSOR/MONITOR'S REPORT NUMBER(S)

12. DISTRIBUTION / AVAILABILITY STATEMENT

DISTRIBUTION STATEMENT A:
APPROVED FOR PUBLIC RELEASE; DISTRIBUTION UNLIMITED.

13. SUPPLEMENTARY NOTES

14. ABSTRACT

In a natural atmospheric environment the troposphere will be the primary source of loss with the ionosphere loss being negligible. If the ionosphere was disturbed from a high altitude nuclear explosion (HANE) more than three times the amount of electrons would be present in the ionosphere and could represent a source of significant loss. In order to determine the amount of electrons distributed from a HANE, GSCENARIO, developed by Defense Threat Reduction Agency was used. The two sources of loss that were examined was signal absorption and amplitude scintillation. Signal loss was determined using GSCENARIO and amplitude scintillation loss was determined by using the multiple phase screen method. Nuclear detonation yields of 100 kt, 500 kt, 1 Mt, 2 Mt, and 5 Mt at explosion heights of 150 km and 200 km were investigated. The results show that signal absorption drops off quickly (within 30 sec), while amplitude scintillation loss can linger for up to 6 min after a HANE. Thus, the signal loss in the V and W bands from a HANE will only disrupt transmissions for the first 6 min after a HANE.

15. SUBJECT TERMS

Ionosphere,Multiple Phase Screens,Split Step Fourier Method,propagation,nuclear effects,V band,W band

16. SECURITY CLASSIFICATION OF:			17. LIMITATION OF ABSTRACT	18. NUMBER OF PAGES	19a. NAME OF RESPONSIBLE PERSON
a. REPORT	b. ABSTRACT	c. THIS PAGE			Dr. A. J. Terzuoli, AFIT/ENG
U	U	U	U	134	19b. TELEPHONE NUMBER *(include area code)* (937) 255-3636, x4717; andrew.terzuoli@afit.edu